

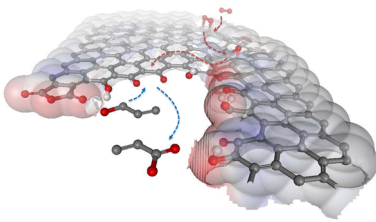
Nanocarbons for the Development of Advanced Catalysts

Dang Sheng Su,*^{†,‡} Siglinda Perathoner,[§] and Gabriele Centi*,[§]

[†]Shenyang National Laboratory for Materials Science, Institute of Metal Research, Chinese Academy of Science, 72 Wenhua Road, Shenyang 110006, China

[‡]Department of Inorganic Chemistry, Fritz Haber Institute of the Max Planck Society, Faradayweg 4-6, 14195 Berlin, Germany

[§]Dipartimento di Ingegneria Elettronica, Chimica ed Ingegneria Industriale, University of Messina and INSTM/CASPE (Laboratory of Catalysis for Sustainable Production and Energy), Viale Ferdinando Stagno, D'Alcontres 31, 98166 Messina, Italy



CONTENTS

1. Introduction	5782
2. Synthesis of Novel Nanostructured Carbon Materials	5784
2.1. Carbon Nanotubes	5785
2.2. Graphene	5786
2.3. Ordered Mesoporous Carbon	5787
2.4. Carbon Hierarchy	5787
2.5. Macroscopic Shaping of Nanocarbon	5788
3. Functionalization of Nanocarbon Materials	5789
3.1. Liquid-Phase Functionalization of Nanocarbon	5789
3.2. Gas-Phase Functionalization of Nanocarbon	5789
4. Characterization and Modeling	5790
4.1. Characterization of Carbon	5790
4.1.1. Microcalorimetry	5791
4.1.2. Temperature-Programmed and Ambient Pressure Photoelectron Spectroscopy	5792
4.1.3. Advanced Electron Microscopy	5792
4.2. Theoretical Modeling	5793
5. Nanocarbons in Catalytic Reactions	5795
5.1. Enhanced Characteristics as a Support for Catalytic Functionalities	5795
5.2. Stabilization of Small Catalytic Particles with Enhanced Catalytic Behavior	5796
5.3. Direct Catalytic Role of Nanocarbon Functional Groups	5798
5.4. Nanoconfinement	5803
5.5. Electron-Transfer Induced Changes in the Properties of Supported Nanoparticles	5804
5.6. Defect-Related Catalytic Reactivity	5805
5.7. Catalysis by Two-Dimensional Carbon Nanomaterials	5807
6. Concluding Remarks and Perspectives	5808
Author Information	5809
Corresponding Author	5809
Author Contributions	5809
Notes	5809

Biographies	5809
Acknowledgments	5810
Abbreviations Used	5810
References	5810

1. INTRODUCTION

Nanocarbon is a term increasingly used^{1–9} to indicate the broad range of carbon materials having a tailored nanoscale dimension and functional properties that significantly depend on their nanoscale features. CNT and graphene belong to this class of materials comprising many more types of carbon materials, such as nanofibers, -coils, -diamonds, -horns, -onions, and fullerene. The alternative definition (also often used) is nanostructured carbon.^{10–15} Both definitions include also ordered mesoporous carbon materials obtained, for example, by a replica method from mesoporous silica or other ordered oxides, which are then removed after the template synthesis of the mesoporous carbon.^{16–20} The nanocarbon class of materials is typically extended to include carbon nanocomposites with metal ions, metal oxide, metals, and quantum dots used in various applications^{21–27} as advanced electrodes for energy conversion and storage, as well as other applications such as catalysis. These carbon/inorganic nanohybrids are at the frontier of research for the development of advanced devices for sustainable energy and development,^{28–31} including artificial leaves.³² Figure 1 provides a schematic illustration of some nanocarbons.

The field of application of nanocarbon materials is large, because they possess electrical and thermal conductivity, as well as a mechanical strength and lightness that conventional materials cannot match. With the diversity of their structure, these characteristic values can be achieved over an extremely wide range of conditions. For these reasons, they are extensively studied in applications going from photonics and optoelectronics to biotech and nanomedicine, advanced electrodes, and polymer composites.^{1–4,9,33}

The global CNT industry turned over around \$668.3 million in 2010, with multiwalled carbon nanotubes (MWCNTs) having a production value of approximately \$631.5 million and single-walled carbon nanotubes (SWCNTs) around \$36.8 million, and the value is forecast to grow to \$1.1 billion by 2016 at a compound annual growth rate (CAGR) of 10.5%.³⁴ Production capacity in 2010 was about 2500 t.³⁴ The largest

Received: September 1, 2012

Published: May 31, 2013

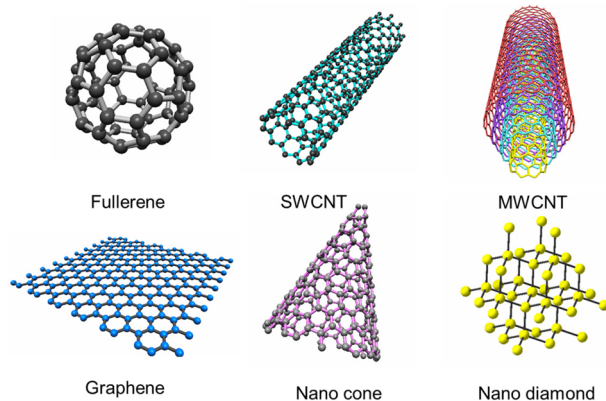


Figure 1. Schematic illustration of some nanocarbon.

share of global CNTs is accounted for by plastics and composites (about 69% of the market). Electrical and electronics industries accounted for 10% of the CNTs market share, followed by energy (8%). The energy sector will also witness rapid growth, with enhanced performance requirements for batteries, wind turbine blades, photovoltaic cells, and other applications in the next 5–10 years.³⁴

In catalysis, even for the relevant research interest,^{14–16,21,26,27,35–44} no major industrial application is already ongoing. A main reason was the higher cost to performance ratio of these materials [with respect to their alternative, for example, active carbon (AC)], but with the actual possibility of mass-production for example of CNTs^{45–47} at costs well-comparable with that of the oxide supports in catalysis applications (alumina, silica) or even of AC, the industrial interest in developing catalysts based on nanocarbons is rapidly raising.^{13,36,39,42}

AC, besides as sorbent, has been used for a long time as an excellent support for catalytic nanoparticles. It is largely applied industrially (worldwide demand of AC in 2011 was about 1.5 Mtions, but a minor part was used for preparing catalysts), particularly in selective hydrogenation and electrocatalytic reactions,^{48–50} due to various valuable properties (with respect to other types of commercial supports or materials for electrochemistry): high surface area; possibility to fine-tune the porosity and graphitic character (e.g., the conductivity properties); robustness and chemical inertness (except in the presence of oxygen at high temperature); availability with different surface properties, such as hydrophilicity and interaction with the supported metal particles (depending on the presence of heteroatoms and inorganic elements, which in turn derive from the starting material and procedure to prepare the AC); and, not least, the low cost. In recent years, thanks to also a better understanding of the surface chemistry of carbon used as support in catalysis, the range of industrial use of AC as catalyst support has been extended to new areas such as (i) environmental protection (volatile organic compound oxidation, chlorinated compound dehalogenation, and advanced oxidation technologies such as catalytic wet-air oxidation), (ii) selective oxidation processes (oxidation of glycerol, for example, or heterogeneous Wacker-type catalysts for the oxidative carbonylation of methanol), (iii) hydroprocessing and selective hydrogenation, and (iv) fine and specialty chemicals synthesis, going from base-catalyzed reactions (for example, Na-, K-, and Cs-AC for N-alkylation of imidazolic rings) and acid-catalyzed reactions to C–C bond formation

(Suzuki, Heck, Sonogashira, and Ullmann reactions) as well.^{48,50} AC surface functional groups may be further tailored for specific needs by secondary functionalization (oxidation, halogenation, impregnation, dry mixing, and heat treatments) to create, for example, O- and N-containing groups, H–C species, S, P, and halogen functionalities or to insert heteroatoms such as B.⁵⁰ Notwithstanding these characteristics of ACs, there are various motivations to develop novel nanocarbon-based catalytic materials for industrial applications. A concise presentation of the difference between AC and CNT (the latter as representative for nanocarbons) is presented below, while details are discussed in the following sections.

Better Pore Structure. AC surface area and porosity can be tuned within some range by controlling the AC preparation procedure, but in large part the high surface area is due to micropores that can be negative in various catalytic reactions, because micropores limit reactant and product diffusion and full accessibility to the supported metal particles. On the contrary, CNT surface area is mainly associated with the external geometrical area of the CNT (except for SWCNT and DWCNT, where inner surface contributes significantly, although different situations are present for open or close nanotubes).⁵¹ CNTs (particularly MWCNT, the most used in catalysis, due to wider availability and lower cost) have thus predominantly mesoporosity associated with the voids created from the CNT network, while in AC most of the surface area is associated with microporosity. Typical AC surface area is around 1000 m²/g (greatly depending on the type and treatment procedure), while that of CNT may range from over 1000 m²/g for SWCNTs to 700–800 m²/g for DWCNT and 200–300 m²/g for MWCNT (5–10 walls).⁵¹ Therefore, when diffusion limitations can be critical in catalytic reactions (e.g., fast gas-phase reactions and/or in liquid phase), the catalytic effectiveness of CNTs can be better than that of ACs, as well as the selectivity,⁵² the latter also being negatively affected by the presence of microporosity (for example, in consecutive reactions).

More Uniform Characteristics. Commercial ACs derive mainly from natural sources (nutshells, peat, etc.) through a process of carbonization by pyrolysis followed by specific treatment in controlled atmosphere to create the porosity. Due to this process and the natural source origin, significant differences in the surface properties, structure, and composition between different regions of the AC are often present on a nanoscale level. This could lead a wide range of chemical and physical properties. Due to the recently developed synthetic procedure of preparation, as will be mentioned in the following session, the uniformity in MWCNTs in terms of size distribution, graphitization degree, and purity has been improved significantly. The controlling of chirality and diameter of single-walled CNTs still remains challenge.

Reduced Number of Defects and Impurities. CNTs and graphene with the well-defined structure have defect sites incorporated in the sp²-bonded carbon network, while ACs with disordered structure have a huge number of different type of defective sites (AC has a complex structure composed primarily of graphitic-like sheets—basal planes—joined by random cross-linking resulting in a highly porous structure with a myriad of cracks and crevices). Therefore, in CNTs and graphene it is potentially possible to have a more defined and controlled type of defect that can be better tuned to have the necessary catalytic functionalities or surface properties. In addition, ACs, deriving from natural sources, contain large

amounts of impurities, which are difficult to remove. AC can be prepared also starting from pure organic reactants,⁵³ but then the cost becomes too high. The metallic impurity in CNTs, mostly being residual catalyst used for their production, is defined and can be removed with well-developed methods.⁵⁴ Purity and more defined structural uniformity are both important aspects in catalytic reactions to minimize side reactions. The synthetic procedure for the preparation of CNT with respect to AC allows a better control of these aspects, as commented on in detail later.⁵⁵

Enhanced Oxidative Resistance for Chemical Reactions. ACs usually do not have a well-defined long-range ordering, while each CNT is a rolled-up graphene with well-defined short-range and long-range ordering. Usually, CNTs are more resistant to oxidation than AC,⁵⁶ because on technical grade CNTs or AC, different from single crystal graphite, the mechanism of carbon combustion starts with oxygen dissociation on active sites related to defects and functional groups at the edges of the basal plane.⁵⁷ This property is of special importance when CNTs are used as catalyst support or catalyst for high-temperature reactions or in electrocatalysis in the presence of oxygen.^{55,57} In hybrid materials, e.g., nanocarbons with supported metal oxide nanostructures, the nature of the metal oxide also plays a special role, with the oxidation stability being inversely proportional to the metal oxides reducibility, i.e., the ability to create oxygen vacancies.⁵⁸

Better Electron and Heat Transport. Due to their characteristics, CNTs allow a faster and more efficient electron and heat transport with respect to AC.⁵⁹ Although the electron and heat transport properties depend greatly on the specific characteristics of carbon material (as discussed later), we could indicate that carbon black (CB), one of the most conductive conventional carbon materials, shows a volume resistivity usually higher than $10^1 \Omega \text{ cm}$, while CNTs show a volume resistivity in the 10^{-2} – $10^{-3} \Omega \text{ cm}$ typical range.⁶⁰ Also these properties are relevant for the development of better catalysts.

In addition to these general differences between nanocarbons and AC, which motivate the development of novel catalysts based on nanocarbon materials, there are many aspects related to the specific characteristics of the nanocarbons and their intrinsic reactivity that allow defining these materials as a novel class of catalysts with large potential for industrial uses. The progress on the understanding of the growth mechanism of CNTs⁵² not only improved the yields of CNTs, putting forward the basis toward their mass production,^{45–47} but especially allow a step forward in the control of the quality and nanostructure (number of walls, graphene sheet orientation, chirality, alignment, defect nature, etc.). An initial problem in the use of CNTs in catalysis was the poor control of CNT homogeneity, which led to a number of contrasting catalytic results.¹⁴ This was an additional factor slowing down the potential use of nanocarbons in catalysis. Today, however, there is a much better understanding of nanocarbon characteristics, surface chemistry, and the presence of defect sites.²⁰ The raising research on the synthesis of nanostructured carbon materials significantly extended also the number of different carbon nanostructures available for catalytic uses (carbon nanofibers, -tubes, -coils, -horns, -diamonds, -onions, graphene, etc.).^{13,61–63} Furthermore, the progress in the controlled doping of these materials (particularly with N and B)^{64–67} and in the assembling of low-dimensional carbon nano-objects into three-dimensional architectures (films, hollow spherical capsules, or hollow nanotubes)^{68–70} has further opened the

possibilities for a tailored use in catalysis. The direct growth of ordered arrays of carbon nanotubes or -fibers (carpet-type) from a nanopatterned catalyst array or using inorganic templates,^{71–73} for example, open new possibilities to develop advanced catalyst architectures⁷⁴ or to develop novel more efficient catalysts for microstructured reactor.

It should be mentioned that for commercial applications a comprehensive understanding of the catalyst structure, bonding, and properties is desirable, but not strictly necessary, provided that the catalysts are well-reproducible and give superior performances. There are many examples of commercial catalysts initially developed on a trial-and-error basis, although their further development was always based on the scientific understanding. Today, even with the availability of high-throughput methods, experimentation is too costly and it is necessary to limit the search domain to a narrow range based on the rational understanding of catalyst mechanism and functionalities. In materials such as nanocarbons, where the catalytic performances are highly related to their specific nanodimension and -architecture more than to the composition, a knowledge-driven development is strongly necessary. In addition, very few studies have been reported in the literature regarding the use of high-throughput experimentation methods in the nanocarbon area,⁷⁵ because this kind of testing does not well adapt to this specific scientific area.

The aim of this review is to evaluate the state of nanocarbons and cast a glance to the future in this very dynamic and active field of research to outline the new possibilities offered to the design of advanced catalysts, evidencing at the same time the critical aspects that have to be investigated in a more detail. Emphasis is given, in particular, to less investigated aspects but those relevant to open practical possibilities to develop new classes of catalysts. The aspects discussed regard both the use of nanocarbons as the support for metal or metal oxide nanoparticles that act as the catalytic centers and of metal-free nanocarbons, where the catalytic properties are associated with the catalytic functionalities of the nanocarbon surface itself. However, no precise separation has been made between these two classes of catalytic materials, because even in the first case the nanocarbon does not play a simple role of support (as will emerge from the following discussion), having a role as cocatalyst or by inducing specific reactivity in the supported metal or metal oxide particles. The terms “carbocatalysis” was proposed recently^{42,43,76–78} to describe carbon-only catalysts as alternative to the term metal-free (nano)carbon catalysts used by other authors.^{79–81}

2. SYNTHESIS OF NOVEL NANOSTRUCTURED CARBON MATERIALS

The synthesis of nanocarbons with tailored properties is the prerequisite for applications and investigations of catalysts and their possible production at industrial scale. Up to now more attention has been dedicated to the synthesis and characterization of novel structured carbon materials themselves, rather than of nanocarbon materials having specific reactivity and nanoarchitecture relevant for their use as advanced catalytic materials. In addition, we believe that still limited effort has been dedicated to the uniformity of the nanocarbon characteristics on a nanoscale. In fact, in commercial samples there are often differences between single CNTs in terms of characteristics. Marked differences in the uniformity of distribution of supported metal particles between different zones of CNTs are often observed by electron microscopy (for example, in

published literature images), implying different local differences in the surface properties of CNTs. Progress has been achieved in recent years to get CNTs with more homogenous surface property, as discussed below, but significant improvement is still needed.

2.1. Carbon Nanotubes

More than 20 years after the Iijima's paper of 1991 on CNTs, the growth mechanism of CNTs has been well-studied and was understood to a large extent.^{52,82} The synthesis of CNTs with arc discharge or laser vaporization methods remains interesting for a laboratory scale investigation,⁸² but they are not suitable for mass production. Chemical vapor deposition (CVD) is the only method to scale-up the production of multiwalled CNTs. Tessonniere et al.⁸³ showed that in an optimized CVD process, 1 g of spinel-type cobalt–manganese-based mixed oxide catalyst can produce about 180 g of MWCNTs, when exposed to an ethylene/hydrogen feed at 650 °C for 2 h (Figure 2). A

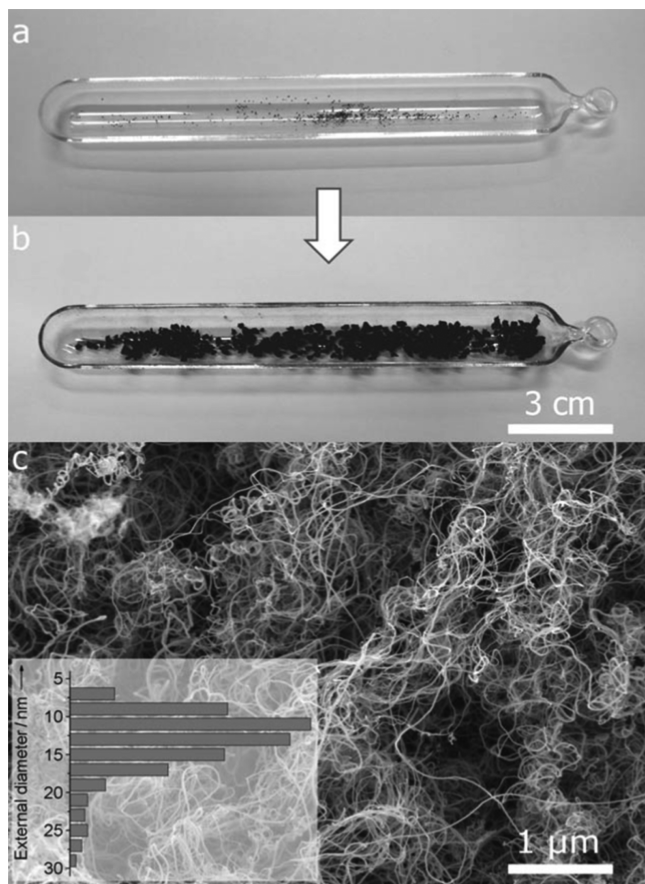


Figure 2. Optical photography of the catalyst before (a) and after (b) the reaction, showing the remarkable increase in volume during CNT growth. The MWCNT yield is 179 g_{CNT}·g_{catalyst}⁻¹. (c) SEM image of the MWCNTs and their external diameter distribution (inset). Reprinted with permission from ref 83. Copyright 2010 Wiley-VCH Verlag.

productivity of 70 kg·h⁻¹ at industrial scale has been realized.^{45,46} The residual catalyst impurities in the obtained MWCNTs were scarce with a purity close to 99.5% carbon, which is sufficient for most applications. The traditional purification step with strong mineral acids is no longer required for many applications, thus rendering the overall process safer, greener, and cheaper. MWCNT are still the main type of

nanocarbon material studied for catalytic applications and also that commercialized for over 95% of global nanocarbon production, as reported in the previous section.

Although SWCNTs are potentially preferable for a number of applications (surface area, for example, may be 5 times higher than that of MWCNTs), the lack of mass production (at a reasonable cost) is still a limit for their practical use. The production of SWCNTs at an industrial scale is underdeveloped, compared with that of MWCNTs. CVD requires high temperature, but under these conditions the rate of pyrolysis of hydrocarbon is often too high and catalytic particles may sinter, making the technology for SWCNT growth unsuitable on an industrial scale. The use of CO as feed was proposed about 10 years ago by Smalley et al.⁸⁴ and later indicated by other groups as a suitable option for the large-scale catalytic synthesis of SWCNTs.^{85–87} This method is applied commercially by small production manufacturers. An example is the CoMoCAT process used by Oklahoma-based SouthWest NanoTechnologies, Inc. (SWeNT), a company founded by Resasco.⁸⁸ SWCNT production with controllable chirality has also progressed significantly in recent years, but still large-scale production remains a far goal, particularly for catalytic applications.⁵²

In view of the sustainability, the use of natural materials containing iron as catalysts for the growth of CNTs is another interesting area of development.^{89–92} The nanocarbon obtained has been successfully tested for ODH (oxidative dehydrogenation) reactions.^{93,94} This method may potentially reduce the costs, but the reproducibility of the starting materials on a large (industrial) scale to have constant-quality products is a major issue.

An interesting advance in CNTs synthesis in the last years is the preparation of vertically aligned CNTs (carpets). This topic was reviewed recently.^{45,70} Aligned CNTs have shown promising applications in electrocatalysis⁹⁵ and in micro-reactors as catalyst support.^{96,97} The production of this specific nanoarchitecture is still mainly at the laboratory scale.

CNTs doped with heteroatoms such as nitrogen (basic-doped) or boron (acid-doped) can be considered different nanocarbons with respect to the undoped CNTs, for their different characteristics both in acid/base-catalyzed reactions and behavior as catalyst support. Significant progress in the synthesis of nitrogen- or boron-doped CNTs has been made using methods similar to those used to produce CNTs, and it is now possible to produce multiwalled structures in a very controlled manner.^{67,98–100} Doping of carbons during CNT synthesis by using nitrogen- or boron-containing precursors can yield a homogeneous incorporation of nitrogen/boron into the entire carbon material.¹⁰¹ The most effective method for N-doped CNTs and CNFs (carbon nanofibers) is the CVD process^{102,103} using N-containing precursors such as melamine;¹⁰⁴ benzylamine;¹⁰⁵ acetonitrile;^{106–108} N-heterocycles;^{109–111} or ammonia, 1,2-ethylenediamine, and pyridine mixed with carbon sources.¹¹² Nitrogen can be incorporated in the CNTs through direct substitution of a carbon atom or a pyridinic bonding configuration. N-doped CNTs do not have a hollow channel, but rather a bamboo-like structure. Incorporation of N in the CVD process requires careful control of the thermodynamic parameters involved in the process of formation. The problem does not lie in the issue that the structures formed exhibit a bamboo-type configuration but that the nitrogen reactivity accelerates the process, leading to the formation of a higher yield of defective coproducts in the

soot.⁶⁷ Also for B-doped CNTs it was observed that structural modifications in the morphology and microstructure of CNTs occur on increasing the level of incorporation of boron.¹¹³

Therefore, even if MWCNTs are today available at low cost and large scale, making them potentially suitable for commercial use in catalysts formulations, an intensified effort is still necessary to ensure (i) higher homogeneity and reproducible quality; (ii) higher uniform characteristics in terms of structure, reactivity, and functional properties at nanoscale-level; and (iii) production at low cost with a higher volume of single- and double-wall CNTs, as well as specific nanoarchitectures, for example, vertically aligned CNTs (carpets). These are the main issues to solve to extend the use of nanocarbon materials as catalysts.

It should be also mentioned that the interest in the synthesis of CNT-like materials is increasing. An example is the production of boron nitride nanotubes (BNNTs).¹¹⁴ They are a structural analog of CNTs, but BNNTs are an electrical insulator with a band gap of ~5 eV, basically independent of tube geometry. In addition, BNNTs possess a high chemical stability, excellent mechanical properties, and high thermal conductivity, making them a potentially interesting material for catalysis. Carbon nitride nanotubes (CNNTs) are also seeing increasing research interest both as support for catalytic nanoparticles^{115,116} and as photocatalytic materials¹¹⁷ and electrocatalysts.¹¹⁸

2.2. Graphene

Graphene, by definition, is a honeycomb-like carbon sheet strictly of one atom thickness. It can be synthesized by micromechanical alleviation of graphite, as reported by Novoselov et al. in 2004,¹¹⁹ but it can also be prepared by other methods that were developed already in the 1960s as described in the historical excursus on graphene reported recently by Bielawski and co-workers.¹²⁰ Graphene can also be obtained by heating silicon carbide to high temperatures (>1100 °C).¹²¹ Epitaxial growth of graphene is also reported on metal substrate.^{122,123} At very low pressure a single graphene layer can form on copper foil.^{124,125} The growth automatically stops after forming a monolayer, and arbitrarily large graphene films can be created. Recently it was also shown that it is possible to produce monolayer graphene films with much larger domain sizes than previously attainable under high-vacuum conditions on Si-terminated SiC(0001) in an argon atmosphere of about 1 bar.¹²⁶ Layers of graphene with dimensions of 3–50 mm may be obtained, as opposed to dimensions of tens of nanometers when the experiments are carried out under high vacuum.

The graphene sheets obtained through these technologies have been used in numerous electronic applications, but they are not suitable for catalysis applications due to their high cost and the small amount of materials available for test reactions. For the preparation of these materials in relatively large quantities, different methods have to be adopted, such as those based on graphite oxide (GO) as raw material, as described later. Recent studies have also shown that graphite can be exfoliated in liquid media into few-layer or even monolayer graphene.^{127–129} This method with further developments may be scalable to industrial production, although probably it will remain too costly for catalytic applications. Despite these achievements, preparation of “pristine” graphene that is free of defects and has lateral dimensions larger than approximately 10–100 mm (a rough upper limit to the lateral size of graphene

from graphitic sources) remains challenging.¹²⁰ It should be also mentioned that for catalytic applications, the graphene layer may stick together, leaving a small exposed surface area, and thus a suitable functionalization is also necessary to create pillars between the graphene layers to leave all of the surface area accessible. This pillarating procedure further enhances the cost of production. Handling these materials to form industrial catalysts with suitable shapes and mechanical resistance for use in industrial reactors is a further great challenge.

On the other hand, this kind of well-defined graphene may be suitable as a model system to study the interaction of gas molecules with the active sites (defects, heteroatoms, or functional groups) of graphene with surface science methods.^{130–133} Systematic studies of this type are still missing, but there are some emerging exciting directions.

The CVD process with its high efficiency remains the only choice for a possible scaled up production of graphene, but this process should occur not on a flat metal substrate, but rather on substrate of high surface area.¹³⁴ In this case, a single-layer graphene is not produced but rather a multilayer (3–10 sheets) material. The removal of the porous support may leave a three-dimensional interconnected graphene network that could be used as catalyst support or as catalyst. This material shows interesting characteristics, but may be better described as a carbon or graphite film (the authors describe it as a three-dimensional interconnected graphene macrostructure or graphene foam, e.g., a porous graphene bulk material that consists of an interconnected network of graphene) rather than pristine graphene.

The chemical production of graphene has been widely explored in the last few years, mainly as a cheap and alternative method for graphene synthesis on a large scale.¹³⁵ This method is based on the so-called Hummers method developed already in 1958 to prepare graphite oxide (GO) by treating graphite in a mixture of sulfuric acid (H_2SO_4), sodium nitrate ($NaNO_3$), and potassium permanganate ($KMnO_4$).¹³⁶ Chemical reduction of these flakes would yield a suspension of graphene flakes, as demonstrated by Boehm et al. in 1962.¹³⁷ This method has recently attracted substantial interest for the manufacture of graphene.¹³⁸ However, the graphene obtained by this route still has many chemical and structural defects. It is misleading to refer to such materials as graphene.¹²⁰ Nevertheless, these materials show interesting catalytic behavior, as described later.

Remarkably, the synthetic procedures used to prepare rGO (reduced graphene oxide)^{139,140} is still similar to that used by Boehm et al.¹³⁷ A modification to the original procedures is that a sonication period is now typically included to exfoliate the oxidized graphite layers into isolated, single sheets dispersed in the aqueous or polar organic media. The resulting dispersions are stable in water at concentrations up to 3–4 mg·mL⁻¹,¹⁴¹ due to the strong polarity of the oxide functional groups present on the surface of rGO. This material is thus potentially usable in catalytic reactions in water, but separation is a major issue in industrial reactors.

A promising method is also to unzip CNTs to graphene nanoribbons either using strong oxidants or catalytic nanoparticles,^{142–146} but the method produces typically few-layer graphene sheets. These nanocarbon materials can be good for catalytic applications or electrodes. It is possible to extend these methods also using a range of novel nanoengineering possibilities, such as using encapsulated Co particle to achieve a precise cutting, repairing, and interconnecting of the nanoribbons.¹⁴⁴ Depending on the cutting angle, graphene

nanoribbons show different chirality, which determines a change in the energy gaps, and the presence of one-dimensional edge states with unusual magnetic structure.¹⁴⁷ Under electron irradiation (or by other mechanisms) it is possible to generate carbon vacancies leading to the formation of extended defect domains (with the presence of pentagonal and heptagonal and even four-membered carbon rings) that often show semiconductor character. This is the mechanism of formation of semiconductor properties in quantum-dot carbon nanoparticles or graphene nanoribbons, which plays an important role in determining their use in the design of advanced photocatalytic materials.

The graphene nanoribbons may thus show different properties depending on the width, length, chirality, and substrate, e.g., on the specific preparation methodology. This opens interesting perspectives for supporting metal nanoparticles on them,^{148–152} because it allows one to change the interaction between the metal nanoparticles and the carbon substrate (thus the intrinsic reactivity of the metal nanoparticles), without a change in composition. A novel, highly challenging area of catalysis is related to the use of subnanometer supported metal clusters and alloys,¹⁵³ because below around 1 nm metal particles have unusual catalytic reactivity. A main challenge is the stabilization of these very small particles and the control of their interaction with the substrate. Magnetic nanocenters in graphene nanoribbons or other nanocarbons as well as controlled defects are between the novel possibilities to stabilize these so small nanoparticles. This is an area of development still at an early stage^{14,21,154,155} but highly promising also to develop advanced solar devices such as artificial leaves.³²

2.3. Ordered Mesoporous Carbon

OMC (with pore size ranging from 2 to 50 nm) can be prepared by hard and soft templating synthetic methods.^{15,16,20,156–159} The hard templating method, typically using OMS (ordered mesoporous silica) as template, has advantages in terms of reliability in producing the OMC (the structure is an exact replica of the template material), but the procedure is complicated, time-consuming, and unsuitable for the mass production. Several steps are required to fabricate the structure matrices and then remove the siliceous template matrices under harsh chemical treatment conditions. Highly ordered mesoporous carbon (for instance, CMK-1) with a pore size of 3 nm was obtained by employing the aluminum silicate MCM-48 as a hard template.¹⁶⁰ OMC demonstrated a significant potential in various catalytic and environmental applications,¹⁶¹ for instance, showing a good performance as catalyst for ODH of ethylbenzene to styrene.¹⁶⁰

The soft templating method uses phenolic resin and block copolymer PEO–PPO–PEO to prepare highly ordered mesoporous carbon via organic–organic assembly of block copolymers and phenolic resins.^{162,163} Liang et al.¹⁶³ reported the self-assembly synthesis of highly ordered mesostructures based on a commercially available triblock copolymer (Pluronic F127) as a template and a mixture of phloroglucinol and formaldehyde as an inexpensive carbon precursor. Highly ordered mesoporous carbon with monolith, fibree, and film morphologies can be obtained after curing of polymer, removal of template, and carbonization. With this method, the large-scale synthesis of OMC materials is potentially viable.^{164,165} Kilogram-scale synthesis of OMC has been reported.¹⁶⁶ Unfortunately, OMC obtained in this way typically do not

offer any macropore character (pore size >50 nm). By combining hard- and soft-templating methods, hierarchically ordered porous carbon with designed porosity on multiple length scales can be obtained.¹⁶⁷

2.4. Carbon Hierarchy

Carbon hierarchy, sometimes defined as carbon nanoarchitecture, is a combination of at least two nanocarbon (graphene, carbon nanotubes or nanofibers, nanodiamond, nanoporous carbons or polymers) building blocks, to induce superior properties with respect to those of the individual elements.¹ It is also often used to indicate hierarchically organized carbon materials having a bimodal pore distribution deriving from the combination of the microporous characteristics of nanoscale carbon elements with the mesoporous characteristics deriving from the arrangement of these building blocks.⁷⁰ An example is the previous cited hierarchically ordered porous carbon with designed porosity on multiple length scales deriving from using in sequence hard- and soft-template methods.^{168,169} Recently, Zhang et al.¹⁷⁰ reported the spherical multiwalled carbon nanotube architectures obtained by exchange of resin with iron, followed by a high-temperature graphitization process with the formation of CNTs from solid-phase carbon. The general objective of carbon hierarchy is to overcome mass transport limitations in catalysts (or other applications like advanced electrodes, for example), combining high surface area with good accessibility. Figure 3 reports a schematic illustration of some hierarchical carbon structures.

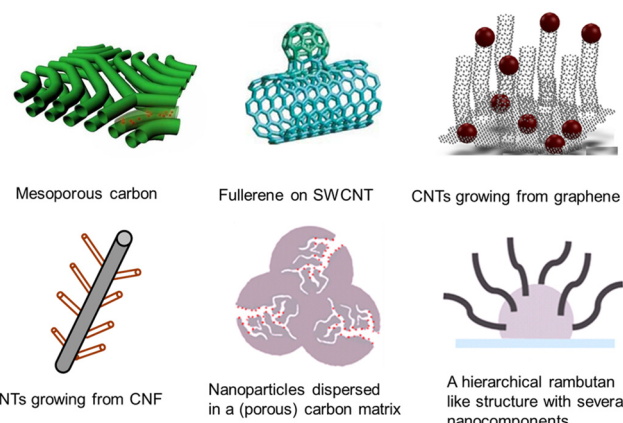


Figure 3. Schematic illustration of some hierarchical carbon structures.

Less investigated, but rather important, is the possibility to combine different specific properties, such as those of carbon nanotubes and nanowires. On the molecular level it is potentially useful to grow dendritic structures of CNTs/CNFs onto each other¹⁷¹ to maximize the surface area exposed and to provide molecular roughness for entanglement of, for instance, polymer strands. A hierarchical organization of the nanocarbon units on itself to form small objects¹⁷² and on a robust carrier structure in larger dimensions is highly desirable, for instance, to immobilize CNTs on carbon macrofibers.^{173–176} This kind of carbon hierarchy shows satisfying performance as catalyst for the ODH of ethylbenzene to styrene.^{173,175} Carbon nanofiber–nanotube hierarchy could be prepared by replacing metal particles inside CNTs (acting as a container) followed by the CVD process.¹⁷⁷ With this approach it is possible to grow CNFs inside large CNTs, developing thus a further level of hierarchy. AC can be used as carrier to

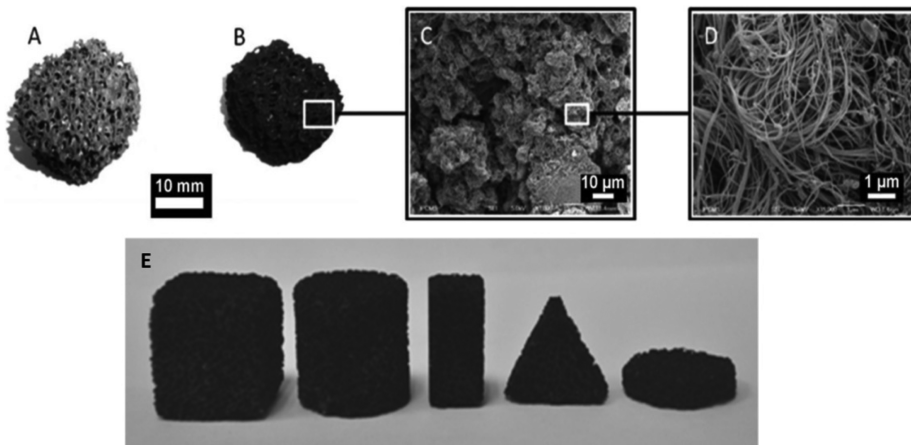


Figure 4. (A, B) Photographs of the SiC foam and N-CNT/SiC foam composite, which show the high accessibility of the macroscopic structure. (C, D) SEM images of the N-CNT/SiC composite, which show the detailed microstructure of the N-CNTs on the surface of the SiC support and the average diameter of the N-CNTs. Reprinted with permission from ref 182. Copyright 2012 Wiley-VCH Verlag. (E) Photograph of CNTs/SiC foam catalyst in various macroscopic forms.

immobilize CNTs/CNFs on its surface and inside its macropores.^{178–180} The obtained carbon hierarchy shows improved behavior in the adsorption of noncondensable chromate in basic solution and condensable heteropolyimido-bdate in solution, but it is unsatisfactory for catalytic purposes, since the micropores of AC can lead to polymerization of reactants and thus carbon deposition.¹⁸¹ In electrocatalysis and in energy storage devices,^{9,21} a single component could not meet the high demanding of, for instance, the batteries or supercapacitors to have either high power or high energy density, respectively.

A large range of possible nanoarchitectures is thus possible. However, the process of synthesis or production of carbon hierarchy on an industrial scale is underdeveloped. In addition, a general problem, not well investigated, is the presence of several interfaces, which may give discontinuities in transport and in chemical properties and possible deterioration of the overall properties and chemical stability.¹⁷⁸

The number of examples on the synthesis of interesting carbon hierarchic structures is increasing, but without a corresponding significant progress in terms of using these carbon materials to develop improved catalytic or functional materials. Without more precise indications on the interface problem, as well as the nanolevel characterization of the materials produced (defect, interfaces, etc.), it is not possible to put on a rational basis the progress in this field. The consequence is an increased number of contrasting results. The bottleneck of the development in the field is thus related to the possibility of detailed characterization at the nanoscale of the interfaces between the nanocarbon elements, because this is the critical element determining many relevant aspects, such as conductivity (electrical, heat) and chemical stability. This is the area on which the future research should be focused to have real progress in using these materials.

2.5. Macroscopic Shaping of Nanocarbon

A further constraint for the use of nanocarbons as catalysts in industrial reactors, in addition to the availability in large amounts with well-defined surface-chemical and mechanical properties, is that they should be formed into larger objects with suitable characteristics to allow good resistance to compressibility (for fixed-bed reactor operations; hardness is instead the requirement for fluid-bed reactor operations), with

the size and shape dictated by the use in the reactor (to minimize pressure drop in fixed bed, allows good fluidizability in fluid bed, etc.), and with the porosity necessary to allow effective contact with reacting matrices at the typical high space velocities used in industrial reactors.

Pham-Huu and co-workers¹⁸² has developed a macroscopic composite-catalyst that consists of a highly entangled N-CNT network supported on an SiC foam with a fully accessible macroscopic structure. Representative photographs and SEM images of the composite catalyst are presented in Figure 4A–D. The supported N-CNTs were well-anchored on the surface of the host structure, so no mass loss was observed after air flushing at high space velocity. Su and Yan¹⁸³ have shown that CNTs with a loading of 0.5–4 wt % could be grown on SiC foam with various forms, as shown in Figure 4E. These CNTs/SiC catalysts have been successfully tested for the ODH of 1-butene to butadiene.¹⁸³ However, for higher loadings in CNTs, it becomes difficult to control the rate of growing and to avoid blocking some parts of the foams.

For large foams, as would be required for industrial-size reactors, it could be difficult to control the uniform growing of the CNTs in the whole SiC foam and to avoid having some preferential paths of gas flow in the foam. An optimization in the synthesis procedures can reasonably minimize these issues, but still the analysis of the optimal design of CNT/SiC foams or monoliths in terms of the fluidodynamics of gas–solid contact (a key question for the development of industrial catalysts) would require more specific studies. The interface between the SiC and CNTs also appears to be critical in terms of reduced effectiveness in the heat transfer. The main advantage of SiC is its high heat transport coefficient, but in the composite during the catalytic reaction, the effectiveness depends on the heat transfer between the CNT (where the heat of reaction is generated) and the SiC (which is the massive element for radial and axial heat transport in the reactor bed). When there are minimal hot-spot temperature profiles (axial and radial) in fixed bed reactor operations, with the heat transfer capacity being better than the heat release (this depends on the rate and heat of reaction, as well as the reactor characteristics), the use of SiC is not critical, as observed for ODH reaction even in industrial reactors. However, there are other examples in which maintaining a more uniform

temperature profile due to the better heat conductivity of SiC is very relevant to keep high selectivity and/or limit deactivation. In these cases, it is necessary to investigate the thermal profile in CNT/SiC foams or monoliths and to optimize the preparation in relation to this aspect, but this is an area scarcely investigated. Current advances in CFD (computational fluid dynamics) of porous media¹⁸⁴ should be integrated into design of CNT/SiC foams or monoliths to optimize the performances.

There is an increasing number of recent studies on CNT/SiC^{185–187} and on CNT/carbon felt,^{173,188} but none of them has investigated the engineering aspects (fluidynamics, heat transport, and dissipation, etc.) of the development of these materials. In addition, a critical factor in heat transport, as discussed also later, is the interface between CNT and SiC or carbon felt. Nanoengineering of the interfaces between CNTs and between the CNTs and a (conductive) support is a critical factor for effective long-range heat transport and dissipation.¹⁸⁹ The aspects that have to be considered include the concept to select CNTs with similar structure or interfacial materials with a similar phonon spectrum. Furthermore, the performance can be improved by increasing the overlap length between CNTs and/or CNT/conductive support and specifically optimizing the nature of the interphase (often, there is amorphous carbon at the base where the CNT grows). By putting the right attention to these aspects, the interfacial thermal conductivity of the CNT interfaces can be significantly improved.¹⁸⁹ Various studies in this specific area are present for CNT–polymer nanocomposites,¹⁹⁰ but there is a lack of investigations in relation to materials for catalytic applications.

The above-mentioned nanocarbon composites are typically prepared by growing CNTs in a CVD process on supports with macroscopic form. Another way to macroscopically shape CNTs is the gelation process.¹⁹¹ Preformed CNTs are used in this process. The synthesis method is based on the coagulation process using alginate as a gelling agent, followed by a thermal step to make entangled CNTs with homogeneous size and shape. The macroscopic shape of the composite can be finely tuned, i.e., beads, extrudates, or plates, depending on the downstream application. The formed CNT beads consist of highly entangled CNTs forming a dense network exhibiting a rather high specific surface ($>180 \text{ m}^2 \cdot \text{g}^{-1}$) and also full porous network accessibility. In view of the CNTs commercially available in bulk and with a reasonable price, this method seems simpler and more practical, but also here, the above-mentioned engineering aspects, especially the mechanical strength of the shaped CNTs, need further investigation.

3. FUNCTIONALIZATION OF NANOCARBON MATERIALS

Functionalization of nanocarbons is one of the important treatments for their applications either as sorbent, catalyst, or catalyst support. Chemical modification of CNTs^{30,77,192} and graphenes^{193,194} remains an important research area in nanocarbon science. According to the interaction of functional groups with nanocarbon, the methodologies of functionalization could be categorized as covalent attachment of chemical groups, through reactions on the conjugated sp^2 carbons skeleton, and the noncovalent supramolecular adsorption (wrapping) of various functional molecules on the nanocarbon. Noncovalent functionalization involves mostly decoration of nanocarbons with (large and in many cases organic) molecules. Noncovalent functionalizations did not disturb the character-

istic π electron system and was widely used in the preparation of both aqueous and organic solutions to obtain highly stable suspensions of individually dispersed nanotubes or graphenes. For catalytic purpose, the covalent oxidation and amination of nanocarbons are the most important and well-studied methods to introduce O- or N-containing groups on the surface.^{195–197} However, the stability of these functional sites during the catalytic reactions have to be verified.

3.1. Liquid-Phase Functionalization of Nanocarbon

Liquid-phase oxidation of CNTs involves mainly acidic etching by hot nitric acid or sulfuric/nitric acid mixtures. This is a simple and well-established method to purify and functionalize simultaneously nanocarbons. The functionalization is not selective, and various O-containing groups could be anchored on the defect sites of sidewall and open caps of CNTs or on the defect sites and edges of graphene, respectively. Hydrogen peroxide has also been used as oxidant for the functionalization.¹⁹⁸ Sonochemical-assisted oxidation of CNT in sulfuric/nitric acid mixture could promote acidic etching and increase the population density of surface oxide groups. With this method, Xing et al.¹⁹⁹ found that some carbonyl groups were formed along with carboxy groups, with the latter being the dominant species. Depending on the time of sonochemical treatment, structural damage to the CNT surface could occur that affected the electronic properties. It was also reported that mild sonication of CNTs in nitric acid followed by subsequent treatment with hydrogen peroxide is a more efficient method for the oxidation of CNTs without damaging the skeleton.²⁰⁰ Liquid-phase purification and functionalization cause the loss of SWCNT metallic character²⁰¹ and change the physicochemical properties of MWCNTs, although the nature of the changes depends significantly on the specific characteristics of the MWCNTs.²⁰²

3.2. Gas-Phase Functionalization of Nanocarbon

Liquid-phase functionalization of nanocarbon is easy but requires filtration, washing, and drying steps. The first studied gas-phase functionalization techniques involved gas-phase oxidation in ozone,²⁰³ carbon dioxide,²⁰⁴ hydrogen peroxide,¹⁹⁸ and oxidative plasmas.²⁰⁵ Recently, a more effective route has been developed for the oxygen functionalization of CNTs in gas phase by means of nitric acid vapors.²⁰⁶ The setup is shown in Figure 5a. CNTs were loaded to the reactor and heated to temperatures between 125 and 250 °C. Concentrated HNO_3 was added to the round-bottom flask and heated under magnetic stirring to 125 °C. The condenser was connected with an open-end exhaust line to air. The design of the setup effectively prevents the reflux of liquid HNO_3 collected by the condenser to the CNT sample. The treatment was fully under gas-phase conditions, and the wetting of CNTs with liquid HNO_3 could be completely avoided. This method is especially suitable for the functionalization of macroscopically shaped CNT catalyst.

Differing from other gas-phase oxidation, this method allows a selective functionalization, but strongly depending on the treatment temperature. A high concentration of carboxyl groups could be obtained at high temperature. The O 1s core level XPS spectra (Figure 5b) show the presence of two major contributions (indicated by the dashed lines) that were assigned to oxygen doubly bound to carbon (i.e., $\text{O}=\text{C}$) in quinones, ketones, and aldehydes at 531.6 eV and oxygen singly bound to carbon (i.e., $\text{O}-\text{C}$) in ethers, hydroxyls, and phenols at 533.2 eV, according to Okpalugo et al.²⁰⁷ Since oxygen

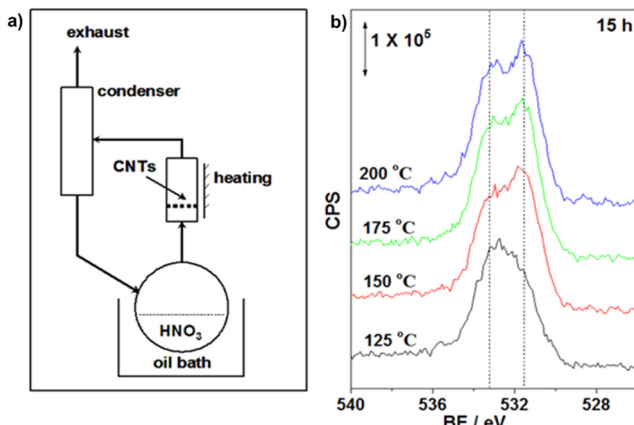


Figure 5. (a) Illustration of the setup used for gas-phase functionalization of CNTs with HNO₃ vapor. (b) XPS spectra of CNTs treated by HNO₃ vapor at different temperatures for 15 h. Reprinted with permission from ref 206. Copyright 2009 Elsevier.

atoms in esters, carboxyls, anhydrides, and pyrones have both single bonds and double bonds with carbon, the oxygen atoms in these groups contribute to both O 1s peaks. It can be seen from the O 1s spectra that the main peak is dominated by O–C at lower treatment temperatures, presumably due to preferred formation of hydroxyls at low temperatures. The contribution of OC increases strongly at higher temperatures. A quantitative analysis of the different oxygen species based on the deconvolution of the O 1s peaks²⁰⁸ confirmed that the decomposition of the carboxylic groups occurs in the lower temperatures range, whereas the phenol, ether, and carbonyl groups are more stable and decompose at higher temperatures. As compared to the conventional treatment with liquid HNO₃, the HNO₃ vapor treatment not only enhances the total amount

but also changes the areal density of different oxygen-containing functional groups on CNTs.

After the HNO₃ vapor treatment, the CNTs can be collected directly without any additional process such as filtration, washing, and drying. This method is especially important to introduce oxygen functional groups on metal-loaded nanocarbons. Bitter and co-workers²⁰⁹ showed that amounts of acidic oxygen groups as high as 0.3 mmol/g can be introduced on Pd-loaded CNFs, an amount that is comparable to that introduced by liquid-phase treatment in 65% HNO₃ on bare CNFs.

4. CHARACTERIZATION AND MODELING

Although significant advances have been made in the past decade in this field and a broad portfolio of techniques for the characterization of nanocarbon materials is available today, there are still contrasting literature results due to the poor characterization of the used materials. For this reason, and taking into consideration of the intrinsic difficulties in studying these materials, it may be useful to apply well-defined systems for catalysis and to adopt a standard characterization protocol for nanocarbon.²¹⁰ It is also useful for the same reason to summarize briefly some of the recent progresses in this field.

4.1. Characterization of Carbon

There is a broad portfolio of techniques for the characterization of nanocarbon materials. Scanning electron microscopy remains the most routine and standard technique to get a general impression of the carbon materials. TEM, electron and X-ray diffraction, and Raman spectroscopy are standard tools for the microstructural characterization of carbon materials. X-ray photoemission spectroscopy, infrared spectroscopy, and temperature-programmed desorption techniques are the first choice to study the surface functionality and adsorption properties of carbon materials. Surface area and pore distribution of nanocarbons can be determined by nitrogen adsorption

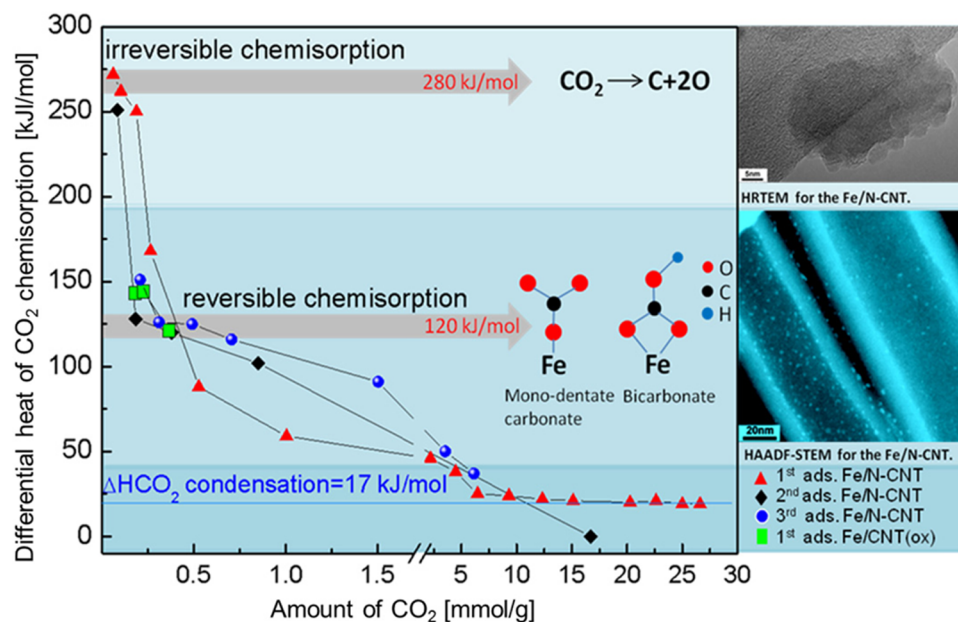


Figure 6. Differential heat of adsorption as a function of CO₂ uptake for an iron catalyst supported on N-functionalized CNT (Fe/C–CNT): first run of adsorption (triangle); second run of adsorption (rhombus); third run of adsorption (cycle). The line indicates the order of the measured points. For comparison, the data of the first run (square) of iron catalyst supported on oxidized CNTs (Fe/CNT(ox)) is given. Adapted from ref 215.

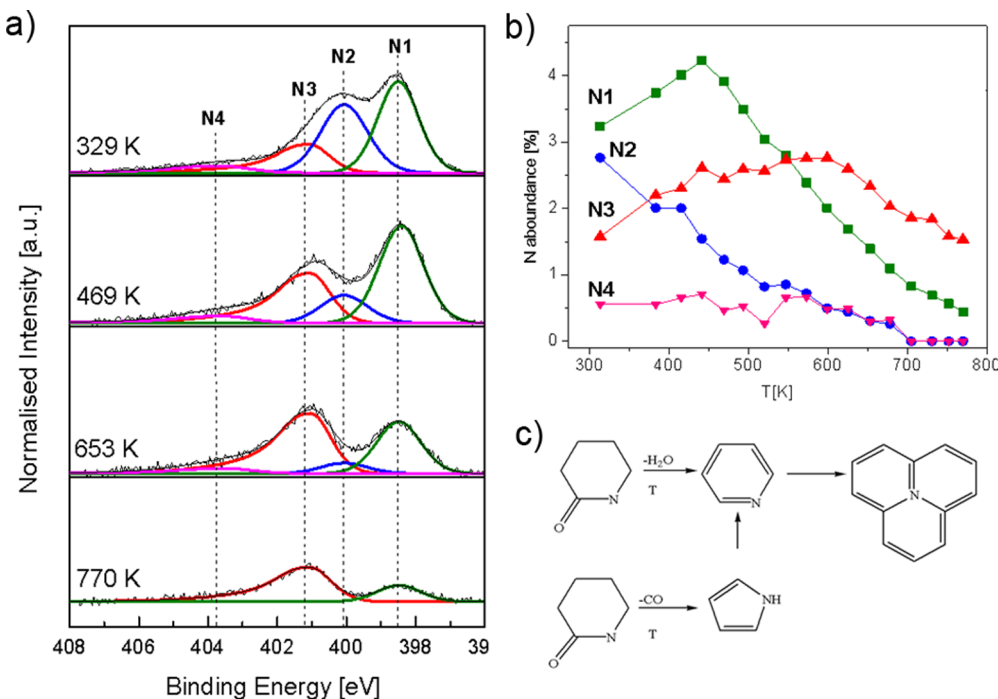


Figure 7. (a) TP-XPS and the deconvoluted N1s core level spectra for sample N-CNT 873K during in situ heating: N1, pyridinic groups; N2, pyrrolic-like groups; N3, quaternary nitrogen; N4, pyridine oxide. (b) Evolution of different N-species during TP-XPS for N-CNT 873K: N1 (green curve); N2 (blue curve); N3 (red curve); N4 (pink curve). (c) Nitrogen insertion pathway in CNT. Elaborated from refs 222, 223.

experiments (BET analysis).²¹¹ HRTEM is the only technique to provide an image of a catalyst at an atomic resolution.^{212,213}

In addition to all these routine characterization methods mentioned above, in-depth characterization of nanocarbon is needed for an understanding of the interaction of molecules with the carbon surface, the dynamics of surface structure and functionality at high temperature, and the spatial distribution of supported catalysts. There are some special techniques available for these purposes, and some representative ones are discussed below.

4.1.1. Microcalorimetry. Catalysis involves specific chemical interactions between the surface of catalyst and the reacting gas molecules. The catalytic cycle is generally composed of adsorption steps, surface reaction processes, and desorption steps. The energetics of these surface chemical events plays an important role in the determination of the catalytic properties of the surface. Adsorption microcalorimetry is a direct method to determine the number, strength, and energy distribution of adsorption sites on a catalyst. It allows for measuring the differential heats evolved when known amounts of gas probe molecules are adsorbed on the catalyst surface.²¹⁴ The released heat is related to the energy of the bonds formed between the adsorbed species and the adsorbent and hence to the nature of the chemical reactivity of the surface. Figure 6 shows the differential heat of adsorption as a function of CO₂ uptake measured on iron nanoparticles on N-functionalized CNTs.²¹⁵ This catalyst is electrocatalytically more active in CO₂ conversion to fuels (these electrocatalysts able to reduce selectively CO₂ to 2-propanol, a very challenging reaction)^{216–219} than iron catalysts supported on oxidized CNTs. The microcalorimetry experiment reveals that there are two types of chemisorption sites on the catalyst: irreversible sites (280 kJ/mol) at the uncoordinated sites of the facets (top HRTEM image of Figure 6) and reversible sites (120 kJ/mol)

at the hydrated oxide surface of the small nanoparticles (bottom STEM image of Figure 6).

An often used simplification is that carbon, differently from other supports such as oxides, is inert. It is assumed that carbon (as the support for other catalytic elements, such as metal nanoparticles) does not participate as cocatalyst nor induce significant modifications in the nature of the supported active particles. Data presented in Figure 6 show that the reversible sites (120 kJ/mol) are correlated to the enhancement of the catalytic performance. These specific reversible sites are suggested to be present at the interface between the catalyst nanoparticles and the carbon support, in order to explain the dependence of the activity on the defective nature of the CNT and the relation with the perimetral area of metal nanoparticles with the performances. The N-doping is important in creating these sites, explaining the superior activity of N-doped CNTs with respect to oxidized CNTs.

The calorimetry can also be used to study the interaction of organic chemicals with the surface of carbon materials. In a recent study, Guerrero-Ruiz and co-workers²²⁰ investigated the interaction of probe organic molecules with CNTs surface of various diameters through the determination of immersion enthalpies by calorimetry. They found that the curvature of CNTs enhances the adsorption of aromatic compounds in comparison with the graphite surface: the adsorption strength of aromatic compounds on CNTs is higher compared to that on the flat graphite. For instance, CNTs adsorb toluene more strongly than graphite. The number of oxygen groups on CNTs modifies the electron density of their surface and thus the interaction mechanism with the adsorbates.²²⁰

It is necessary, however, to make a next step and use adsorption microcalorimetry to characterize the surface chemical properties of nanocarbons under conditions close to catalytic reaction. This is a challenging but possible task. One example is the quantification of the different adsorption sites

and their correlation to the catalytic activity of CNT catalysts in the ODH of propane.²²¹ Frank et al.²²¹ showed that the adsorption of hydrocarbons on carbon surfaces favorably occurs on oxygenated sites, providing experimental evidence for the interpretation of differences in the catalytic activity of various CNTs in the ODH of propane.

The key to the effective utilization of adsorptive microcalorimetry in heterogeneous catalysis is the judicious choice of gas-phase molecules for study. Reactants and products of the catalytic reaction can be employed when adsorption of these gases leads to well-defined adsorption species. The data obtained are of substantial value for comparing theoretical and experimental hypotheses about reaction pathways.

4.1.2. Temperature-Programmed and Ambient Pressure Photoelectron Spectroscopy. Chemical functionalization is a fundamental step in the view of exploring the properties of nanocarbons as catalyst or as catalyst support. In addition to understand how to create and control the surface sites present in nanocarbons (particularly, the nature of O- and N-containing functional groups), it is also necessary to understand their stability and thermal transformation and the dynamics of their transformation during catalytic reactions. Nitrogen-functionalized carbons have been explored as catalyst or as catalyst support. The stability and transformation of various N-containing functional groups at high temperature are thus of importance for gas-phase catalytic reactions typically occurring at high temperature, but they need a combination of many advanced characterization techniques to obtain reliable conclusions.

Arrigo et al.^{222,223} investigated the dynamic nature of nitrogen functional groups on CNTs by means of TP-XPS and TPD-MS. By relating mass signals and binding energy to certain specific functional groups, the dynamic surface rearrangement and the thermal stability of postfunctionalized CNTs were revealed (Figure 7). The decomposition of the functional group competes with the conversion to another functional group. It was found that functional groups with a binding energy at 400.3 eV (mostly pyrrole-like groups) partly decompose through formation of HCN and partly convert into pyridine groups. Above 450 K, the pyridine is transformed into the so-called “quaternary nitrogen” or decomposes, giving rise to further formation of HCN. The quaternary nitrogen is the most thermally stable N species in carbon materials.

Synchrotron-based APPES^{224,225} has been shown to be a unique tool to study the dramatic changes of liquid and solid surfaces in the presence of gases and vapors,^{226–228} as encountered in industrial catalysis and atmospheric environments. It has been used to monitoring the redox behaviors of quinic groups on carbon surface during the oxidative dehydrogenation of *n*-butane,²²⁹ the interaction of Ni nanoparticles with carbon support,²³⁰ and the reaction mechanism of nanosized PdGa intermetallic compounds on CNTs in selective hydrogenation reaction.²³¹

4.1.3. Advanced Electron Microscopy. Although TEM remains the most important tool to “see” the size and morphology of a catalyst, TEM provides only a projected two-dimensional image so that the information along the electron beam is lost. With the help of electron diffraction, image simulation, and crystallographic analysis, facets and the shape of the nanocatalyst may be retrieved.^{211,213} Electron tomography is nowadays an indispensable tool for the local three-dimensional characterization of supported catalysts and zeolite.^{232–234} This technique is especially important for

localizing the metal nanoparticles when CNTs or porous materials are used as support. The exact locations of nanoparticles must be known, if, for instance, the confinement effect of nanoparticles inside CNTs should be investigated. Electron tomography is obtained by taking multiple images of a single sample tilted through a series of angles. A set of images (known as a “tilt series”) can be collected. In the same way as in established X-ray tomography,^{235,236} the information from the tilt series of two-dimensional projections is analyzed to yield a detailed three-dimensional construction of the structure.²³⁷

Figure 8a shows a typical 2D image of a CNT with supported Ni nanoparticles. From such a 2D projected bright-field image,

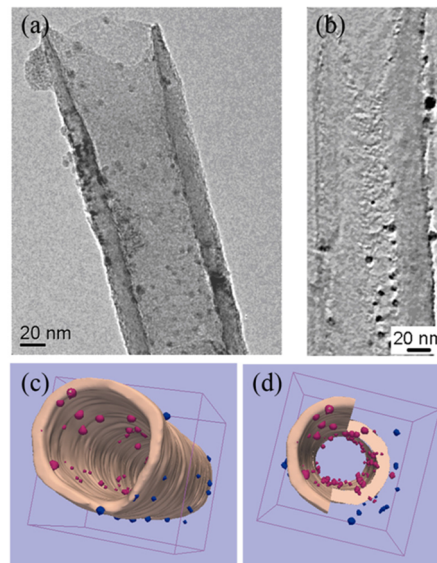


Figure 8. (a) Typical 2D-TEM image of a CNT with Ni nanoparticles, used to reconstruct the 3D image; (b) longitudinal section through the reconstructed volume; and (c and d) modeling of the reconstructed volume (pink, carbon nanotube; red, Ni particles inside the tube; blue, Ni particles on the external surface). Reprinted from ref 238. Copyright 2009 American Chemical Society

it is not possible to determine the exact location of the Ni nanoparticles. The very small size of Ni nanoparticles gives a very weak mass–thickness contrast between Ni and carbon. In the sections through the reconstructed volume (a longitudinal section is presented in Figure 8b), the individual analysis of their size is facilitated by the increase of the signal-to-noise ratio due to the redundancy of information coming from several images. Using the 3D positions of these particles with respect to the inner and outer surfaces of the tube obtained by modeling, the Ni nanoparticles inside or outside CNTs can be clearly distinguished (Figure 8c,d): 75% of the Ni particles are found located inside the tube.²³⁸

It should be commented that the specific CNT used by Tessonniere et al.²³⁸ is a commercial sample supplied by Pyrograf Products, Inc. Pristine MWCNTs have both ends opened and present lengths up to several micrometers. Statistical analysis reveals that they exhibit an outer diameter of 90 ± 30 nm with wall thickness ranging between 5 and 20 nm. The large inner diameter, which is larger than the typical one for CNTs, facilitates the filling of the CNTs with either organic or aqueous solutions. For this reason, these samples show a predominant localization of Ni particles inside the CNT, but this is not necessarily true for other types of CNTs

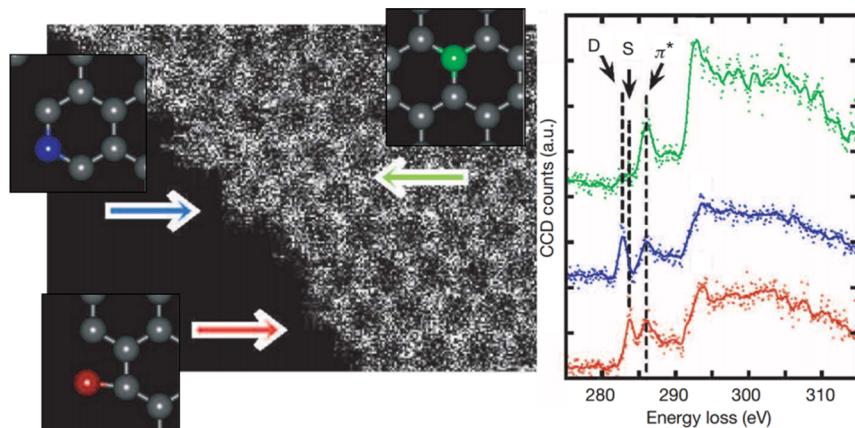


Figure 9. Graphene edge spectroscopy. Left: ADF image of a single graphene layer at the edge region with the colored arrows indicating different atomic positions for carbon illustrated in the related insets. Right: carbon K-edge (1s) fine structure spectra extracted using sequential EELS spectroscopy. The color of the spectra (green, blue, and red) corresponds to the normal sp^2 carbon atom, a double-coordinated atom, and a single-coordinated atom, respectively. Adapted from ref 247.

with smaller diameter. However, de Jong and co-workers²³⁹ studying by electron tomography the deposition of Ru particles on two types of commercial CNTs (from Chengdu Organic Chemicals) with inner and outer diameters of 5/15 and 8/20 nm, respectively, showed that the amount of Ru particles inside was 91 and 66%, respectively. In addition, the average particle–particle distance inside/outside CNTs were 10.7/38.4 nm and 7.1/7.3 nm, respectively. Therefore, even for apparently similar CNTs to which the metal was added with the same procedure (ultrasound-assisted wet impregnation), different inner/outer distributions could be observed.

Electron tomography of CNTs also revealed that the structure of CNTs is more complex than the commonly assumed cylinder model. If electron tomography is not available, a single tiling of the specimen could provide a clue to distinguish the particles on the interior and exterior surfaces of CNTs.^{238,240}

There is a tendency to use STEM in HADDF (high angle annular dark field) mode instead of TEM in bright/dark field mode to study metal particles supported on carbon.^{241–243} This is due to the fact that image contrast in HADDF mode is proportional to atomic number Z (Z-contrast) and the metal particles usually have much higher atomic number than carbon. The integration of STEM mode and HADDF detector in a modern TEM makes the use of HADDF–STEM images nearly routine.

The recently developed aberration-corrected (S)TEM has an improved resolution down to subangstrom and eliminates the Fresnel diffraction at the perimeter of a specimen, allowing sharp imaging of the surface structure of a catalyst.^{244,245} In general, carbon materials could suffer electron beam radiation damage when a TEM is operated at high voltage and at high electron dose. This damage is drastically minimized or even reduced to a minimum level at a voltage lower than 80 kV. Low-voltage electron microscopy, equipped with aberration correctors to compensate the loss of resolution, provides a new possibility to study the point defects and doping of carbon materials.²⁴⁶ Both are of essential importance for understanding how to use nanocarbon as catalyst and catalyst support and for understanding the nature of defect and perimetral sites, which play a key role on the catalytic properties of nanocarbon materials, as will be discussed later. For example, Suenaga and Koshino²⁴⁷ have studied graphene by low-voltage STEM, in

annular dark field configuration (ADF) and energy-loss near-edge fine structure (ELNES) for single-atom spectroscopy, in order to determine the exact local electronic structure of graphene edges (Figure 9). This is a first step for the correlation with their reactivity.

Other advanced developments in electron microscopy methods, for instance, environmental TEM for in situ probing of catalysis at the atomic level,^{248–250} energy filtered imaging and element mapping for elucidating the structure and chemistry of catalysts,²⁵¹ and electron holography for studying the charge transfer between nanoparticle and support,²⁵² are transforming heterogeneous catalysis research and have become indispensable tools for a fundamental understanding of catalytic phenomena, mechanism, principles, and design of sustainable catalyst. Further aspects are discussed in an introductory paper to a special issue dedicated to “advanced electron microscopy for catalysis” (see ref 253 and the references therein). With all these new and very helpful developments in mind, it should be remarked that TEM is not an integral technique. Care must be given to analyze enough individual particles to obtain statistically relevant data not only valid for a few specific nanoparticles analyzed.

4.2. Theoretical Modeling

Parallel with the increased research interests in carbon as catalyst and catalyst support is the increase of theoretical modeling and simulation of the reactivity of nanocarbons. A driving force for the theoretical computational studies may be also the enormous interest in the chemical properties of graphene, especially those on the edges of a graphene sheet, as an emerging star in nanocarbon materials.^{254,255} However, molecular-level engineering of carbon-based catalysis cannot be successful until and unless the issues such as (re)active sites, doping effects, activation of reactant molecules on carbon, and microreaction kinetics are clarified by first-principle computational simulations.²⁵⁶

Graphene and also SWCNTs provide the simplest platform to investigate theoretically their chemical reactivity and their interaction as well as reactivity with small molecules. Reactions of H_2S with quinones and a model carbonic cluster, mimicking an active center on the surface of active carbon, have been theoretically modeled.²⁵⁷ Pathways and rate constants for reactions of CO and CO_2 with vacancy defects on graphite

(0001) surfaces can be predicated by quantum chemistry calculations.²⁵⁸ The catalytic ability of the metal-free N-CNT was investigated by Hu et al.,²⁵⁹ who found that N-functionalized CNT alone (no metal particles, even in traces) is able to activate the C–H in methane, a very challenging reaction. The reactivity of N-functionalized CNT is comparable to that reported for noble metal catalysts. The energy diagram for methane to methanol oxidation and the optimized transition state on N-doped CNT are shown in Figure 10.²⁵⁹

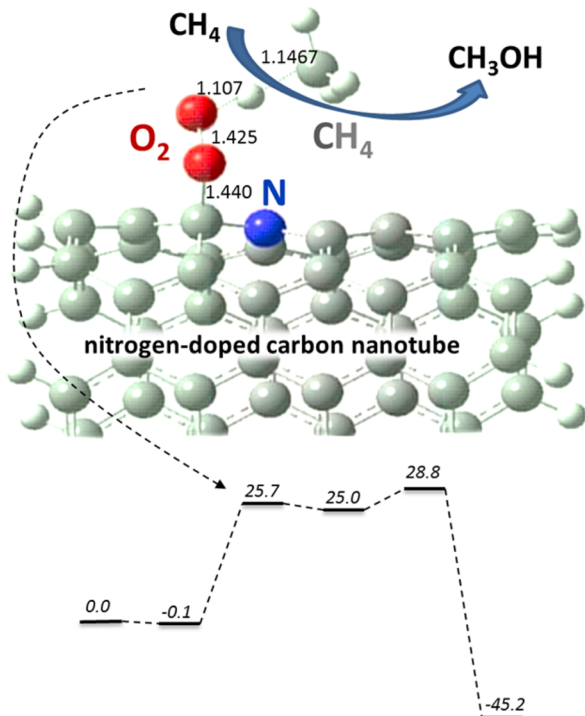


Figure 10. The energy diagram for methane oxidation to methanol on metal-free N-doped CNT [armchair N-CNT (4,4)-8.0, where (N,N) represents the nanotube type and 8.0 is the length in angstroms of the nanotube] and the optimized transition state for methane activation on N-doped CNT. Adapted from ref 259.

O₂ chemisorbs side-on on a carbon atom close to a nitrogen site in N-doped CNT. The presence of near-lying N is necessary, because it induces an electron transfer to oxygen, which thus interacts with CH₄ through a weak O···H–CH₃ bond. The energy for this transition state is about 26 kcal/mol, thus relatively low for the activation of methane. Following the hydrogen transfer process, the OH group rebounds via another transition state having a low barrier height (about 4 kcal/mol) and it will produce the final product CH₃OH. Although the mechanism was only proven by theoretical calculations, it shows a novel possible reaction mechanism and active sites for this challenging reaction of direct conversion of methane to methanol.

Oxygen adsorption and dissociation on graphene and nanotubes are crucial to study the oxidation of the nanocarbon and to understand the overall process of the oxygen reduction reaction as well of selective oxidation, as discussed above. This aspect was investigated theoretically by several groups.^{260–263} Shan and Cho²⁶¹ showed that oxygen molecule dissociation is facilitated on carbon atoms neighboring a nitrogen dopant, with the dissociation barrier reduced from 2 to 0.68 eV. The activation barrier can be further reduced to 0.03 eV in the

vicinity of a N-doped SW defect.²⁶¹ On a SWCNT with N-doped SW defect, nitrogen preferentially segregates to a five-membered ring site in the vicinity of the rotated bond and reduces the oxygen dissociation barrier to ca. 0.03 eV. Figure 11 shows the model proposed by Shan and Cho²⁶¹ for these barrierless sites for oxygen dissociation on defects of N-doped single-wall carbon nanotubes.

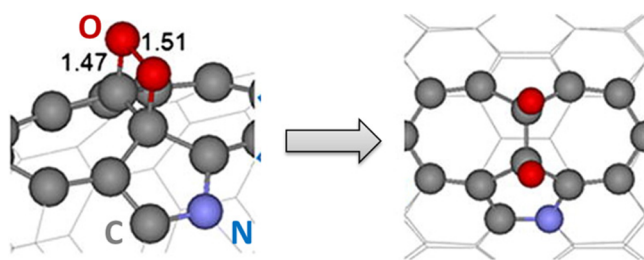


Figure 11. Oxygen dissociation over N-doped SWCNTs. A nitrogen atom in vicinity of a SW defect will enhance the oxygen dissociation. The energetically most favorable site for nitrogen doping on the SW defect is on the five-membered ring. The barrier for oxygen dissociation is 0.03 eV. Adapted from ref 261.

Carbon nanotubes, particularly at defect sites close to N atoms (which favor the electron charge transfer to chemisorbed oxygen and its dissociation and enhance as well the formation of double heptagonal carbon rings stabilized by two pentagonal rings containing the N atom, as shown in Figure 11), are thus able to promote the easy dissociative chemisorption of oxygen. This is an important aspect for the use of these materials in the cathode of PEM (proton exchange membrane) fuel cells, where the O₂ reduction reaction occurs, although the application of a potential between the electrodes of the fuel cell certainly influences the mechanism of O₂ dissociation. In addition, the surface chemistry of nanocarbons toward oxygen (a relevant aspect to understand their use in selective oxidation reactions, as discussed later) is richer in terms of the type of species which may form. Radovic²⁵⁶ recently investigated the nature of oxygen species formed at graphene edges and at nanotube ends, as well as at various types of defects within the basal plane of sp²-hybridized carbon materials, with reference to carbon oxidation. By quantum chemistry calculations he found that the basal-plane sites of a graphene are neither as inert as nor as (re)active as earlier supposed. These sites react with oxygen, forming epoxide-type species, but the C–C is stable enough to prevent desorption of CO₂, while the C–O bond not enough strong to avoid the “mobility” of oxygen. The activity of these species is limited to providing a “reservoir” of mobile oxygen. Oxygen insertion (graphene unzipping) and desorption of CO₂ is favored at oxygen-saturated edges, thus accounting for the well-documented phenomenon of induced heterogeneity of carbon surfaces. There is the need, however, of more comprehensive studies that analyze from the theoretical point of view the nature of the different species formed at the different possible (defect) sites of nanocarbons and determine their reactivity to correlate with the increasing knowledge on the catalytic chemistry of metal-free nanocarbon (see later).

Another relevant area in theoretical modeling of nanocarbon regards the influence of carbon nanostructure on the characteristics of supported metal particles. Li et al.²⁶⁴ studied the confinement effect of Au_n (*n* = 1–5) clusters in CNTs by DFT calculations. They found that gold clusters encapsulated

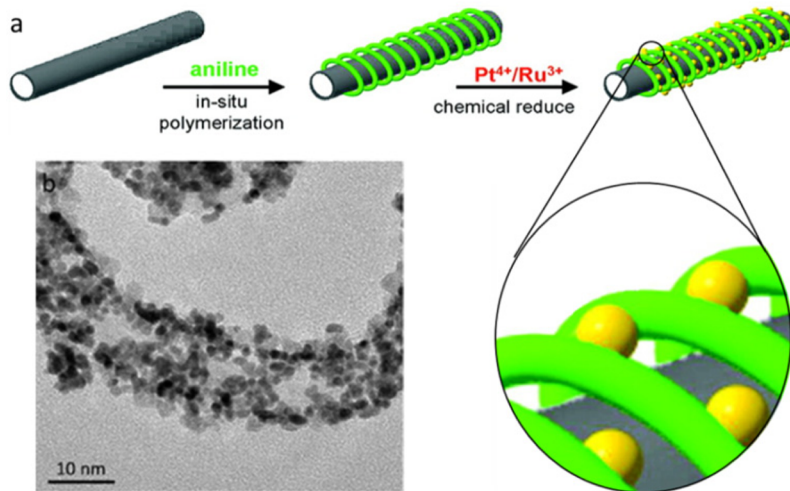


Figure 12. (a) Schematic illustration of the preparation of Pt–Ru binary catalysts on a polyaniline-functionalized multiwalled carbon nanotube (PANI/MWCNT). (b) TEM micrographs of the Pt–Ru/PANI/MWCNT. Adapted from ref 272.

inside the tubes interact with the tube via charge transfer from the inner sidewall to the clusters, resulting in negatively charged clusters. Clusters deposited outside the tubes are usually more stable than those encapsulated inside CNTs. H₂ generally binds to CNT supported gold clusters less strongly than to bare clusters, indicating that H₂ is less activated. Consistently, H₂ dissociation is suppressed on CNT-supported gold clusters except for Au monomer deposited outside the CNTs and Au dimer inside the CNTs. Their study demonstrates that CNT does not show a positive effect on H₂ dissociation. Its promotion effect depends not only on the reaction but also on the size of the catalysts. This study further demonstrates that the confinement effect is not effective for all types of reactions (see also later section 5.4).

On the other hand, it was also shown by theoretical modeling that supported metal nanoparticles are modified by the interaction with the carbon support,²⁶⁵ possibly being a specific interaction between carbon and the metal particles that creates bond length disorder deriving from interactions of the bottom metal layer in contact with the carbon surface.²⁶⁶ A number of other intriguing aspects are emerging recently. Qin and Li²⁶⁷ have shown by molecular dynamics simulations and DFT calculations that CuO nanoparticles confined in CNT have different reactivity with respect to when they are supported on the outside walls of CNTs. Zoberbier et al.²⁶⁸ have also demonstrated that clusters of transition metals (W, Re, and Os), upon encapsulation within a single-walled carbon nanotube (SWNT), exhibit marked differences in their affinity and reactivity. Point defects in carbon nanotubes have a large effect on anchoring sites of Au nanoparticles, as shown by DFT.²⁶⁹ Other defect sites in carbon (specifically ordered mesoporous C), such as sulfur, can equally play a critical role in the enhancement of the electrochemical stability and catalytic activity of supported Pt nanoparticles.²⁷⁰

There is thus a rich surface chemistry of nanocarbon materials that is progressively better understood due to the synergistic integration of experimental and theoretical studies. There are a number of emerging aspects, from the confinement inside CNT to the role of defects in creating special reactive sites at the nanocarbon surface or those that can interact with surface metal nanoparticles, modifying their reactivity and characteristics. These are the key aspects on which future

research should be focused, because they are the necessary elements for the rational use of nanocarbons in catalysis and other applications.

5. NANOCARBONS IN CATALYTIC REACTIONS

In parallel to the growing knowledge on the synthesis and understanding of nanocarbon materials, their use as advanced catalysts moved to more rational bases, although a gap may be still noted between the exponential increase of new carbon materials available, the rising level of their in-depth understanding, and the slowing growing of their use as advanced catalysts. The largest area of use as catalysts still remains in the clean and sustainable energy sector. New opportunities are emerging in the chemical synthesis area, although this is a more conservative sector, less prone to introduce new catalysts. We will mention here some of the new possibilities offered to catalysis by the use of nanocarbons, in terms of novel concepts that can be used rather than as a list of reactions in which they have been tested.

However, it is useful to comment that it is not always proven that functionalized nanocarbons act as real catalysts; e.g., they are not consumed during the reaction. Tests are often made in batch-type reactions, and stability is typically tested by reusing the samples in a few cycles. This type of test does not prove that nanocarbons (or functional sites on them) are not consumed during the reaction. This is particularly important in tests using metal-free carbon materials, for which it is highly recommended to use continuous flow reactors in order to prove the stability of the performances.

5.1. Enhanced Characteristics as a Support for Catalytic Functionalities

In several applications, when a complex mixture is present (a typical case is in fine chemicals synthesis), it is necessary to control the hydrophobic character of the support to limit side reactions and/or to control how the reactant(s) chemisorb. Seo et al.²⁷¹ showed that covering carbon fibers by a thin polydimethylsiloxane film made the superhydrophobic behavior of the surface possible in a wide pH range (1–13). This is interesting in a number of applications, for example, to limit water chemisorption on active sites, which often inhibits the reaction. However, surface functionalization of CNT may induce also additional intriguing effects for catalysis. An

interesting example is offered by MWCNT covered with polyaniline (PANI) (Figure 12).

Lee et al.²⁷² showed that the presence of PANI on the MWCNT surface induces a modification in the supported Pt–Ru (1:1) nanoparticles with respect to when they are supported directly on the bare MWCNT. In the latter, a Pt-rich core and a Ru-rich shell nanostructure is present, while the presence of PANI induces a surface composition analogous to that of bulk. This effect allows higher activity, superior Pt utilization efficiency, and a better durability when compared to other catalyst supports on bare MWCNT or on Vulcan XC-72 for methanol electro-oxidation. This is an example of application to catalysis of the knowledge gained in developing nanostructured PANI/CNT array composite electrode for electrochemical energy storage.²⁷³

Although problems of stability can be present for other catalytic applications, the concept is interesting, because it shows how an inorganic–organic composite as support (possible only using nanocarbon materials) offers the possibility of intrinsic change of the characteristics of bimetallic alloy nanoparticles. The use of bimetallic nanoparticles supported on carbon is becoming of increasing relevance in the sector of biofuels. For the conversion of levulinic acid to γ -valerolactone (GVL), an important conversion step in the development of novel second-generation biofuels,^{274,275} a RuRe/C catalyst is significantly more active than a Ru/C catalyst.²⁷⁶ Dumesic and co-workers²⁷⁷ reported recently that also RuSn/C shows superior properties with respect to Ru/C catalyst. The possibility of tuning the surface composition of these bimetallic nanoparticles by the presence of a secondary electron donor or acceptor element (using PANI or other conductive polymers) can be an interesting possibility, still not explored. Note also that the modification of MWCNT by PANI increases significantly their dispersion in aqueous solutions, another relevant aspect for biofuel applications.

5.2. Stabilization of Small Catalytic Particles with Enhanced Catalytic Behavior

Another attractive property of nanocarbons, still not investigated in enough detail, is the possibility to stabilize subnano metal particles. As mentioned before, this is a novel, attractive area, because subnanoparticles not only have higher activity but often show unusual properties. It is necessary to clarify that extremely small metal nanoparticles are not always necessary and it may be instead necessary to have metal nanoparticles above some threshold diameter. A typical case is the Fischer–Tropsch (FT) reaction. For cobalt-based FT catalysts, the turnover rate is nearly independent of the size of Co particles above a size of about 6 nm, while the turnover rate decreases almost linearly below this value.^{278,279} Chorkendorff and co-workers²⁸⁰ also found recently that larger Pt particles on carbon have a higher specific activity in ORR (oxygen reduction reaction). Many methods are known to prepare metal particles above a size of about 1–2 nm.²⁸¹ It is also possible to obtain rather narrow size distributions, for example, using colloidal-type solutions.²⁸² However, the preparation of stable subnanometer metal particles is highly challenging, and in this case, the support plays a critical role both in forming and stabilizing these very small metal nanoparticles. For these reasons, we focus discussion here on the role of nanocarbon in forming subnanometer metal particles, but this does not exclude that larger metal nanoparticles could be interesting. However, specific structural motivations should be present. On

the contrary, for structurally sensitive reactions or for those reactions having the active sites located at the interface between the metal nanoparticle and the support, subnanometer metal particles are highly interesting, because activity exponentially increases on decreasing the metal particle size.

Subnanometer particles are essentially all surface atoms, and thus show a quite different surface energy. Lei et al.²⁸³ showed a very high selectivity in direct propylene epoxidation using subnanometric silver particles (Ag_3 clusters), because of the open-shell nature of their electronic structure. Larger silver particles are completely unselective in the reaction. Furthermore, in these so small metal nanoparticles it is not possible to stabilize subsurface atom species that influence the surface reactivity. In the selective alkyne hydrogenation in the presence of carbon–carbon double bonded compounds (an important large-scale industrial process), the catalytic behavior of Pd nanoparticles is strongly influenced by the presence of interstitial atoms in the subsurface region.²⁸⁴ Hydrogen diffusion in Pd may form a β -hydride-like phase that is unselective in the hydrogenation, but dissolution of also carbon atoms in the subsurface results in a selective hydrogenation.²⁸⁵ Similarly, in the direct synthesis of H_2O_2 (reaction discussed in a more detail later), the formation of subsurface hydrogen and oxygen species may induce lattice strain,^{286,287} which decreases the selectivity in H_2O_2 synthesis, favoring both parallel and consecutive conversion. In subnanometer Pd nanoparticles, these processes are inhibited, thus allowing one to obtain an enhanced selectivity.²⁸⁸ There are thus both practical and fundamental motivations for the interest in developing subnanometer metal particles, and nanocarbons offer a great potential to stabilize these particles.

Yoo et al.²⁸⁹ showed that subnano Pt clusters show peculiar reactivity and high CO tolerance when supported on a graphene nanosheet. Shim et al.²⁹⁰ prepared Pd nanoparticles on a carbon support by using ethylene glycol containing PVP. The size of Pd nanoparticles was determined by the PVP concentration. For a PVP/Pd ratio of 80, particles with mean dimension of 0.8 ± 0.3 nm were obtained that showed more efficient ORR properties, e.g., a more positive ORR onset potential and increased number of electrons transferred in the ORR, and better methanol tolerance. Below about 1 nm, almost all metal atoms in the particles are on the surface, and for this reason the particles may show unusual properties. This is confirmed from the results of Ji et al.,²⁹¹ who reported that palladium subnanoparticles supported on “bamboo”-type MWCNTs exhibit metastability in the electrochemical oxidation of hydrazine, e.g., allowing the sensing of hydrazine in the pH range where Pd metal would normally be voltammetrically stripped (oxidized) from the surface of conventional electrodes.

The technique of preparation is indicated as sol immobilization, because a sol of Pd nanoparticles is first prepared, which is then immobilized over the support. In order to avoid the coagulation, the aqueous colloidal solution of metal particles should be stabilized by different methods:²⁹² (a) surface potential and/or charge density are increased by the adsorption of surface active long-chain ions (i.e., surfactants); (b) van der Walls forces are reduced by adsorption of relatively rigid hydrophilic macromolecules (i.e., dextrin, starch); (c) “steric stabilization” is produced by large adsorbed organic species. However, the sol characteristics determine not only the size distribution of metal nanoparticles on the final catalyst but also the interaction of the individual nanoparticles with support, in

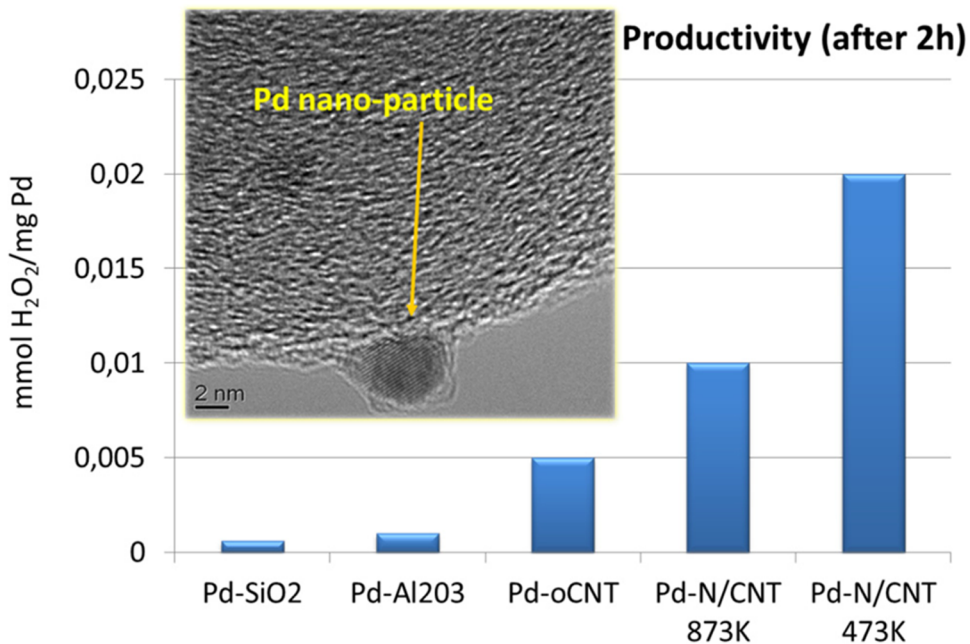


Figure 13. Comparison of the catalytic behavior (amount of H_2O_2 formed per milligram of Pd) in the direct synthesis of H_2O_2 from H_2/O_2 using Pd nanoparticles supported over different type of supports (SiO_2 , $\gamma\text{-Al}_2\text{O}_3$, and CNT; see the text for an explanation of the different types of CNTs). An analogous preparation by sol immobilization (PVP as organic sol stabilizer) was used. About 1 wt % of Pd was used in all catalysts. Reaction conditions: $P = 7.5$ bar (rt), feed: 7.5 vol % of H_2 with a H_2/O_2 ratio of 1:2, 20% CO_2 , flow semibatch reactor. In the inset, a TEM image of the Pd-CNT (SI) catalyst. Based on the data reported in refs 293, 297, 298.

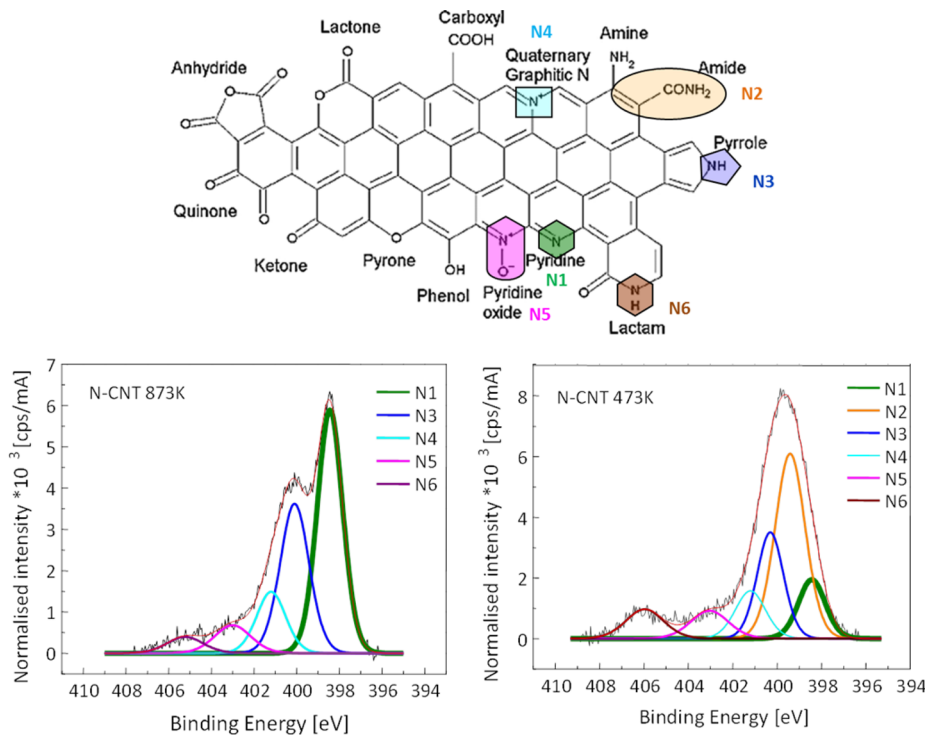


Figure 14. Different types of O and N functionalities in CNTs and synchrotron-radiation XPS spectra in the N_{Is} core region of N-CNT 473K and 873K samples (see the text). The XPS spectra report also the deconvolution in the different N species highlighted in the top part of the figure. Based on the data reported in refs 222, 223, 293.

particular the interaction of the organic capping agent with the functional sites of the support.

An example of the relevance of these aspects is given in Figure 13, which compares the catalytic behavior of catalysts prepared by the same procedure (using PVP as organic

stabilizer for the sol and about the same amount of 1% Pd in the final catalyst) over three types of supports: SiO_2 , $\gamma\text{-Al}_2\text{O}_3$, and CNT. Three different types of CNTs have been used: after the conventional oxidative treatment of activation (oCNT) and after subsequent functionalization by NH_3 at two different

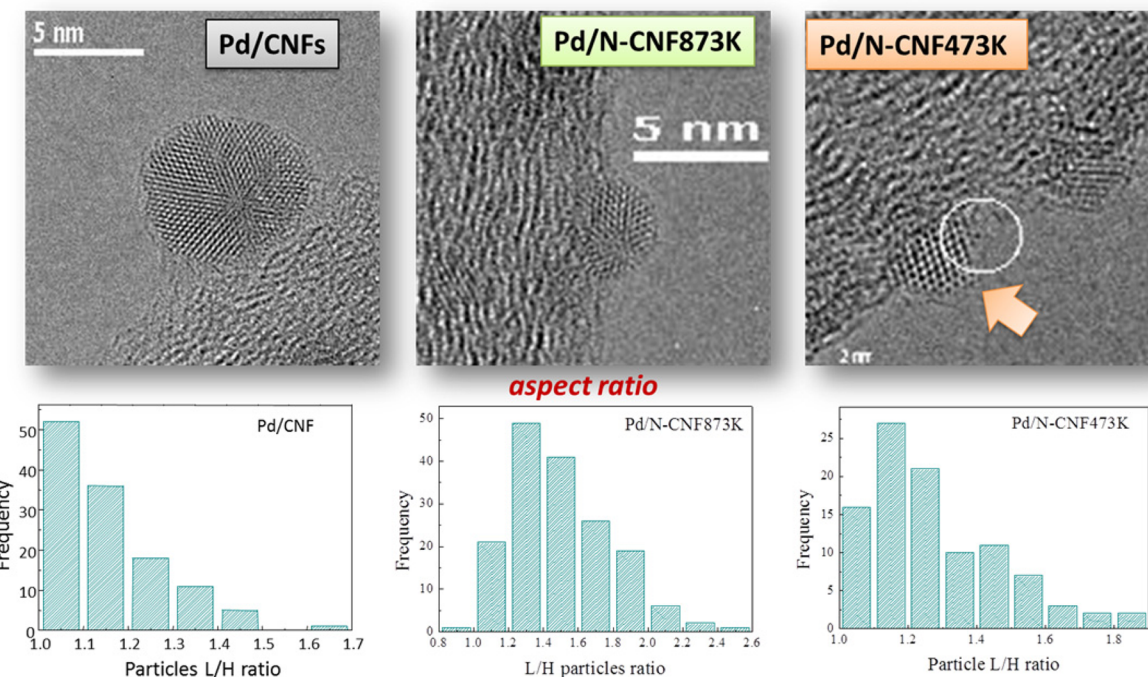


Figure 15. Distribution of the aspect ratio (length to height ratio; L/H) in Pd/CNF samples and TEM images of the corresponding samples (see the text for an explanation of the different types of CNTs). Adapted from ref 288.

reaction temperatures (N-CNT 473K and 873K, respectively).²⁹³ The pristine carbon nanotube was a commercial multiwalled sample from Pyrograph. The catalytic reaction is the direct synthesis of H_2O_2 from H_2/O_2 , an important industrial reaction of increasing relevance as an alternative to the multistep antraquinone-based commercial process having significant impact on the environment and large energy consumption.^{294–297}

Pd supported on CNTs²⁹³ gave in general significantly better performances than when deposited over other type of supports, including Pd supported over graphitic-type active carbon.^{297,298} In part, the explanation is related to the better Pd dispersion over CNT, particularly using the sol immobilization procedure, leading to very small and well-dispersed Pd nanoparticles having size in the 1–2 nm range (see image in Figure 13). In the case of alumina, the mean size is about 2–3 nm, while it is around 5 nm and with a broader size distribution for silica. However, this different size distribution of the Pd nanoparticles cannot explain alone the large differences observed in the activities in H_2O_2 formation as well as the large influence on the reactivity of the type of functional groups present on CNTs.

Different types of functional species are present on the surface of CNTs, depending on the type of treatment (oxidative treatment and consecutive treatment with ammonia at different reaction temperatures, e.g., oCNT and N-CNT 473K, N-CNT 873K). An overview of the different type of species present is shown in the top of Figure 14, while the bottom part of Figure 14 reports the high-resolution synchrotron-radiation XPS spectra in the N_{1s} core region of N-CNT 473K and 873K samples. The XPS spectra report also the assignment of the different components of the spectra, outlined in the top part of the Figure 14.^{222,223,293}

It is possible on these bases to correlate the maximum activity in the direct synthesis of Pd/N-CNT 473K (Figure 13) to the higher presence of amine- and amide-type surface species on CNTs (Figure 14). However, what is the effect of the

presence of these species on the characteristics of Pd particles and thus their reactivity in the direct synthesis of H_2O_2 ?

The Pd nanoparticles on CNTs have a slightly elongated shape due to the interaction with the surface sites present on CNTs, and in turn, there is an influence on the characteristics of the nanoparticles. This is as evidenced by the distribution of the aspect ratios (the length to height ratio) of these nanoparticles from the distribution of surface functional sites on CNTs, which in turn depends on the procedure of functionalization of the CNTs (Figure 15).²⁸⁸

The optimization of the preparation leads to very active catalysts, having over 80% of the nanoparticles below 1.5 nm, including about 10% below 1 nm, and showing also very high selectivity (over 95%) in the direct synthesis of H_2O_2 .²⁸⁸ However, in the reaction conditions of H_2O_2 synthesis, the PVP capping agent, which decorates the Pd nanoparticles, is progressively removed during reaction, leading to sintering of the Pd particles and a consequent worsening of the catalytic performances.

5.3. Direct Catalytic Role of Nanocarbon Functional Groups

The surface functional groups of the nanocarbon show interesting catalytic properties. It was already mentioned in the previous sections that metal-free nanocarbon materials show interesting catalytic properties due to the presence of surface O- and N-type functional groups. Su et al.⁸⁰ have recently reviewed this topic, evidencing how metal-free heterogeneous catalysts based on nanocarbon or carbon nitride are an interesting alternative to some current commercial catalysts and may be considered a new class of catalysts. Yu et al.⁸¹ also discussed the progress in development of C-based, metal-free catalysts for industrial process applications, with particular emphasis on the use of CNT for ODH of aromatic hydrocarbons and alkanes (the same topics originally developed by Su et al.⁸⁰) and O reduction reactions in alkaline medium. As mentioned, a different name to indicate the same type of

chemistry is carbocatalysis. Two recent reviews on this topic, with a focus on graphene oxide, were done by Dreyer and Bielawski⁴² and Su and Loh.⁴³ The use of graphitic carbon nitride materials as metal-free catalysts was also recently reviewed by Thomas et al.⁷⁹

This section does not aim to give a systematic list of all the reactions tested, but only to use selected examples, mainly with reference to industrially important reactions, such as styrene synthesis, acrolein, and cyclohexane oxidation, benzene hydroxylation, and ORR, in order to highlight how this class of material represents a potential breakthrough, novel catalysts for industrially relevant reactions. The use of nanocarbons, in particular graphene oxide, in organic syntheses and polymerization reactions will be instead discussed in section 5.7, because this type of chemistry is interesting and often involves different types of surface sites than those discussed in this section, but in terms of potential industrial impact it is less relevant. In fact, there are other types of catalyst which perform similar catalytic chemistry, often with better performances (productivity, selectivity) and/or with easier application (preparation in a form suitable for industrial use, with easy recovery and handling).

It should be also commented that the use of metal-free carbon in catalysis and electrocatalysis is not new. Phosgene, even with its well-known safety issues (highly toxic and hazardous nature), is still produced in an annual amount of about 5–6 Mtons using carbon as catalyst, although essentially all for immediate *in situ* use without storage.²⁹⁹ Phosgene is a chemical intermediate used in the manufacture of important industrial products such as polyurethanes, polycarbonates, pharmaceuticals, and agrochemicals. Alternative phosgene-free routes to manufacture these products, although appealing in terms of sustainability, still suffer in large part from higher costs. Phosgene is manufactured industrially via the gas-phase reaction of carbon monoxide with chlorine in the presence of an activated carbon catalyst. This reaction has been known for over a century, and it is known that the specific nature of the carbon catalyst strongly influences the catalytic performances,³⁰⁰ although the exact nature of the active sites is still largely unknown. It is known that Cl₂ dissociation with halogenation of carbon, probably the first step in the reaction to phosgene, is considerably dependent on the structure of the nanocarbon.³⁰¹ It is thus likely that by combining advances in understanding the nature of nanocarbon surface sites with those on the reaction mechanism of phosgene generation, it will be possible to develop improved nanocarbon-based catalysts for this old but still relevant reaction.

The use of carbon (particularly graphite) in the electro-reduction of nitrobenzene to aniline, another industrially important reaction, has also been known for a long time, although the current process is based on the catalytic hydrogenation of nitrobenzene using copper-chromite or Ni Raney catalysts. However, several recent developments have increased the interest in the electroreduction of nitrobenzene. Li et al.³⁰² have investigated the electrochemical reduction of nitrobenzene at a pyrolytic graphite electrode modified with CNTs and observed a large increase in the activity with respect to bare graphite electrode. Qi et al.³⁰³ showed that an ordered mesoporous carbon material modified with didodecyldimethylammonium bromide and supported on a glassy C electrode (GCE) exhibits high electrocatalytic activity toward the reduction of nitrobenzene. The capability of graphite to reduce nitrobenzene to aniline in the presence of hydrazine (known

for many years³⁰⁴) is also related to an electrocatalytic mechanism, because hydrazine decomposition generates two electrons, which are used for the four-electron reduction of nitrobenzene at graphite sites.³⁰⁵ It was shown recently that reduced graphene oxide shows significantly larger activity than carbon black, natural or expanded graphite, and pyrolytic graphene oxide in the reduction of nitrobenzene to aniline at room temperature in the presence of hydrazine.³⁰⁶ Fullerenes were also used in the catalytic reduction of nitrobenzene to aniline, but using H₂ directly as coreactant.³⁰⁷ The hydrogenation of nitrobenzene is achieved with high conversion and selectivity under 1 atm of H₂ and light irradiation at room temperature (for UV radiation and 4 h of reaction, 100% conversion and 92% selectivity) or under conditions of 120–160 °C and 4–5 MPa of H₂ pressure without light irradiation (using C60/C60⁻ anion in a 2:1 ratio as catalyst, 5 MPa H₂, 160 °C, THF solvent, and 12 h of reaction time gave nearly complete conversion and selectivity). Although productivity in comparison with the industrial process of catalytic reduction of nitrobenzene is still too low, these data indicate interesting perspectives to develop an alternative process. Another possible industrially relevant application is the reduction of *p*-nitrobenzene to the corresponding amine as an intermediate to form diisocyanate (to be reacted with polyols in the production of polyurethanes, an important class of polymers).

It should be also commented that in metal-free carbon catalysis (carbocatalysis), care should always be taken to demonstrate the real role of carbon functional groups in the reaction mechanism and not of impurities present in carbon. For example, van Bokhoven et al.³⁰⁸ argued whether Ni contamination in C60 anion is responsible for the observed activity, because when preparing C60 anion using sodium naphthalenide instead of reduction using a Ni-Al alloy (as in Li and Xu³⁰⁷ experiments), no catalytic activity was observed. The reaction discussed below in this section was proven to be unrelated to contaminants in the nanocarbon materials, but in general, careful attention to this aspect should be given.

For sp² nanocarbons, high-energy sites provided by the dangling bond of the sp² hybridization are located at the edges (prismatic sites). These sites are saturated by hydrogen or by heteroatoms (depending on the pretreatment), providing a rich surface catalytic reactivity (see the top of Figure 11) for both acid–base and redox chemistry. If the graphitic sheets contain pentagonal, heptagonal, or larger nonhexagonal defects, the additional charge present in such units can assist the activation or dissociation of adsorbing molecules. In addition, if the graphitic sheets are curled, then the strain on the sp² centers leads to charge localization and increases the poor reactivity of the basal plane. There is thus an interesting possible surface catalytic chemistry of nanocarbons, which is starting to be explored. In turn, the catalytic performances strongly depend on the type of nanocarbons, as shown in Figure 16, which reports the rate and selectivity in styrene formation by dehydrogenation of ethylbenzene (a multimillion-ton scale industrial reaction).³⁰⁹

Nanodiamond nanoparticle has a diamond–graphene core–shell structure. The surface graphene layer is highly defective and rich in oxygen-containing groups, among which the ketone-like C=O species can be stable even at temperature as high as 550 °C (high temperatures are necessary due to thermodynamic limitations in reversible dehydrogenation reactions). Nanodiamond shows about 3 times the steady-state activity of the K-promoted Fe₂O₃ catalyst that is commercially used. In

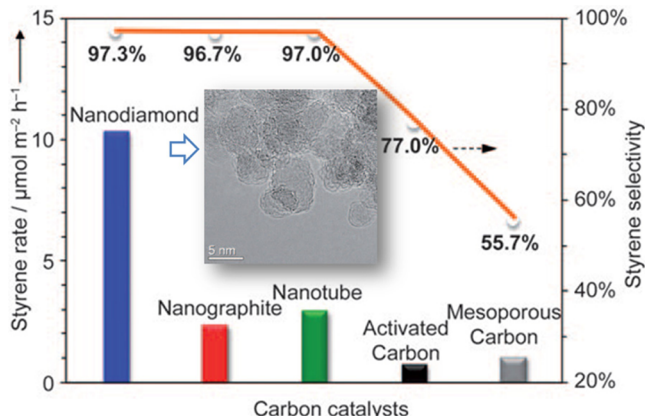


Figure 16. Comparison of the rate and selectivity of styrene formation in the steam-free dehydrogenation at 555 °C of ethylbenzene on different types of nanocarbons. Conditions: 50 mg of catalyst, 2.8% ethylbenzene in helium, gas flow rate 10 mL/min, 1 atm. In the inset, HRTEM image of fresh nanodiamond. Adapted from ref 309.

addition, nanodiamond displays remarkable stability over a long period of time.³⁰⁹ The yield and selectivity are greater than 20.5 and 97.3%, respectively, indicating the potential industrial exploitation of these materials, although the cost of manufacture is still high. The suggested mechanism is based on coupled surface ketonic C=O groups, which abstract H-atoms from ethylbenzene, forming styrene and hydroxyl groups (C-OH). The reaction cycle is closed by the thermal decomposition of C-OH to C=O and molecular hydrogen, which is thermodynamically favorable at high temperatures. The critical issues for maintaining this cycle are avoiding reconstruction of the surface sites, hydrogen passivation, deposition of carbon, etc. The role of the nanocarbon structure is critical with respect to these aspects, and for this reason, the unique sp²-sp³ hybrid structure in nanodiamond results in different behavior with respect to other carbons, with superior activity and stability from coke formation.^{310,311}

The synthesis, structure, properties, and surface chemistry of nanodiamonds has been reviewed recently.³¹²

Metal-free nanocarbons show interesting catalytic properties also in alkane activation and ODH^{229,311,313,314} and in oxygen insertion catalysis, in particular, the selective gas-phase oxidation of acrolein to acrylic acid.³¹⁵ Figure 17 reports the proposed reaction pathway for the oxidation of C₃H₄O at the graphitic carbon surface.

The sp² carbon acts as a bifunctional catalyst in acrolein oxidation to acrylic acid. The nucleophilic oxygen atoms terminating the graphite (0001) surface abstract the formyl hydrogen and the activated aldehyde gets oxidized by epoxide-type mobile oxygen.³¹⁶ Liang et al.³¹⁷ reported that graphitic edges, present in open cages of fullerene-like sites in glassy carbon, display high activity for the ODH of isobutane in comparison to the not-opened ones. Ni et al.³¹⁸ showed that graphite-like nitrogen and Stone-Wales defect nitrogen decrease the energy barrier more efficiently than pyridine-like nitrogen, and a dissociation barrier lower than 0.2 eV can be obtained. Higher nitrogen concentration reduces the energy barrier much more efficiently for graphite-like nitrogen, due to partial occupation of π^* orbitals and change of work functions.

Another challenge for industrial processes in the direct benzene hydroxylation to phenol^{294,296} to avoid the multistep process currently used via cumene and cumene hydroperoxide. A recent result showed that defective MWCNTs are active also in this reaction.³¹⁹ Although benzene conversion is low (around 6%), the selectivity is very high (about 99%). A clear correlation with the number of defects in MWCNTs (produced by heating and ultrasonication methods) was determined. The proposed reaction mechanism (Figure 18) involves active monoatomic oxygen (with electrophilic character) attacking benzene to form directly phenol. The active oxygen was generated by H₂O₂ decomposition on the defect of MWCNTs with dangling incomplete bonding.

Although the mechanism is still speculative and direct evidence on the nature of the sites involved was not provided, it presents analogies with the mechanism of benzene direct

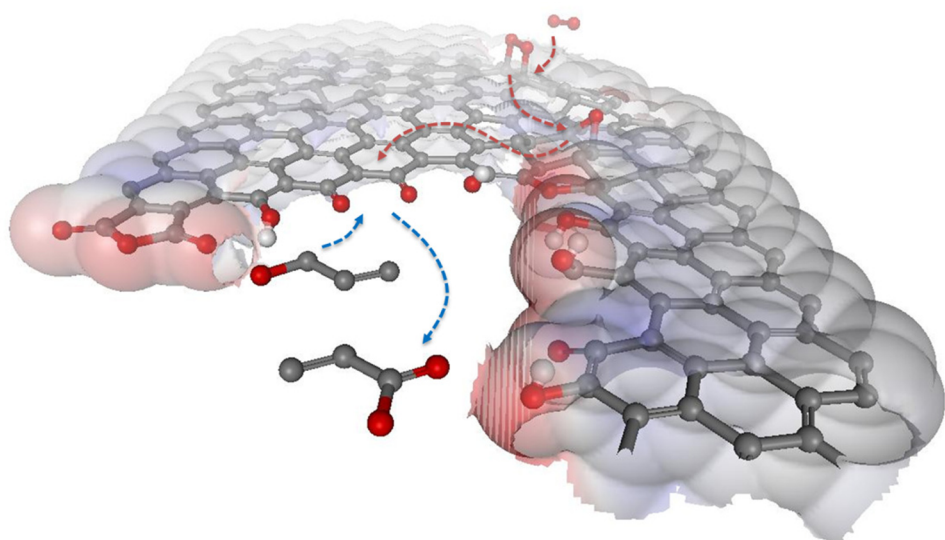


Figure 17. Reaction pathway proposed for the oxidation of C₃H₄O at the graphitic carbon surface. The active domain is illustrated as a rectangular section of a planar graphene sheet with a hole defect, which is terminated by arbitrarily positioned oxygen functionalities. O₂ adsorbs dissociatively at the (0001) surface to form mobile epoxy groups, which migrate to the prismatic edge sites. The adsorption of C₃H₄O at the nucleophilic oxygen sites, i.e., the ketones/quinones, initiates its oxygenation by epoxy oxygen atoms to form acrylic acid. Based on the mechanism proposed in ref 315.

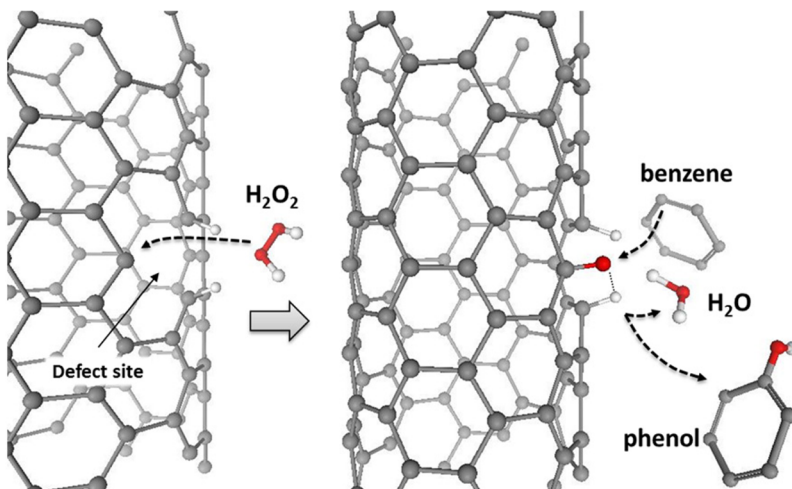


Figure 18. Mechanism of benzene hydroxylation on defective carbon nanotubes. H_2O_2 reacts with dangling incomplete bonding defect site of MWCNTs, forming water and an electrophilic monatomic oxygen species, stabilized by hydrogen bonds with near-lying C–H sites. This species reacts with benzene, forming phenol. Based on the mechanism proposed by Song et al.³¹⁹

hydroxylation to phenol on Ti-silicalite.²⁹⁴ However, it is probable that the exact nature of the “defective” sites and surface oxygen species is slightly different from that proposed, on the basis of the indications discussed before.

CNTs as metal-free catalyst were also reported to exhibit interesting performances in other industrially relevant reactions, such as the catalytic oxidation of cyclohexane with O_2 ^{320,321} and of benzyl alcohol.³²² The reaction of cyclohexane oxidation to cyclohexanol and cyclohexanone [the so-called KA oil; they are further oxidized to adipic acid (AA), an important industrial reaction with world annual production of about 3–4 Mtons] is currently mainly made in two steps. The first step is the oxidation of cyclohexane with O_2 to give KA oil using Co or Mn organic salts (e.g., naphthenate), which catalyze the start of a radical homolytic autoxidation mechanism (reaction temperature is typically in the 150–180 °C range and pressure in the 10–20 atm range). The second step is the oxidation of KA oil to AA using a large excess of 50–60% HNO_3 , and Cu(II) and ammonium metavanadate as catalysts.²⁹⁴ The possibility to use CNT instead of the above outlined chemistry is thus potentially interesting, especially to avoid the second step using HNO_3 (for its environmental impact), although one must remember that the second stage can occur also using air instead of nitric acid, and Co and Mn acetate as catalysts (at 70–80 °C, in acetic acid solvent).²⁹⁴ Using O_2 instead of nitric acid has the advantages of lower environmental impact (NO_x and N_2O emissions) and corrosion problems, but the yields of AA (typically not higher than 70%) are lower than those obtained using nitric acid. The quality of produced AA is also poor. AA can be thus formed from cyclohexane using O_2 through a radical homolytic autoxidation mechanism, which can be activated from redox metals such as Co, Mn, or even Fe. Co and Fe are also the catalysts used to synthesize CNTs, and by acting as promoters of a radical mechanism, even when present in traces, can catalyze the reaction. In the second published paper by Peng and co-workers,³²¹ they show that iron nanowires confined in CNTs enhance the aerobic oxidation of cyclohexane to AA. As may be argued from the above discussion, in this radical-type autoxidation chemistry, great care must be taken to really proof that functionalities of CNTs or nanocarbons are really acting as catalysts and eventually not as simple radical-chemistry promoters. In terms of application,

the productivities reported are still far from those industrially relevant, and thus, further experimentations on these materials are needed to look at their exploitability.

By doping the CNTs with nitrogen, the reaction rate in cyclohexane oxidation increases about 5 times with respect to AC and about doubles with respect to undoped CNT.³²⁰ These results could indicate a specific role of the surface sites of CNTs in catalyzing the reaction, but they are also consistent with a radical-type autoxidation mechanism, given the still low reaction rate (at the best around $1 \text{ mmol}\cdot\text{h}^{-1}\cdot\text{g}^{-1}$)³²⁰ with respect to industrial process (around $1\text{--}2 \text{ kmol}\cdot\text{h}^{-1}\cdot\text{m}^{-3}$).³²³ The encapsulation of metallic Fe within CNTs improves electron transfer between the metal and the CNTs, resulting in a higher catalytic activity in the oxidation of cyclohexane,³²¹ although it is not demonstrated that traces of leached iron do not catalyze the autoxidation process. In the selective liquid-phase oxidation of benzyl alcohol catalyzed by carbon nanotubes,³²² an autoxidation mechanism is also possible. Although the presence of CNT (HNO_3 -treated) increases by about 5 times the reaction rate and good results are reported (benzyl alcohol conversion of 96.2% and benzaldehyde selectivity of 88.3% under optimal conditions), the data are well consistent with a promotion of a radical mechanism by CNTs. Localized electrons can be trapped in CNT defects, and this is another mechanism by which radical-type chemistry can be promoted. In addition, it should be remarked that, from an application perspective, the industrially relevant reaction is toluene oxidation to benzaldehyde (or benzoic acid) not benzyl alcohol oxidation.

Another industrially relevant reaction in which metal-free nanocarbons are active is that of oxygen reduction in PEM fuel cells. A number of new interesting results have been reported recently. Morozan et al.³²⁴ showed that metal-free N-CNTs prepared from triazole and tetrazole derivatives (heat-treatment of N-containing precursors and MWCNTs at 700 °C under argon) show high electrocatalytic activity toward the ORR (assessed by cyclic voltammetry, rotating disk and rotating-ring disk electrode) measurements in alkaline media (O_2 -saturated 0.1 M KOH). The onset potentials of the ORR on N-CNTs are more positive than on CNTs, although still negatively shifted from the value for Pt/C catalyst (an overpotential ca. 80 mV higher than for Pt/C catalyst). A

good stability was also observed.³²⁴ After 200 cycles (e.g., approximately 14 h of tests), the current density decreases only 10%.

Boron-doped carbon nanotubes (B-CNTs) also show rather interesting behavior as metal-free electrocatalyst for ORR.³²⁵ The electrocatalytic performances are improved progressively with increasing boron content, as reflected in the increased reduction current and the positive shifted onset and peak potentials. Boron doping enhances the O₂ chemisorption on B-CNTs. The electrocatalytic ability for ORR stems from the electron accumulation in the vacant 2p orbital of boron dopant from the π^* electrons of the conjugated system; thereafter, the transfer readily occurs to the chemisorbed O₂ molecules with boron as a bridge. The transferred charge weakens the O—O bonds and facilitates the ORR on B-CNTs. The two key factors for the doped CNTs as metal-free ORR catalysts are the following: (1) breaking the electroneutrality of CNTs to create the charged sites favorable for O₂ adsorption, despite whether the dopants are electron-rich (as N) or electron-deficient (as B), and (2) effective utilization of carbon π electrons for O₂ reduction.

The use of more dopants (B, N, and P) in synergy is a strategy for developing electrocatalysts for fuel cells, because the functions cited above may be optimized. However, there are other aspects in terms of nanocarbon functionalities that are emerging from recent papers and suggest the possibility of more complex synergic strategies to reach ORR performances equal to and perhaps better than those of noble-metal-based ORR electrodes:

(1) CNTs were modified by liquid ionic salts to induce polarization of the π electrons of CNTs, thus accelerating interfacial electron transfer. Kim et al.³²⁶ have shown recently that imidazolium salt-functionalized MWCNTs show a high ORR activity, attributed to the induced polarization of the π electrons of CNTs. The zwitterionic MWCNTs functionalized with poly(vinylimidazolium sulfonate) have a more positive surface charge and exhibit a better electrocatalytic activity than the poly(vinylbutylimidazolium chloride)-functionalized MWCNTs.

(2) Nanocarbon hybrids were created. Ma et al.³²⁷ have prepared a three-dimensional N-CNT/graphene (N-CNT/G) composite by pyrolysis of pyridine over a graphene-sheet-supported Ni catalyst characterized by tangled N-CNTs with lengths of several hundred nanometers sparsely, but tightly, distributed on the graphene sheets, forming quasialigned N-CNT arrays. The N content in the N-CNTs/G was about 6.6 atom %. The N-CNTs/G shows a high activity and selectivity in ORR in alkaline electrolyte.

(3) Zones with controlled hydrophobic/hydrophilic character were produced. Jo et al.³²⁸ reported metal-free hybrid electrocatalyst composed of reduced graphene oxide (rGO) and polyelectrolyte-functionalized MWCNTs. The ratio between the hydrophilic rGO with respect to the hydrophobic MWCNTs is critical in optimization of the effective oxygen transport to the catalytic surfaces, which results in a varying number of electrons being involved during the ORR. It was found that dual interfaces with a fine ratio of rGO/MWCNT and the electron-withdrawing effect of poly(diallyl dimethylammonium chloride) (PDAC), which is used to functionalize CNTs, contributed to the enhanced electrocatalytic ORR activity.

In addition to the N-doped CNTs discussed before, ordered mesoporous carbon nitrides with graphitic frameworks are also

active catalysts.³²⁹ The role of graphitic edge plane exposure in carbon nanostructures for ORR was discussed in detail by Biddinger and Ozkan.³³⁰ Nanostructure on its own is not a factor for improved ORR activity. Rather, nanofibers with high edge plane exposure, like stacked platelets, provide the appropriate locations for N to incorporate into the graphitic matrix. Also gross N content did not play a role in ORR activity. N had to be incorporated into the graphitic matrix, not attached as part of a surface functional group. Lyth et al.³³¹ showed that metal-free carbon nitride shows also high ORR activity, while Morozan et al.³²⁴ showed that the treatment of MWCNTs with nitrogen-containing precursors (in particular, BTA) at 700° under argon produces carbon structures enriched in nitrogen with enhanced ORR properties. Choi et al.³³² evidenced that a dual N and P doping improves the performances, in particular reducing the amount of H₂O₂ formed during ORR, compared to only N-doped samples. Doped nanocarbon materials for ORR is an area of intense research interest recently. Feng and co-workers prepared phosphorus-doped graphite layers,³³³ multiwalled CNTs,³³⁴ and carbon nanospheres,³³⁵ which exhibited high electrocatalytic activity for O₂ reduction in alkaline medium. A review was recently published on this specific topic.³³⁶ The reaction mechanism is still under debate, because often the change of surface properties is not considered when a potential is applied, e.g., during working conditions.³³⁷ They indicate that both a two-electron pathway, where molecular oxygen is reduced to hydrogen peroxide, and a four-electron pathway operate in parallel in the ORR reaction mechanism on N-doped CNTs and Pt catalysts. Kim et al.³³⁸ showed by DFT that in N-doped carbon materials (graphene nanoribbon) the edge structure and doped-N near the edge enhance the oxygen adsorption, the first electron transfer, and also the selectivity toward the four-electron, rather than the two-electron, reduction pathway. The proposed catalytic cycle around these N-doped graphitic sites at the surface involves a ring-opening of the cyclic C—N bond at the edge of graphene, which results in the pyridinic nitrogen (Figure 19).

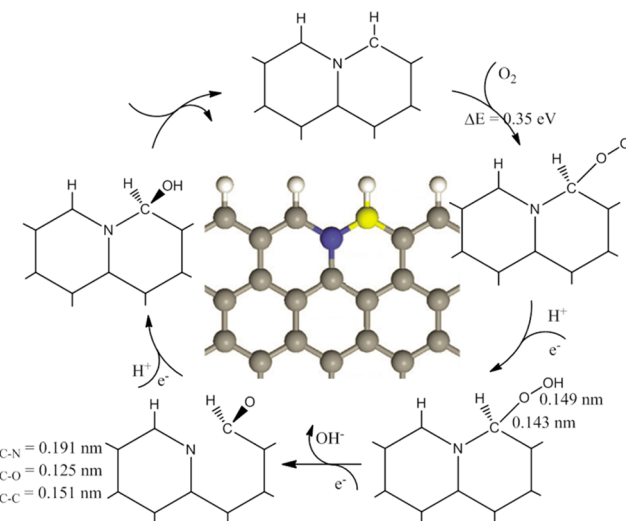


Figure 19. The proposed ORR catalytic cycle for N-doped graphic edge sites and the model structure for this site (nitrogen, oxygen, and hydrogen atoms are colored blue, red, and white, respectively). Elaborated from ref 338.

Wiggins-Camacho and Stevenson³³⁹ instead proposed that the ORR at N-CNTs involves a dual site reduction in which O₂ is initially electrochemically reduced in a two-electron process to form HO₂⁻. This step is then followed by a rapid chemical disproportionation step at surface metal nanoparticles (Fe_xO_y/Fe site stabilized by the presence of pyridinic type surface functionalities.

Although there are still discordances in the nature of surface sites and active species in nanocarbon materials (edge sites, defects, metal impurities, etc.), the data presented above show the very rich catalytic chemistry of metal-free nanocarbons, due to their surface functionalities related to heteroatoms and/or surface defects. The applications range from energy applications (novel ORR electrodes) to novel classes of catalysts for chemical processes. This is an area only recently explored, and thus, a rapid growth of new examples, in parallel with the better understanding of the surface chemistry and reactivity of nanocarbons, is expected.

5.4. Nanoconfinement

It is well-established in catalysts such as zeolite and mesoporous ordered-silica materials that the presence of size constrains in the growth of hosted particles largely influences the catalytic reactivity.^{340,341} CNTs, OMCs, and other nanocarbon materials having ordered nanocavities show analogous characteristics but very different chemical properties of the inner surface with respect to silica-type materials. The interaction with nanoparticles located inside these nanocavities is thus different from that present inside silica-type materials.

It is also known that surface effects tend to become dominant in fluids confined at the mesoscale and that the molecular properties may become anisotropic close to the channel walls, depending on the Gaussian curvature of the latter.⁶⁹ These confinement aspects influence the catalytic behavior, and in CNT, due to the different surface characteristics of inner walls with respect to silica-type mesoporous materials, the effect of confinement could be quite different and can be exploited for interesting applications. De Jongh and Adelheim³⁴² have reviewed the recent research on the concept of nanoconfinement as a new strategy toward meeting hydrogen storage goals.

Tessonniere et al. reported in 2005 the confinement effect of Pd nanoparticle catalysts deposited on the inner walls of CNTs for the selective hydrogenation of cinnamaldehyde to hydrocinnamaldehyde,³⁴³ explained by the unusual interaction between Pd nanoparticles and the inner walls of the CNTs coupled with the relative lack of oxygenated surface groups on them. Bao and co-workers^{26,27,344} studied systematically how the nanoconfinement in CNT influences the properties of metal nanoparticles, especially in relation to the modification of the redox properties. The reduction of Fe₂O₃ nanoparticles is significantly facilitated inside CNTs compared to those on the outside.³⁴⁵ In situ HRTEM indicated that the CNT-confined Fe₂O₃ particles transformed to metallic iron at 600 °C, while the outside particles remained oxidic at this temperature. They also showed³⁴⁶ that the reactivity of iron catalysts in Fischer-Tropsch (FT) synthesis was enhanced by confining iron nanoparticles within CNTs. The iron species encapsulated inside CNT are stabilized in a more reduced state, and the formation of iron carbides under the reaction conditions is enhanced. The latter have been recognized to be essential to obtain high FT activity. The yield of C5+ hydrocarbons over the encapsulated iron catalyst is twice that over iron catalysts outside CNT and more than 6 times that over activated-carbon-

supported iron catalysts. FeN nanoparticles confined in CNTs show enhanced reactivity in CO hydrogenation.³⁴⁷ We also showed that, in the electrochemical reduction of CO₂ to 2-propanol and other alcohols/hydrocarbons, the iron particles located inside the CNT show enhanced properties with respect to those located on the outer surface.¹⁴ In the syngas conversion to C2 oxygenates such as ethanol, acetic acid, and acetaldehyde, Rh–Mn particles located inside the CNTs show a higher activity than when located on the outer surface,³⁴⁴ being present in a more reduced state than that on the exterior. In addition, theoretical studies combining first-principles and Monte Carlo simulations evidence the stronger interactions of both H₂ and CO with the interior nanotube surface than with the exterior surface, but the effect is different for the two molecules. As a result, not only a pseudoenhanced pressure within the CNT is present but also the CO/H₂ ratio is altered. The effects are depending on the diameter of the CNTs. The enrichment generally becomes more significant inside smaller nanotubes at lower temperatures and higher pressures.

The adsorption and reactivity of the reactants and the nature of the active sites (metal nanoparticles) are influenced by the environment and confinement inside nanocarbons. Locating metal nanoparticles inside CNTs is thus an opportunity to control and enhance the catalytic performances,³⁴⁸ although a more in-depth investigation is necessary. For instance, currently it is still not clear up to which diameter the confinement plays a role, since CNTs may have a diameter distribution from a few nanometers to hundreds of nanometers. In addition, CNTs have a huge aspect ratio, and the in and out transfer of reactant and product molecule could be significantly lowered by the small opening on the tip.³⁴⁹ The mass transport may further be hindered by the metal particles in the narrow channel of CNTs.

The confinement is not beneficial for all reactions.²⁶⁴ Zheng et al.²⁴⁰ reported that Ru particles supported outside CNTs have a better catalytic performance in ammonia decomposition than when Ru particles are inside CNTs. Ammonia decomposition requires the difficult step of N–N recombination through surface diffusion from two sites of ammonia cleavage on weakly adsorbing sites (terraces).³⁵⁰ This requires high support ordering and large particles of Ru rather than small particles in a confined space.²⁴⁰

The current study on the influence of the confinement effect provided by CNT channels was solely related to the enhancement of the catalytic performance. Another confinement effect that is not well studied, but could be important for the catalytic reaction, is the modification of the size and shape of the particles in a CNT. Until now, the study on the confinement assumes that the shape and size of nanoparticles inside or outside CNTs do not differ. A recent work shows that the confinement effect also impacts the size and shape of cobalt-based nanoparticles inside the CNTs.³⁵¹ Faceted and highly porous cobalt-based NPs were formed in CNT channels by introducing the CNTs in an octadecene suspension containing a cobalt stearate complex and oleic acid as surfactant and by submitting the mixture to a thermal decomposition at 318 °C. The reasons for the faceted shape and porous structure of obtained particles are still not clear, but such particles are only found inside CNTs. The above-mentioned work by Zheng et al.²⁴⁰ reveals that the inner walls of CNTs may have less ordered graphitic degree, resulting in the formation of smaller, less faceted and more defective Ru nanoparticles compared with those formed on the outer surface of a CNT.

Another important confinement effect is the modification of physical or chemical properties of molecules in a confined space, which still needs to be explored more systematically for catalytic reactions. Compared with the fluids in the bulk phase, the inner surface and the confinement of a CNT can induce a dramatic change in the transport property of water in nanochannels.^{352–356} Moreover, inside the channels of size comparable to molecular diameter, the molecular thermal fluctuations play an unforeseen role for the equilibrium property of fluids. This finding is also valid for gas-phase molecules.³⁵⁷

In addition, some other interesting phenomena may appear in the confined space of a CNT. For instance, methanol molecules inside CNTs opening to a liquid methanol reservoir may form a monowire, in which the molecules are one-dimensionally hydrogen-bonded.³⁵⁸ Stemming from the coexistence of the hydrophobic and the hydrophilic groups, the formation of a methyl–hydroxyl “biwall” along the CNT wall and a subsequent “biwire” consisting of two methanol subwires running through the CNTs is observed to precede the monowire as the diameter size of CNTs decreases. All these unpredictable factors indicate that the conventional behavior of the macroscopic fluids or gases may be no longer applicable for those confined in nanochannels.^{359,360}

How these changed properties interact with or influence the catalytic reaction in the confined space of CNTs is still unknown. However, there is some potential application that may be indicated, although still not explored. For example, nanotube membranes (with vertically aligned CNTs) show superfast flow.³⁶¹ The magnitude of the fluxes is 15–30-fold higher than predicted from Knudsen diffusion kinetics and consistent with specular momentum reflection inside smooth pores. Polar liquids, such as water, ethanol, and isopropyl alcohol, and nonpolar liquids, such as hexane and decane, were dramatically enhanced, with water flow over 4 orders of magnitude larger than “no-slip” hydrodynamic flow predictions. While these interesting properties have been considered mainly for developing new membranes for water purification and gas separation,³⁶² they have great potential for novel catalytic applications.

An ultrashort (millisecond) contact time reactor is a concept developed by Schmidt (University of Minnesota) originally for the selective oxidation of alkanes³⁶³ (but later for a variety of other catalytic reactions, particularly biomass-related applications recently, such as butanol and ethanol dehydration to the corresponding olefins^{364,365}), in order to increase the selectivity by avoiding the consecutive conversion of the reaction products due to the very fast passage through the reactor. However, this concept may be applied only to gas-phase reactions, because it is not possible to realize these ultrashort contact times in a liquid-phase reactor. The very fast diffusion of polar liquids in the straight channels of a CNT-based nanomembrane, where the active catalytic nanoparticles could be localized, enables the possibility to implement this concept also in the liquid phase. A number of rather interesting applications could be suggested, particularly in the area of biomass-related reactions (in liquid phase), where the presence of complex reaction networks determines often rather poor selectivities.

Another area of potential large interest is related to the use of membranes to shift the equilibrium in reversible reactions. While this concept is well-established (for example, for the *in situ* removal of water during catalytic reactions in the food, pharmaceutical, cosmetics, and petrochemical sectors),³⁶⁶ the

application, particularly in liquid-phase reactions, is often limited by the low diffusion rate through the membrane, which is often the rate-limiting step. The use of these ultrafast membranes based on aligned CNTs could thus significantly potentially enhance the performances in these reversible reactions, as well as induce interesting effects on the selectivity, being that diffusivity greatly depends on molecular characteristics.

5.5. Electron-Transfer Induced Changes in the Properties of Supported Nanoparticles

Some of these nanocarbons have semiconductor characteristics,^{367,368} and it may be possible to induce changes in the reactivity of supported nanoparticles by electron-transfer. In SWCNTs a semiconductor–metal transition occurs due to Coulombic charge transfer between the metal nanoparticles (Pt and Au supported on the SWCNT) and the semiconducting SWCNTs.³⁶⁹ In subnanometer titania clusters dispersed within DWCNTs (inner diameter ranging from 1.0 to 1.5 nm), the confined titania exhibits a much higher activity than the titania particles attached on the outside walls in the epoxidation of propylene by H₂O₂,³⁷⁰ an important industrial reaction.²⁹⁴ XPS, XANES, and Raman spectroscopy data indicate electron transfer from titanium to the inner surfaces of the DWNTs.³⁷⁰ In contrast, no electron transfer has been observed for the outside titania. Combining TiO₂ with carbonaceous nanomaterials is being increasingly investigated as a means to increase photocatalytic activity and to develop novel catalysts.³⁷¹

Incorporation of low dimensional carbon nanostructures (in particular, CNTs and graphene sheets) into the semiconductor electrodes is a common approach to improve the charge collection and the photovoltaic performance of dye-sensitized solar cells (DSSC).³⁷² However, the modification of the properties of the oxide semiconductor by the interaction with nanocarbon is an aspect not well investigated. We reviewed recently the importance of the electron transfer mechanism from TiO₂ nanoparticles to CNTs in determining the performances of dye-sensitized solar cells.^{20,21} Recently, the effect of incorporation of different types of SWCNTs (pristine, metallic, and semiconducting) into TiO₂ photoanodes to improve the DSSC was studied.³⁷³ Although all three types of SWCNTs are found to have comparable structural morphologies and a reduced charge transport resistivity for the photoanodes, only the semiconducting one has a large effect on improving the DSSC performances, in agreement with above indications. A better understanding of the nature of the interaction between nanocarbons and semiconductor nanoparticles would be necessary to improve the performances of these solar cells and to develop novel catalysts. There are many aspects in the design of nanocarbon–semiconductor hybrid materials for catalytic and energy applications that allow the development of materials with potential higher performances, but the following deserve more attention:^{374,375}

(1) The nanocarbon offers an effective way for an efficient dispersion of the semiconductor, preventing agglomeration but also providing an hierachic structure for efficient light harvesting and eventually easy access from gas/liquid-phase components (in photocatalytic reactions) or electrolyte (in DSSC).

(2) The interfacial interaction between the nanocarbon and semiconductor particle stabilizes different morphologies for the

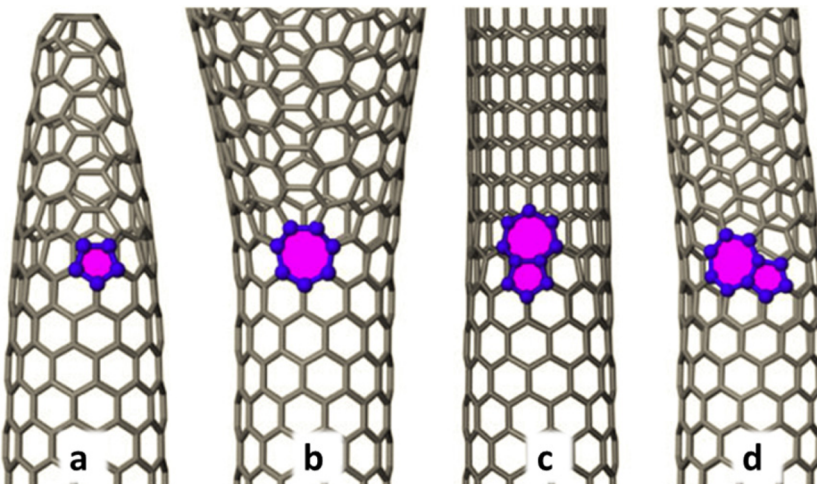


Figure 20. An isolated pentagon turns a (10,0) SWCNT into a cone shape (a) and a heptagon turns it into a horn (b). A 5/7 defect that, along the direction of the tube axis, changes the chirality of the tube to (9,0) (c) and a 5/7 with a different orientation changes the tube to (9,1) (d). Adapted from ref 377.

supported semiconductor nanoparticle, which in turn influence the performances.

(3) The interaction of semiconductor with nanocarbon induces a modification of the intrinsic properties of semiconductor particles (band gap, charge carrier density, lifetime of charge separation, nonradiative paths, etc.) as well as of the surface properties.

(4) Carbon nanodots and other carbon surface species may act as efficient solid-state sensitizers to promote visible light absorption. Carbon may also dope the semiconductor (TiO_2), inducing a shift in the band edge toward the visible region.

(5) Nanocarbons may show excellent electronic conductivity, but defects and other aspects can decrease largely the conductivity.

(6) Nanocarbon hybrids with semiconductors can act as a sink for electrons, enhancing the lifetime of charge separation. Fermi levels of the nanocarbons are generally below the conduction band minimum of most semiconductors. However, depending on the specific characteristics of the nanocarbons, the Fermi level may also be above that of TiO_2 .

(7) Due to their thermal conductivity, nanocarbons can help maintain a more uniform temperature of the semiconductor–nanocarbon hybrid upon irradiation.

(8) A further role of nanocarbon is to provide an optimal nanoarchitecture in the photoanode for light absorption.

There are thus various aspects, some positive and others negative, which have to be all considered for a proper design. As a consequence, there is no a simple relation between conductivity of nanocarbons and the promotion effect in TiO_2 photoelectrodes or -catalysts.

Controlling the effective charge on supported nanoparticles through the semiconductor nanocarbon can be used in principle to modify the catalytic reactivity, although the influence of the redox reaction (typically present during catalytic reactions) on this effect has to be verified. The combination of nanocarbon with inorganic nanostructures to develop hybrid architectures is an area of rising interest both from the scientific and application points of view.^{30,374,376}

These hybrid architectures find an increasing interest in many fields ranging from energy storage and conversion, to catalysis, sensing, and medical diagnosis and treatment. In the field of energy conversion, there is also an urgent need to develop

novel nanocarbon-based materials, in particular for fuel and solar cells.³⁷⁵ In terms of application, nanocarbons for polymer solar cells appear as one of the main drivers for research in the short–medium term, while solar fuel cells, to develop PEC and artificial-leaf type devices, are a priority in a longer-term vision.

5.6. Defect-Related Catalytic Reactivity

The previous sections have already pointed out the role of defects in nanocarbons and on their surface reactivity. This is an unique characteristic of these materials, because a higher number of defects is possible in nanocarbons with respect to most of other types of catalysts (in oxides, for example, a higher concentration of defects leads typically to a structural rearrangement) due to the capability of graphitic networks to reorganize their structures. As illustrated in Figure 20a,b, an isolated pentagon turns a SWCNT into a sharp cone and a heptagon turns a SWCNT into a horn.³⁷⁷ A pentagon–heptagon pair (5/7), one of the simplest and most common type of defects, changes the tube's chirality in SWCNTs. As shown in Figure 20c,d, two 5/7 pairs with different orientations change a (10,0) SWCNT into a (9,0) and (9,1) one, respectively.³⁷⁷ The formation energies of a 5/7 defect site in SWCNTs depends on the tube diameter, but it is low, ranging between 2 and 4 eV.

Defect healing (the process of defect removal during growth) is a condition for chirality-controlled SWCNT growth.³⁷⁸ It is also known that the conditions of CNT growth (temperature, precursor pressure, etc.)³⁷⁹ and the rate of CNT length increase³⁷⁹ influence the defect density. Hembra and Roa³⁸⁰ proposed a generalized model for the growth of defective MWCNTs. It is also known that low-energy irradiation is a tool to further modify postsynthesis concentration and types of defects in CNTs.³⁸¹ There are thus different tools for nanoengineering of CNTs in terms of defects (type and concentration), and it is known that defects in nanocarbons play a relevant role on the catalytic reactivity,³⁸² as shown before and further below.

Tessonner et al.³⁸³ showed that defects in carbon nanotubes mediate their functionalization and are thus important for the design of single-site basic heterogeneous catalysts (to be used in biomass conversion). Chen and Jafvert³⁸⁴ showed how the

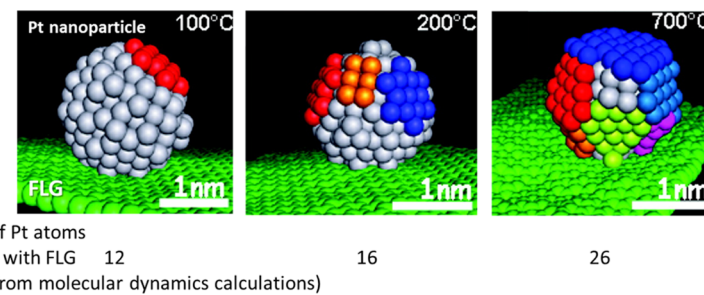


Figure 21. Configuration of Pt nanoparticles sitting on defects of FLG layer (estimated from molecular dynamics simulations) as a function of the annealing temperatures (the different colorations for the Pt atoms denote their attachment to the [111] crystallographic planes; the fraction of Pt atoms in contact with FLG support is reported below). Adapted from ref 390.

CNT characteristics (diameter, chirality, number and type of defects, functionalization, etc.) determine the production of reactive oxygen species during irradiation and in turn the photocatalytic activity of these materials. Luo et al.³⁸⁵ reported that highly defective CNTs show high photocatalytic activity for this reason, but also because defects introduce the capability to operate also in the range of visible light, through probably the mechanisms discussed before of creating semiconducting patches. Gray and co-workers³⁸⁶ instead indicated that graphene nanoplatelets with the lower defect densities are preferable to form nanocomposites with titania active in the photoreduction of CO₂, especially under visible light. This different role of defects is reasonably related to the different prevailing mechanisms of promotion of the catalytic behavior, being the generation of active centers in the first case and the enhancement of electron mobility (facilitating the diffusion of photoexcited electrons to reactive sites) in the second case. Similarly, Huang et al.³⁸⁷ indicate the need of low-defect MWCNTs to prepare high-performance electrocatalyst for direct methanol fuel cells, because the low-defect MWCNTs exhibit higher electrical conductivity. This contrasts with the other literature results discussed before on the role of defects to prepare highly active electrodes for fuel cells.

The problem lies clearly in the fact that the introduction of defects in nanocarbon modifies several properties, from the surface reactivity to the surface mobility of adspecies, the electron conductivity, the surface hydrophilicity, etc. All these aspects have to be analyzed in depth to determine the relation with the catalytic behavior and/or the relative contribution to the catalytic performances.

Few studies have analyzed in a more comprehensive way how the presence of these defects influences the properties relevant for the catalytic behavior of nanocarbons. Centi et al.³⁸⁸ have investigated this aspect in relation to the use of CNTs in PEM electrodes. The presence of defects, induced mechanically by ball-milling, was shown to influence several properties, including the dispersion of supported Pt nanoparticles. The performance could be not correlated to the geometrical surface area of the Pt particles, nor to the electrochemical active surface area. The presence of defects enhanced the amount of surface functional groups on CNTs, influencing (i) the contact interface between the CNT (on which the active metal nanoparticles are supported), (ii) the surface mobility of protons, (iii) the adsorption of water, and (iv) the chemisorption of gas reactants. In addition, as commented before, the presence of defects modifies the electron conductivity. In PEM fuel cell electrodes, a critical parameter governing the cell efficiency, especially at high power densities,

is the three-phase boundary between the electron (transported to the metal nanoparticle active site through the carbon conductive substrate, the protons being transported through the proton-conductive membrane and then surface diffusing to the metal nanoparticle) and the gas-phase reactant. It is thus evident how many aspects, not fully rationalized, determine the relationship between the presence of defects in nanocarbon and performances in PEM fuel cells, but experiments have to be made under relevant experimental conditions.

The presence of defects in nanocarbon, influencing the nature and dispersion of supported metal nanoparticles, modifies also the intrinsic reactivity. Centi et al.³⁸⁸ showed that, in the presence of defects, supported Pt nanoparticles show an enhanced tolerance to deactivation by CO in PEM fuel cells. This aspect was further demonstrated recently by Kim and Jhi,³⁸⁹ who reported ab initio calculations to demonstrate the presence of CO-tolerant platinum nanoparticles on defect-engineered graphene. Pt d-band center is a key parameter that is tailored by such defect formation.

Defects also play a critical role in stabilizing metal nanoparticles. This is an area of critical relevance for catalysis, although still at the beginning in terms of systematic investigation. It is worth mentioning in this area the recent elegant work of Pham-Huu and co-workers³⁹⁰ regarding the evolution of Pt nanoparticles on FLG support in the high-temperature range. These authors have evidenced the relatively high reactivity of the graphene border and basal plane to anchor metal nanoparticles. This interaction seems to be strong enough to prevent metal nanoparticles from sintering, even under high thermal annealing temperature (600–700 °C). By *in situ* TEM they have demonstrated that Pt nanoparticles chemically deposited on a highly defected few-layer graphene (FLG) support with nanoparticles located preferentially at the topographical defects (as shown by electron tomography) show a reduced rate of surface diffusion and sintering. Such defects can be seen as paths for NP diffusion and subsequent sintering and appear to stabilize the particle size and shape, even at high temperatures such as 600–700 °C. The suggested mechanism is that the presence of oxygen and carboxyl groups preferentially at the edges of FLG determines the preferential localization of the metal nanoparticles in the low-temperature range. In the high-temperature range, the nanoparticles diffuse along these topological defects. The interaction energy between the nanoparticles and the support increases with the temperature in the same manner as the number of metallic atoms in contact with the support, as highlighted by the molecular dynamics calculations. They also observed that the oxygen-free defect sites localized at the FLG edges also participate in the

anchoring and stabilization of metal clusters during high-temperature annealing. These defect sites can be generated by catalytic cutting of FLG with iron clusters to form trenches across the support surface before depositing the active-phase metal clusters. Therefore, the preparation method determines the type of defects present in nanocarbons, and this is a way to control the stability of supported metal particles.

The diffusion and coalesce of metal nanoparticles along these defects determines also a change in their shape, from nearly spherical Pt nanoparticles with average sizes of 2 nm located preferentially at the support topographical defects (e.g., steps and edges) to more facets nanoparticles (of average size about 5 nm) showing a larger number of Pt atoms in contact with the one-layer graphene support (Figure 21). This is the motivation for the higher interaction energy between the metal nanoparticle and FLG support.

5.7. Catalysis by Two-Dimensional Carbon Nanomaterials

Research on the catalytic use of graphene and other two-dimensional sp^2 -hybridized carbon nanomaterials,^{42,43,61,391–400} particularly graphite oxide (GO) and graphene oxide (frequently used as precursors to obtain graphene-like materials, as discussed in section 2.2), has significantly increased over the last 5 years, following the general trend in chemistry, physics, and materials science and engineering after the seminal report by Geim and co-workers.¹¹⁹ Already various examples have been discussed in the previous sections, particularly in relation to the use of surface functionalized graphene and graphene-like materials as supports for catalytically active transition metals. These supports allow one to prepare interesting catalysts, but care has to be taken in considering the practical use. For example, Mülhaupt and co-workers⁴⁰¹ reported that palladium nanoparticles dispersed on graphite oxide (prepared by immobilization of Pd^{2+} on graphite oxide via cation exchange and subsequent chemical reduction) catalyze the Suzuki–Miyaura coupling reactions with turnover frequencies up to over 39 000 h^{-1} . Even though these authors indicate these catalysts as an attractive alternative to commercially available palladium-based catalysts such as Pd on charcoal, the loss of activity (conversion decreases from 100% to 19% in four cycles) and the comparison on more practical bases (activity per total catalyst weight instead of turnover frequencies) as well as the difficulty in shaping these catalysts in the form of suitable materials for industrial reactor uses and their cost indicate that more research is needed before the possible use of these catalysts.

For catalytic applications, it is thus preferable to investigate the use of these materials in areas for which conventional carbon-based catalysts (or other catalysts as well) do not show good performances, because in this case new possibilities are open, less depending on a strict cost-performance comparison. From this perspective, the use of nanocarbons as metal-free catalysts is rather interesting, avoiding the problems of leaching of supported metal particles in liquid-phase reactions and opening new routes in terms of patents, in addition to the other advantages discussed in section 5.3. We focus discussion in this section on the use of GO and graphene oxide particularly in organic syntheses and polymerization reactions to complement the picture presented in section 5.3 focused on potentially industrial applications of other nanocarbon materials. GO and graphene oxide can be produced with relatively low cost methods from graphite, using potassium permanganate and sodium nitrate in concentrated sulfuric acid (Hummers

method) or strong acids (e.g., sulfuric or nitric acid) and potassium or sodium chloride (Brodie and Staudenmaier methods), although the industrial use of these methods poses severe problems due to harsh conditions and environmental impact. Nevertheless, these materials can be considered as potentially low-cost carbon materials suitable for industrial exploitation. These treatments produce delamination/exfoliation and oxidation of the graphite sheets, with the transformation from a hydrophobic to a hydrophilic material. The obtained materials are characterized from the presence of oxygen-containing functional groups that catalyze oxidation or acid reactions, as discussed in section 5.3, as well as defects like nanovoids and vacancies, which may play a role in the activation of small molecules by a spin flip process. In addition, the aromatic scaffold provides a template to anchor active species such as organocatalysts or other functional groups that may synergistically interact with GO sites and/or adsorbing molecules to enhance the catalytic performances.

Bielawski and co-workers⁷⁶ were among the first groups investigating the reactivity of GO for various synthetic reactions. The authors demonstrated the efficient oxidation of benzyl alcohol to benzaldehyde in the presence of GO as a heterogeneous catalyst. Although the work opened the use of GO in various other catalytic reactions, it has to be mentioned that turnover numbers (TON) were quite low (about 1×10^{-2}), and yields above 80% in benzaldehyde require catalyst loading above 100% wt (thus by definition not a catalytic reaction), temperatures above 100 °C, and reaction times of several hours. The benzyl alcohol to benzaldehyde transformation could be realized selectively under similar conditions, but with significantly faster reaction rates, using radical mechanisms catalyzed by Co^{2+} and Mn^{2+} ions. Bielawski and co-workers⁷⁶ exclude the presence of radical species by adding butylated hydroxytoluene, a known radical inhibitor. However, the large amount of catalyst necessary and the slow rates of reaction do not allow one to exclude that the catalytic behavior is associated with the presence of traces of metals in GO. It is worth mentioning, however, that various other benzylic and aliphatic alcohols could be converted selectively to their respective aldehyde or ketone products using GO,⁷⁶ although large amounts of GO (200 wt % GO) are necessary as well as long times of reaction (24 h at 100 °C). Also unsaturated hydrocarbons, such as *cis*-stilbene, could be oxidized to the corresponding dione, while alkynes under similar conditions are converted to their respective hydration products.

GO also catalyzes at about 60 °C the ring-opening polymerization of various cyclic lactones and lactames, such as ϵ -caprolactone, δ -valerolactone, and ϵ -caprolactam.⁴⁰² The idea is that in this way it is possible to obtain directly in one step a carbon-reinforced composite, where the monomer may be reacted directly with the carbon (GO) that ultimately acts as the composite reinforcer. The resulting polymers show moderate average molecular weights (4.8–12.8 kDa) with a homogeneous dispersion of GO that transforms from the lamellar structure commonly observed for GO primarily into multiwalled fullerenes. The long reaction times (14 h at 60% with 10 wt % GO) and low molecular weight of the obtained polymeric material indicate the need to improve the method and characteristics of the produced composites, particularly with respect to an industrial process.

GO is also active in the polymerization of various olefin monomers, including *n*-butyl vinyl ether, *N*-vinylcarbazole, styrene, and sodium 4-styrenesulfonate.⁴⁰³ The GO-catalyzed

polymerization of *n*-butyl vinyl ether (0.1–5.0 wt % GO relative to monomer) proceeds rapidly under solvent-free conditions and affords polymers with moderate number-average molecular weights and broad polydispersities. GO also catalyzes the polymerization of *N*-vinylcarbazole and styrene, although only low molecular weight polymers are obtained. Sodium 4-styrenesulfonate polymerizes in the presence of GO to afford poly(sodium 4-styrenesulfonate) (PSS) composites. Also in this case, the characteristics of the polymers produced (molecular weight in the 5000–8000 Da region) and low reaction rates (about 4 h at rt to obtain about complete monomer conversion using about 1–2 wt % GO and solvent-free conditions) are still far from industrial conditions. However, the GO retained in the polymer improves the conductivity and specific capacitance of the material. Another example of application of GO as polymerization catalysts is in the conversion of benzyl alcohol to produce carbon-reinforced poly(phenylene methylene) (PPM) composites.⁴⁰⁴

Other fields of use of GO include the selective oxidation of thiols to disulfides, and sulfides to sulfoxides⁴⁰⁵ and as oxidant in a broad range of reactions,⁴⁰⁶ including the oxidation of olefins to their respective diones, methylbenzenes to their respective aldehydes, and diarylmethanes to their respective ketones. GO is also active as an autotandem oxidation–hydration–aldol coupling catalyst for the formation of chalcones in a single reaction vessel.⁴⁰⁷ Various alkynes or alcohols could be hydrated or oxidized *in situ* to their corresponding Me ketones or aldehydes, respectively, which underwent a subsequent Claisen–Schmidt condensation.

GO is thus active in various type of reactions, from organic synthesis to polymerization reactions, indicating its potentially high versatility, although more attention is necessary to compare the performances and quality of obtained products with industrial state-of-the art. The high catalyst loading necessary in some cases also puts to question whether the reaction is catalytic or stoichiometric. While for oxidation reactions it is necessary to better analyze this aspect, the use of GO as solid acid catalyst is proven and confirmed in various reactions, including Michael-type Friedel–Crafts reaction⁴⁰⁸ and aza-Michael additions.⁴⁰⁹ However, in general a careful comparison with conventional solid acid catalysts for these reactions is missing. The properties of GO can be further improved, for example, by addition of sulfonated groups to produce a water-tolerant solid acid catalyst with strongly acidic sites ($2.0 \text{ mmol}\cdot\text{g}^{-1}$).⁴¹⁰ In this case, the catalytic activity of the sulfonated graphene was shown to have better performance than NRSO, a commercial solid acid for hydrolysis of ethyl acetate.

Recently, reduced GO (rGO) has been found to be a reusable and efficient catalyst for the hydrogenation of nitrobenzene.³⁰⁶ rGO shows comparable reactivity to noble metal (1% Pt) supported on SiO₂ under reflux conditions in hydrazine hydrate. The zigzag edges of rGO are suggested to be the catalytically active sites. Mechanistic insights from DFT calculations suggest that interaction between carbon atoms at the zigzag edges and terminal oxygen atoms of nitrobenzene weakens the N–O bond. In the oxidation of benzyl alcohol to benzaldehyde, DFT calculations⁴¹¹ instead indicate that the reaction occurred via the transfer of hydrogen atoms from the organic molecule to the GO surface. In particular, the neighboring epoxide groups that decorate the GO basal plane were ring-opened, which resulted in the formation of diols, followed by dehydration.

The great potential of graphene-like materials as a catalyst material⁴¹³ lies in the synergistic interaction they can have with enzyme, organocatalyst, electrocatalyst, and photocatalyst. The physical binding between GO and conjugated polymer, organometallic catalyst, or organic dye ranges from covalent binding or noncovalent binding to long-range interactions in solutions.⁴³ Enhanced conversion and yield were obtained compared with the case when GO was absent. The examples include GO hybridized with poly(3-hexylthiophene-2,5-diyl) (P3HT) to form a charge transfer complex.⁴¹² In the photocatalytic Mannich reaction, the catalytic yield of GO–P3HT (2.5 wt %) is 93% (same weight P3HT, 65%), which is markedly superior to that of TiO₂ (P25) (33.5 wt %, 58%), a known standard photocatalyst. The cooperative interaction allows the P3HT/GO to function as a dyad in photocatalysis. The reaction is initiated by photoexcited electron and hole pairs of P3HT. The tertiary amine is oxidized by the positive hole on the HOMO of P3HT via single electron transfer to form the radical cation. At the same time, the excited electron is injected from the LUMO of P3HT into GO, which is then used to activate molecular oxygen to form the dioxygen radical anion, the latter being stabilized by the aromatic scaffold in GO. There is thus a synergistic effect between P3HT and GO, which may be generalized, suggesting that GO scaffold can potentially act as an efficient electron relay for photoexcited holes generated in a wide range of organic dyes.

rGO–metalloporphyrin hybrid shows rather interesting performances in ORR. Iron–porphyrin is known to facilitate ORR via four-electron reaction with water.⁴¹³ rGO shows poor performances in ORR, but the GO–metalloporphyrin composite has a rather interesting behavior. The overpotential for ORR in the GO–metalloporphyrin is shifted positively by 120 mV compared with GO, and the ORR current density of the composite is higher than that of either GO or MOF constructed from porphyrin alone. These improvements in catalytic activities can be explained by the synergistic effects of framework porosity, a larger bond polarity due to nitrogen ligand in the pyridinium-terminated GO, and the catalytically active iron–porphyrin in the hybrid MOF. Furthermore, methanol crossover is minimized due to the inactivity of the hybrid MOF for methanol oxidation.

Graphene and graphene-like materials have thus the potential to be main players in catalysis.⁴¹⁴ GO can be readily functionalized, making it useful in a wide range of synthetic reactions, but more care has to be given to analyze when these catalysts show real better performances with respect to state-of-the-art and the industrial scalability and economic viability. On the other hand, new possibilities and concepts, particularly in terms of nanocarbon hybrids, are continuously reported in literature, showing the richness of the catalytic chemistry of these materials.

6. CONCLUDING REMARKS AND PERSPECTIVES

The growing knowledge on the (i) controlled synthesis (in terms of not only the type of materials and nanoarchitecture but especially uniform characteristics, including type and density of defects), (ii) post-treatment procedures to introduce controlled doping and surface functional sites, and especially (iii) an advanced understanding of the nature of defects and surface functional groups by combining novel characterization methodologies to theoretical modeling have completely changed the landscape and perspectives for the use of nanocarbons as conceptually new catalysts or catalytic supports.

Due to the lack of understanding of the rich surface chemistry of nanocarbons, their possible application in industrial catalysts has been considered questionable. In fact, besides the argument about their cost, their use as catalysts or catalytic support gives rise to contradictory results.

From one side, the mass production of CNTs and other types of nanocarbons now makes them available in large amounts at competitive costs. From the other side, a number of rather interesting applications, both for metal-free nanocarbons and metal nanoparticles supported over nanocarbons, were thoroughly investigated in the past decade. Some examples discussed here are their use in ORR and advanced electrodes, as well as in selective oxidation and hydrogenation reactions. In addition, a detailed understanding of the surface properties of defect and other functional sites in nanocarbon and the possibility of their tailored tuning have opened the door to a new development area for catalysis. The examples discussed show clearly that they can be considered as a new class of catalysts, with reaction mechanisms and active sites different from those of most of the current catalysts and which show for this reason very interesting properties in some challenging reactions such as methane direct oxidation to methanol and benzene direct oxidation to phenol.

We have remarked, however, that systematic studies of the relationship between the nature of the active sites in nanocarbons and their catalytic reactivity are still limited. This is a direction in which research should be intensified. The reactivity of nanocarbons is largely associated with the presence of defects and edge sites, doping heteroatoms, and the interaction between these sites. Although conclusive evidence on the nature of these sites and their catalytic reactivity is still missing, also because *in situ/operando* studies are lacking, large progress in this direction has been definitively made in the last years. We have to remark, however, that often many aspects relevant to the catalytic behavior are influenced by defects and heteroatoms. This complexity has not always been correctly taken into account.

The role of architecture engineering of nanocarbons for catalytic applications (carbon hierarchy and macroscopic shaping of nanocarbons) was emphasized also. This is a bottleneck to expand their application in industrial catalysis, but the possibility to synergistically combine the properties of different nanocarbons also exists. This is a research area on which already various studies are present, but which should be further intensified.

The characterization and modeling are clearly the key enabling elements for a rational design of nanocarbons in advanced catalytic applications. This is a fast growing area. Spectacular developments in microscopy are opening completely new possibilities (aberration-corrected TEM, 4D electron microscopy, electron tomography, dynamic TEM, etc.), but only by combining these methods with other advanced characterizations and theoretical modeling as well is it possible to understand in detail the surface chemistry of nanocarbons, as shown here. However, it should be remarked that a gap still exists between well-defined nanocarbon materials and those used as catalysts.

In the section related to the use of nanocarbons in catalysis, a number of different aspects were highlighted: (i) enhanced characteristics as a support for catalytic functionalities, (ii) stabilization of small catalytic particles with enhanced catalytic behavior, (iii) the direct catalytic role of nanocarbon functional groups, (iv) nanoconfinement, (v) electron-transfer-induced

changes in the properties of supported nanoparticles, and (vi) defect-related catalytic reactivity. Although the mechanistic understanding of these aspects has made giant progress with respect to a decade ago, it is evident that still further effort is necessary. The next step is to take advantage of the unique possibility in nanocarbons for the tuning of their characteristics, largely related to the flexibility of their nanostructure to account for different types of defects, heteroatoms, and functional groups. It is thus necessary to focus on the design of nanocarbons and their nanoengineering to develop novel active and selective catalysts.

This review thus forecasts a bright future in catalysis by nanocarbon-based materials, which can be considered an emerging and conceptually new area of catalytic materials but also remarks that to foster their larger-scale industrial use it is necessary to put on a stronger rational basis for the exploitation of their nanoscale-dependent, unique features. Not discussed in this review is the work to prepare nanocarbon via an organic route, an effort to *synthesize* nanocarbon catalysts with desired molecular and functional structure, a new direction that is worth following.

AUTHOR INFORMATION

Corresponding Author

*E-mail: dssu@imr.ac.cn, dangsheng@fhi-berlin.mpg.de (D.S.S.), centi@unime.it (G.C.).

Author Contributions

The manuscript was written through contributions of all the authors. All authors have given approval to the final version of the manuscript.

Notes

The authors declare no competing financial interest.

Biographies



Dang Sheng Su completed his Ph.D. at the Technical University of Vienna (Vienna, Austria) in 1991, and then moved to the Fritz Haber Institute (FHI) of the Max Planck Society in Berlin, Germany, as a postdoctoral fellow in the Department of Electron Microscopy. After a short stay at the Hahn Meitner Institut GmbH and the Humboldt Universität zu Berlin (Berlin, Germany), he rejoined the FHI in 1999, where he worked on nanomaterials in heterogeneous catalysis and energy storage until 2011. He is now a Professor and Head of the Catalysis and Materials Division of the Shenyang National Laboratory for Materials Science, Institute of Metal Research, Chinese Academy of Sciences, Shenyang, PR China. His research interests are nanomaterials and nanocatalysis, energy storage and conversion, electron microscopy, and electron energy-loss spectroscopy.



Siglinda Perathoner took her degree in Chemistry at the University of Bologna (Bologna, Italy) in 1984 and her Ph.D. in Chemical Science in 1988 working on photophysics and photochemistry of supramolecular systems. From 2001 she joined the University of Messina and is Associate Professor of Industrial Chemistry presently. Her recent research interests include nanostructured zeolites, catalytic membranes, catalysts for wastewater purification and remediation, photo-(electro)catalytic conversion of carbon dioxide, and fuel cells.



Gabriele Centi completed his industrial chemistry studies at the University of Bologna (Bologna, Italy) and is actually Professor of Industrial Chemistry at the University of Messina (Messina, Italy). He is a former President of the European Federation of Catalysis Societies, and was Coordinator of the European Network of Excellence on Catalysis IDECAT. He is Co-Chairman of the Editorial Board of *ChemSusChem* and Chief Editor of the book series *Studies in Surface Science and Catalysis* (Elsevier) and *Green Energy* (De Gruyter). His research interests lie in the development of industrial heterogeneous catalysts for sustainable chemical processes, environmental protection, and clean energy.

ACKNOWLEDGMENTS

D.S.S. is thankful for the financial support of MOST (2011CBA00504), NSFC (21133010, 212111074, 50921004) of China. D.S.S. also thanks the Liaoning province government, China, for financial support.

ABBREVIATIONS USED

AA, adipic acid; AC, active carbon; APPES, ambient pressure photoelectron spectroscopy; BET, Brunauer–Emmett–Teller (indicates the methodology for determining surface area and porosity by physical N₂ multilayer adsorption using the BET theory); B-CNT, boron-doped carbon nanotube; BNNT, boron nitride nanotube; BTA, benzotriazole; CB, carbon

black; CNF, carbon nanofiber; CNNT, carbon nitride nanotube; CNT, carbon nanotube; Da, dalton, unit of measure of molar mass; DFT, density functional theory; DWCNT, double wall carbon nanotube; FLG, Fe layer graphene; GO, graphite oxide; HRTEM, high-resolution transmission electron microscopy; MOF, metal–organic framework; MWCNT, multiwall carbon nanotube; N-CNT, nitrogen-functionalized carbon nanotube; KA oil, mixture of cyclohexanol and cyclohexanone; ODH, oxidative dehydrogenation (for example, the reaction of ethylbenzene to styrene); OMC, ordered mesoporous carbon; OMS, ordered mesoporous silica (for example, MCM-41 and SBA-15); ORR, oxygen reduction reaction (occurs in the anode of proton–electrolyte–membrane fuel cells); P2S, a commercial type of titania; P3HT, poly(3-hexylthiophene-2,5-diyl); PEM, proton exchange membrane; PVP, poly(1-vinyl-2-pyrrolidone); rGO, reduced graphite oxide; rt, room temperature; SEM, scanning electron microscopy; SWCNT, single wall carbon nanotube; TEM, transmission electron microscopy; TPD-MS, temperature-programmed desorption mass spectrometry; TP-XPS, temperature-programmed X-ray photoelectron spectroscopy; STEM, scanning transmission electron microscopy; XPS, X-ray photoelectron spectroscopy.

REFERENCES

- (1) Vilatela, J. J.; Eder, D. *ChemSusChem* **2012**, *5*, 456.
- (2) D’Souza, F.; Ito, O. *Chem. Soc. Rev.* **2012**, *41*, 86.
- (3) Rahman, A.; Ali, I.; Al Zahrani, S. M.; Eleithy, R. H. *NANO* **2011**, *6*, 185.
- (4) Roth, S.; Park, H. *J. Chem. Soc. Rev.* **2010**, *39*, 2477.
- (5) Zhao, M.-Q.; Zhang, Q.; Huang, J.-Q.; Wei, F. *Adv. Funct. Mater.* **2012**, *22*, 675.
- (6) Su, D. S. *ChemSusChem* **2009**, *2*, 1009.
- (7) Enoki, T.; Takai, K.; Osipov, V.; Baidakova, M.; Vul, A. *Chem.-Asian J.* **2009**, *4*, 796.
- (8) Rao, C. N. R.; Biswas, K.; Subrahmanyam, K. S.; Govindaraj, A. *J. Mater. Chem.* **2009**, *19*, 2457.
- (9) Su, D. S.; Schlögl, R. *ChemSusChem* **2010**, *3*, 136.
- (10) Balandin, A. *Nat. Mater.* **2011**, *10*, 569.
- (11) Lee, S. W.; Gallant, B. M.; Byon, H. R.; Hammond, P. T.; Yang, S.-H. *Energy Environ. Sci.* **2011**, *4*, 1972.
- (12) Hoheisel, T. N.; Schrettl, S.; Szillarweit, R.; Frauenrath, H. *Angew. Chem., Int. Ed.* **2010**, *49*, 6496.
- (13) Bitter, J. H. *J. Mater. Chem.* **2010**, *20*, 7312.
- (14) Centi, G.; Perathoner, S. *Catal. Today* **2010**, *150*, 151.
- (15) Ryoo, R.; Joo, S. H. *Stud. Surf. Sci. Catal.* **2004**, *148*, 241.
- (16) Liang, C.; Li, Z.; Dai, S. *Angew. Chem., Int. Ed.* **2008**, *47*, 3696.
- (17) Wan, Y.; Shi, Y.; Zhao, D. *Chem. Mater.* **2008**, *20*, 932.
- (18) Chang, H.; Joo, S. H.; Pak, C. J. *Mater. Chem.* **2007**, *17*, 3078.
- (19) Lee, J.; Kim, J.; Hyeon, T. *Adv. Mater.* **2006**, *18*, 2073.
- (20) Centi, G.; Perathoner, S. *ChemSusChem* **2011**, *4*, 913.
- (21) Centi, G.; Perathoner, S. *Eur. J. Inorg. Chem.* **2009**, *26*, 3851.
- (22) Ghosh, A.; Lee, Y. H. *ChemSusChem* **2012**, *5*, 480.
- (23) Liang, Y.; Wang, H.; Zhou, J.; Li, Y.; Wang, J.; Regier, T.; Dai, H. J. *Am. Chem. Soc.* **2012**, *134*, 3517.
- (24) Bose, S.; Kuila, T.; Mishra, A. K.; Rajasekar, R.; Kim, N. H.; Lee, J. H. *J. Mater. Chem.* **2012**, *22*, 767.
- (25) Campuzano, S.; Wang, J. *Electroanalysis* **2011**, *23*, 1289.
- (26) Pan, X.; Bao, X. *Acc. Chem. Res.* **2011**, *44*, 553.
- (27) Pan, X.; Bao, X. *Chem. Commun.* **2008**, *47*, 6271.
- (28) Marquis, F. D. S. *JOM* **2011**, *63*, 48.
- (29) Guerra, J.; Herrero, M. A. *Nanoscale* **2010**, *2*, 1390.
- (30) Eder, D. *Chem. Rev.* **2010**, *110*, 1348.
- (31) Wang, J.; Blau, W. J. *J. Opt. A: Pure Appl. Opt.* **2009**, *11*, 024001/1.
- (32) Bensaid, S.; Centi, G.; Garrone, E.; Perathoner, S.; Saracco, G. *ChemSusChem* **2012**, *5*, 500.
- (33) Komatsu, N. *Jpn. Petrol. Inst.* **2009**, *52*, 73.

- (34) Patel, V. Global carbon nanotubes market—Industry beckons. *Nanowerk Spotlight* **2013**. Accessed on Jan 10, 2013: <http://www.nanowerk.com/spotlight/spotid=23118.php>
- (35) Pahmy, R. H.; Mohamed, A. R. *Recent Pat. Eng.* **2012**, *6*, 31.
- (36) Yang, Y.; Chiang, K.; Burke, N. *Catal. Today* **2011**, *178*, 197.
- (37) Mabena, L. F.; Sinha Ray, S.; Mhlanga, S. D.; Coville, N. J. *J. Appl. Nanosci.* **2011**, *1*, 67.
- (38) Oosthuizen, R. S.; Nyamori, V. O. *Platinum Met. Rev.* **2011**, *55*, 154.
- (39) Castillejos, E.; Serp, P. Carbon nanotubes for catalytic applications. In *Carbon Nanotubes and Related Structures*; Guldin, D. M., Martin, N., Eds.; Wiley-VCH: Weinheim, Germany, 2010; p 321.
- (40) Upare, D. P.; Yoon, S.; Lee, C. W. *Korean J. Chem. Eng.* **2011**, *28*, 731.
- (41) Wu, B.; Kuang, Y.; Zhang, X.; Chen, J. *Nano Today* **2011**, *6*, 75.
- (42) Dreyer, D. R.; Bielawski, C. W. *Chem. Sci.* **2011**, *2*, 1233.
- (43) Su, C.; Loh, K. P. Carbocatalysis: Graphene oxide and its derivatives. *Acc. Chem. Res.* **2013**, DOI: 10.1021/ar300118v.
- (44) Wang, Y.; Wang, X. C.; Antonietti, M. *Angew. Chem., Int. Ed.* **2012**, *51*, 68.
- (45) Zhang, Q.; Huang, J.-Q.; Zhao, M.-Q.; Qian, W.-Z.; Wei, F. *ChemSusChem* **2011**, *4*, 864.
- (46) Wei, F.; Zhang, Q.; Qian, W.-Z.; Yu, H.; Wang, Y.; Luo, G.-H.; Xu, G.-H.; Wang, D. Z. *Powder Technol.* **2008**, *183*, 10.
- (47) Kumar, M.; Ando, Y. J. *Nanosci. Nanotechnol.* **2010**, *10*, 3739.
- (48) Calvino-Casilda, V.; Lopez-Peinado, A. J.; Duran-Valle, C. J.; Martin-Aranda, R. M. *Catal. Rev. Sci. Eng.* **2010**, *52*, 325.
- (49) Daud, W. M. A. W.; Houshamnd, A. H. *J. Nat. Gas Chem.* **2010**, *19*, 267.
- (50) Bandosz, T. J. Surface chemistry of carbon materials. In *Carbon Materials for Catalysis*; Serp, P., Figueiredo, J. L., Eds.; Wiley & Sons: Hoboken, NJ, 2009; p 45.
- (51) Peigney, A.; Laurent, Ch.; Flahaut, E.; Bacsa, R. R.; Rousset, A. *Carbon* **2001**, *39*, 507.
- (52) Tessonner, J.-P.; Su, D. S. *ChemSusChem* **2011**, *4*, 824.
- (53) Ncibi, M. C.; Mahjoub, B.; Seffen, M.; Gaspard, S. *Recent Pat. Chem. Eng.* **2008**, *1*, 126.
- (54) Hou, P. X.; Liu, C.; Cheng, H. M. *Carbon* **2008**, *46*, 2003.
- (55) Villa, A.; Wang, D.; Dimitratos, N.; Su, D. S.; Trevisan, V.; Prati, L. *Catal. Today* **2010**, *150*, 8.
- (56) Serp, P.; Corrius, M.; Kalck, P. *Appl. Catal. A* **2003**, *253*, 337.
- (57) Frank, B.; Rinaldi, A.; Blume, R.; Schlägl, R.; Su, D. S. *Chem. Mater.* **2010**, *22*, 4462.
- (58) Aksel, S.; Eder, D. J. *Mater. Chem.* **2010**, *20*, 9149.
- (59) Bandaru, P. R. *J. Nanosci. Nanotechnol.* **2007**, *7*, 1.
- (60) Wen, M.; Sun, X.; Su, L.; Shen, J.; Li, J.; Guo, S. *Polymer* **2012**, *53*, 1602.
- (61) Pyun, J. *Angew. Chem., Int. Ed.* **2011**, *50*, 46.
- (62) Resasco, D. E. Carbon nanotubes and related structures. In *Nanoscale Materials in Chemistry*, 2nd ed.; Klabunde, K. J., Richards, R. M., Eds.; John Wiley & Sons, Inc.: Hoboken, NJ, 2009; p 443.
- (63) Su, D. S.; Centi, G. Carbon nanotubes for energy applications. In *Nanoporous Materials for Energy and the Environment*; Rios, G., Centi, G., Kanellopoulos, N., Eds.; Pan Stanford: Singapore, 2012; p 173.
- (64) Yu, S.-S.; Zheng, W.-T. *Nanoscale* **2010**, *2*, 1069.
- (65) Panchakarla, L. S.; Govindaraj, A.; Rao, C. N. R. *Inorg. Chim. Acta* **2010**, *363*, 4163.
- (66) Stoyanov, S. R.; Titov, A. V.; Kral, P. *Coord. Chem. Rev.* **2009**, *293*, 2852.
- (67) Ayala, P.; Arenal, R.; Ruemmeli, M.; Rubio, A.; Pichler, T. *Carbon* **2010**, *48*, 575.
- (68) Lee, S.-H.; Lee, D.-H.; Lee, W.-J.; Kim, S.-O. *Adv. Funct. Mater.* **2011**, *21*, 1338.
- (69) Centi, G.; Perathoner, S. *Coord. Chem. Rev.* **2011**, *255*, 1480.
- (70) Lei, Y.; Yeong, K.-S.; Thong, J. T. L.; Chim, W.-K. *Chem. Mater.* **2004**, *16*, 2757.
- (71) Janowska, I.; Hajiesmaili, S.; Begin, D.; Keller, V.; Keller, N.; Ledoux, M.-J.; Pham-Huu, C. *Catal. Today* **2009**, *145*, 76.
- (72) Xiong, W.; Du, F.; Liu, Y.; Perez, A.; Supp, M.; Ramakrishnan, T. S.; Dai, L. M.; Jiang, L. *J. Am. Chem. Soc.* **2010**, *132*, 15839.
- (73) Liu, Y.; Janowska, I.; Romero, T.; Edouard, D.; Nguyen, L. D.; Ersen, O.; Keller, V.; Keller, N.; Pham-Huu, C. *Catal. Today* **2010**, *150*, 133.
- (74) Su, D. S. *ChemSusChem* **2011**, *4*, 811.
- (75) Jayatissa, A. H. High throughput carbon nanotube growth system, and carbon nanotubes and carbon nanofibers formed thereby. *PCT Int. Appl.* WO 2009145959 A1 20091203, 2009.
- (76) Dreyer, D. R.; Jia, H.-P.; Bielawski, C. W. *Angew. Chem., Int. Ed.* **2010**, *49*, 6813.
- (77) Schaetz, A.; Zeltner, M.; Stark, W. J. *ACS Catal.* **2012**, *2*, 1267.
- (78) Su, C.; Acik, M.; Takai, K.; Lu, J.; Hao, S.-J.; Zheng, Y.; Wu, P.; Bao, Q.; Enoki, T.; Chabal, Y. J.; Ping, L. K. *Nat. Commun.* **2012**, *3*, 1298.
- (79) Thomas, A.; Fischer, A.; Göttmann, F.; Antonietti, M.; Müller, J.-O.; Schlägl, R.; Carlsson, J. M. *J. Mater. Chem.* **2008**, *18*, 4893.
- (80) Su, D. S.; Zhang, J.; Frank, B.; Thomas, A.; Wang, X.; Paraknowitsch, J.; Schlägl, R. *ChemSusChem* **2010**, *3*, 169.
- (81) Yu, D.; Nagelli, E.; Du, F.; Dai, L. *J. Phys. Chem. Lett.* **2010**, *1*, 2165.
- (82) Harris, J. F. *Carbon Nanotube Science*, 2nd ed.; Cambridge Univ. Press: Cambridge, UK, 2011.
- (83) Tessonner, J. P.; Becker, M.; Xia, W.; Girgsdies, F.; Blume, R.; Yao, L. D.; Su, D. S.; Muhler, M.; Schlägl, R. *ChemCatChem* **2010**, *2*, 1559.
- (84) (a) Hafner, J. H.; Bronikowski, M. J.; Azamian, B. R.; Nikolaev, P.; Rinzler, A. G.; Colbert, D. T.; Smith, K. A.; Smalley, R. E. *Chem. Phys. Lett.* **1998**, *296*, 195. (b) Nikolaev, P.; Bronikowski, M. J.; Bradley, R. K.; Rohmund, F.; Colbert, D. T.; Smith, K. A.; Smalley, R. E. *Chem. Phys. Lett.* **1999**, *313*, 91.
- (85) Herrera, J. E.; Balzano, L.; Borgna, A.; Alvarez, W. E.; Resasco, D. E. *J. Catal.* **2001**, *204*, 129.
- (86) Alvarez, W. E.; Kitayanan, B.; Borgna, A.; Resasco, D. E. *Carbon* **2001**, *39*, 547.
- (87) Resasco, D. E.; Alvarez, W. E.; Pompeo, F.; Balzano, L.; Herrera, J. E.; Kitayanan, B.; Borgna, A. *J. Nanopart. Res.* **2002**, *4*, 131.
- (88) (a) Jansen, R.; Wallis, P. *Mater. Matters* **2009**, *4*, 1, 23. (b) Thayer, A. M. *C&EN* **2007**, *85*, 29.
- (89) Su, D. S.; Chen, X. W. *Angew. Chem., Int. Ed.* **2007**, *46*, 1823.
- (90) Endo, M.; Takeuchi, K.; Kim, Y. A.; Park, K. C.; Ichiki, T.; Hayashi, T.; Fukuyo, T.; Linou, S.; Su, D. S.; Terrones, M.; Dresselhaus, M. S. *ChemSusChem* **2008**, *1*, 820.
- (91) Chen, X. W.; Timpe, O.; Hamid, S. B. A.; Schlogl, R.; Su, D. S. *Carbon* **2009**, *47*, 340.
- (92) Su, D. S.; Rinaldi, A.; Frandsen, W.; Weinberg, G. *Phys. Status Solidi B* **2007**, *244*, 3916.
- (93) Su, D. S.; Chen, X. W.; Liu, X.; Delgado, J. J.; Schlogl, R.; Gajovic, A. *Adv. Mater.* **2008**, *20*, 3597.
- (94) Rinaldi, A.; Zhang, J.; Mizera, J.; Girgsdies, F.; Wang, N.; Hamid, S. B. A.; Schlogl, R.; Su, D. S. *Chem. Commun.* **2008**, *48*, 6528.
- (95) Wang, S.; Iyyamperumal, E.; Roy, A.; Xue, Y.; Yu, D.; Dai, L. *Angew. Chem., Int. Ed.* **2011**, *50*, 11756.
- (96) Ishigami, N.; Ago, H.; Motoyama, Y.; Takasaki, M.; Shinagawa, M.; Takahashi, K.; Ikuta, T.; Tsuji, M. *Chem. Commun.* **2007**, *16*, 1626.
- (97) Janowska, I.; Winé, G.; Ledoux, M.-J.; Pham-Huu, C. *J. Mol. Catal. A: Chem.* **2007**, *267*, 92.
- (98) Terrones, M.; Souza-Filho, A. G.; Rao, A. M. Doped carbon nanotubes: Synthesis, characterization and applications. In *Carbon Nanotubes*; Jorio, A., Dresselhaus, G., Dresselhaus, M. S., Eds.; Topics of Applied Physics; Springer: New York, 2008; Vol. 111, p 531.
- (99) Lyu, S. C.; Han, J. H.; Shin, K. W.; Sok, J. H. *Carbon* **2011**, *49*, 1532.
- (100) Panchakarla, L. S.; Govindaraj, A.; Rao, C. N. *ACS Nano* **2007**, *1*, 494.
- (101) Florea, I.; Ersen, O.; Arenal, R.; Ihiawakrim, D.; Messaoudi, C.; Chizari, K.; Janowska, I.; Pham-Huu, C. *J. Am. Chem. Soc.* **2012**, *134*, 9672.

- (102) (a) Podyacheva, O. Y.; Ismagilov, Z. R.; Shalagina, A. E.; Ushakov, V. A.; Shmakov, A. N.; Tsybulya, S. V.; Kriventsov, V. V.; Ischenko, A. V. *Carbon* **2010**, *48*, 2792. (b) Shalagina, A. E.; Podyacheva, O.Yu.; Kvon, R. I.; Ushakov, V. A.; Ismagilov, Z. R. *Carbon* **2007**, *45*, 1808.
- (103) van Dommelle, S.; Romero-Izquierdo, A.; Brydson, R.; de Jong, K. P.; Bitter, J. H. *Carbon* **2008**, *46*, 138.
- (104) (a) Terrones, M.; Redlich, P.; Grobert, N.; Trasobares, S.; Hsu, W. K.; Terrones, H.; Zhu, Y. Q.; Hare, J. P.; Reeves, C. L.; Cheetham, A. K.; Ruhle, M.; Kroto, H. W.; Walton, D. R. M. *Adv. Mater.* **1999**, *11*, 655. (b) Terrones, M.; Terrones, H.; Grobert, N.; Hsu, W. K.; Zhu, Y. Q.; Hare, J. P.; Kroto, H. W.; Walton, D. R. M.; Kohler-Redlich, P.; Ruhle, M.; Zhang, J. P.; Cheetham, A. K. *Appl. Phys. Lett.* **1999**, *75*, 3932.
- (105) Terrones, M.; Kamalalaran, R.; Seeger, T.; Ruhle, M. *Chem. Commun.* **2000**, *1*, 2335.
- (106) Glerup, M.; Castignolles, M.; Holzinger, M.; Hug, G.; Loiseau, A.; Bernier, P. *Chem. Commun.* **2003**, 2542.
- (107) Kudasov, A. G.; Okotrub, A. V.; Bulusheva, L. G.; Asanov, I. P.; Shubin, Yu.V.; Yudanov, N. F.; Yudanova, L. I.; Danilovich, V. S.; Abrosimov, O. G. *J. Phys. Chem. B* **2004**, *108*, 9048.
- (108) Tian, G.-L.; Zhao, M.-Q.; Zhang, Q.; Huang, J.-Q.; Wei, F. *Carbon* **2012**, *50*, 5323.
- (109) Sen, R.; Satishkumar, B. C.; Govindaraj, S.; Harikumar, K. R.; Renganathan, M. K.; Rao, C. N. *J. Mater. Chem.* **1997**, *7*, 2335.
- (110) Kim, D. P.; Lin, C. L.; Mihalisin, T.; Heiney, P.; Labes, M. M. *Chem. Mater.* **1991**, *3*, 686.
- (111) Liu, J.; Czerw, R.; Carroll, D. L. *J. Mater. Res.* **2005**, *20*, 538.
- (112) Huang, J.-Q.; Zhao, M.-Q.; Zhang, Q.; Nie, J.-Q.; Yao, L.-D.; Su, D. S.; Wei, F. *Catal. Today* **2012**, *186*, 83.
- (113) Handuja, S.; Srivastava, P.; Vankar, V. D. *Nanoscale Res. Lett.* **2009**, *4*, 789.
- (114) Golberg, D.; Bando, Y.; Huang, Y.; Terao, T.; Mitome, M.; Tang, C.; Zhi, C. *ACS Nano* **2010**, *4*, 2979.
- (115) Bian, S.-W.; Ma, Z.; Song, W.-G. *J. Phys. Chem. C* **2009**, *113*, 8668.
- (116) Yue, B.; Ma, Y.; Tao, H.; Yu, L.; Jian, G.; Wang, X.; Wang, X.; Lu, Y.; Hu, Z. *J. Mater. Chem.* **2008**, *18*, 1747.
- (117) Zhou, X.; Jin, B.; Li, L.; Peng, F.; Wang, H.; Yu, H.; Fang, Y. *J. Mater. Chem.* **2012**, *22*, 17900.
- (118) Lyth, S. M.; Nabae, Y.; Islam, N. M.; Kuroki, S.; Kakimoto, M.; Miyata, S. *J. Nanosci. Nanotechnol.* **2012**, *12*, 4887.
- (119) Novoselov, K. S.; Geim, A. K.; Morozov, S. V.; Jiang, D.; Zhang, Y.; Dubonos, S. V.; Grigorieva, I. V.; Firsov, A. A. *Science* **2004**, *306*, 666.
- (120) Dreyer, D. R.; Ruoff, R. S.; Bielawski, C. W. *Angew. Chem., Int. Ed.* **2010**, *49*, 9336.
- (121) Sutter, P. *Nat. Mater.* **2009**, *8*, 171.
- (122) Yu, Q. K.; Lian, J.; Siriponglert, S.; Li, H.; Chen, Y. P.; Pei, S. S. *Appl. Phys. Lett.* **2008**, *93*, 113103/1.
- (123) Keun Soo, K.; Yue, Z.; Houk, J.; Sang Yoon, L.; Jong Min, K.; Kim, K. S.; Jong-Hyun, A.; Kim, P.; Jae-Young, C.; Byung Hee, H. *Nature* **2009**, *457*, 706.
- (124) Li, X. S.; Cai, W. W.; An, J. H.; Kim, S.; Nah, J.; Yang, D. X.; Piner, R.; Velamakanni, A.; Jung, I.; Tutuc, E.; Banerjee, S. K.; Colombo, L.; Ruoff, R. S. *Science* **2009**, *324*, 1312.
- (125) Bae, S.; Kim, H.; Lee, Y.; Xu, X. F.; Park, J. S.; Zheng, Y.; Balakrishnan, J.; Lei, T.; Kim, H. R.; Song, Y. I.; Kim, Y. J.; Kim, K. S.; Ozilmez, B.; Ahn, J. H.; Hong, B. H.; Iijima, S. *Nat. Nanotechnol.* **2010**, *5*, 574.
- (126) Emtsev, K. V.; Bostwick, A.; Horn, K.; Jobst, J.; Kellogg, G. L.; Ley, L.; McChesney, J. L.; Ohta, T.; Reshanov, S. A.; Röhrl, J.; Rotenberg, E.; Schmid, A. K.; Waldmann, D.; Seyller, H. B. W. *Nat. Mater.* **2009**, *8*, 203.
- (127) Coleman, J. N. *Adv. Funct. Mater.* **2009**, *19*, 3680.
- (128) Vadukumpully, S.; Paul, J.; Valiyaveettil, S. *Carbon* **2009**, *47*, 3288.
- (129) Khan, U.; O'Neill, A.; Lotya, M.; De, S.; Coleman, J. N. *Small* **2010**, *6*, 864.
- (130) Huang, B.; Li, Z.; Liu, Z.; Zhou, G.; Hao, S.; Wu, J.; Gu, B.-L.; Duan, W. *J. Phys. Chem. C* **2008**, *112*, 13442.
- (131) Zhou, S. Y.; Siegel, D. A.; Fedorov, A. V.; Lanzara, A. *Phys. Rev. Lett.* **2008**, *101*, 086402/1.
- (132) Feng, X.; Maier, S.; Salmeron, M. *J. Am. Chem. Soc.* **2012**, *134*, 5662.
- (133) Hossain, Md. Z.; Johns, J. E.; Bevan, K. H.; Karmel, H. J.; Liang, Y. T.; Yoshimoto, S.; Mukai, K.; Koitaya, T.; Yoshinobu, J.; Kawai, M.; Lear, A. M.; Kesmodel, L. L.; Tait, S. L.; Hersam, M. C. *Nat. Chem.* **2012**, *4*, 305.
- (134) Chen, Z. P.; Ren, W. C.; Gao, L. B.; Liu, B. L.; Pei, S. F.; Cheng, H. M. *Nat. Mater.* **2011**, *10*, 424.
- (135) Park, S.; Ruoff, R. S. *Nature Nanotechnol.* **2009**, *4*, 217–224; Corrigendum: *Nature Nanotechnol.* **2010**, *5*, 309.
- (136) Hummers, W. S.; Offeman, R. E. *J. Am. Chem. Soc.* **1958**, *80*, 1339.
- (137) Boehm, H. P.; Clauss, A.; Fischer, G. O.; Hofmann, U. Z. *Anorg. Allg. Chem.* **1962**, *316*, 119.
- (138) Guo, S. J.; Dong, S. J. *Chem. Soc. Rev.* **2011**, *40*, 2644.
- (139) Loh, K. P.; Bao, Q.; Ang, P. K.; Yang, J. *J. Mater. Chem.* **2010**, *20*, 2277.
- (140) Allen, M. J.; Tung, V. C.; Kaner, R. B. *Chem. Rev.* **2010**, *110*, 132.
- (141) Si, Y.; Samulski, E. T. *Nano Lett.* **2008**, *8*, 1679.
- (142) Rangel, N. L.; Sotelo, J. C.; Seminario, J. M. *J. Chem. Phys.* **2009**, *131*, 031105/1.
- (143) Janowska, I.; Ersen, O.; Jacob, T.; Vennégués, P.; Bégin, D.; Ledoux, M.-J.; Pham-Huu, C. *Appl. Catal. A* **2009**, *371*, 22.
- (144) Wang, M.-S.; Bando, Y.; Rodriguez-Manzo, J. A.; Banhart, F.; Golberg, D. *ACS Nano* **2009**, *3*, 2632.
- (145) Kosynkin, D. V.; Higginbotham, A. L.; Sinitskii, A.; Lomeda, J. R.; Dimiev, A.; Price, B. K.; Tour, J. M. *Nature* **2009**, *458*, 872.
- (146) Jiao, L.; Zhang, L.; Wang, X.; Diankov, G.; Dai, H. *Nature* **2009**, *458*, 877.
- (147) Tao, C.; Jiao, L.; Yazyev, O. V.; Chen, Y.-C.; Feng, J.; Zhang, X.; Capaz, R. B.; Tour, J. M.; Zettl, A.; Louie, S. G. *Nat. Phys.* **2011**, *7*, 616.
- (148) Kamat, P. V. *J. Phys. Chem. Lett.* **2010**, *1*, 520.
- (149) Yang, X.; Xu, M. S.; Qiu, W. M.; Chen, X. Q.; Deng, M.; Zhang, J. L.; Iwai, H.; Watanabe, E.; Chen, H. Z. *J. Mater. Chem.* **2011**, *21*, 8096.
- (150) Machado, B. F.; Serp, P. *Catal. Sci. Technol.* **2012**, *2*, 54.
- (151) Siamaki, A. R.; Khder, A. E. S.; Abdelsayed, V.; El-Shall, M. S.; Gupton, B. F. *J. Catal.* **2011**, *279*, 1.
- (152) Dongil, A. B.; Bachiller-Baeza, B.; Guerrero-Ruiz, A.; Rodriguez-Ramos, I. *J. Catal.* **2011**, *282*, 299.
- (153) Negreiros, F. R.; Apra, E.; Barcaro, G.; Sementa, L.; Vajda, S.; Fortunelli, A. *Nanoscale* **2012**, *4*, 1208.
- (154) Chen, H.; Li, Y.; Zhang, F.; Zhang, G.; Fan, X. *J. Mater. Chem.* **2011**, *21*, 17658.
- (155) Koo, H. Y.; Lee, H.-J.; Noh, Y.-Y.; Lee, E.-S.; Kim, Y.-H.; Choi, W. S. *J. Mater. Chem.* **2012**, *22*, 7130.
- (156) Sahu, A. K.; Sridhar, P.; Pitchumani, S. *J. Indian Inst. Sci.* **2009**, *89*, 437.
- (157) Ryoo, R.; Joo, S. H.; Kruk, M.; Jaroniec, M. *Adv. Mater.* **2001**, *13*, 677.
- (158) Ryoo, R.; Joo, S. H.; Jun, S. *J. Phys. Chem. B* **1999**, *103*, 7743.
- (159) Su, F.; Zhou, Z.; Guo, W.; Liu, J.; Tian, X. N.; Zhao, X. S. *Chem. Phys. Carbon* **2008**, *30*, 63.
- (160) Su, D. S.; Delgado, J. J.; Liu, X.; Wang, D.; Schlögl, R.; Wang, L. F.; Zhang, Z.; Shan, Z. C.; Xiao, F. S. *Chem.-Asian J.* **2009**, *4*, 1108.
- (161) Taguchi, A.; Schüth, F. *Microporous Mesoporous Mater.* **2005**, *77*, 1.
- (162) Meng, Y.; Gu, D.; Zhang, F. Q.; Shi, Y. F.; Yang, H. F.; Li, Z.; Yu, C. Z.; Tu, B.; Zhao, D. Y. *Angew. Chem., Int. Ed.* **2005**, *44*, 7053.
- (163) Liang, C. D.; Dai, S. *J. Am. Chem. Soc.* **2006**, *128*, 5316.
- (164) Huang, C. H.; Doong, R. A.; Gu, D.; Zhao, D. Y. *Carbon* **2011**, *49*, 3055.
- (165) Wang, X.; Liang, C.; Dai, S. *Langmuir* **2008**, *24*, 7500.

- (166) Wang, J.; Xue, C.; Lv, Y.; Zhang, F.; Tu, B.; Zhao, D. *Carbon* **2011**, *49*, 4580.
- (167) Huang, C. H.; Zhang, Q.; Chou, T. C.; Chen, C. M.; Su, D. S.; Doong, R. A. *ChemSusChem* **2012**, *5* (5), 563.
- (168) Wang, D. W.; Li, F.; Liu, M.; Lu, G. Q.; Cheng, H.-M. *Angew. Chem., Int. Ed.* **2008**, *47*, 373.
- (169) Zeng, Q.; Wu, D.; Zou, C.; Xu, F.; Fu, R.; Li, Z.; Liang, Y.; Su, D. *Chem. Commun.* **2010**, *46*, 5927.
- (170) Zhang, J.; Wang, R.; Liu, E.; Gao, X.; Sun, Z.; Xiao, F.-S.; Girgsdies, F.; Su, D. S. *Angew. Chem., Int. Ed.* **2012**, *51*, 7581.
- (171) Ma, H. L.; Su, D. S.; Klein-Hoffmann, A.; Jin, G. Q.; Guo, X. Y. *Carbon* **2006**, *44*, 2254.
- (172) Xia, W.; Su, D. S.; Biner, A.; Ruppel, L.; Wang, Y. W.; Woll, C.; Qian, J.; Liang, C. H.; Marginean, G.; Brandl, W.; Muhler, M. *Chem. Mater.* **2005**, *17*, 5737.
- (173) Delgado, J. J.; Su, D. S.; Rebmann, G.; Keller, N.; Gajovic, A.; Schlägl, R. *J. Catal.* **2006**, *244*, 126.
- (174) Vieira, R.; Pham-Huu, C.; Keller, N.; Ledoux, M. *J. Chem. Commun.* **2002**, *9*, 954.
- (175) Delgado, J. J.; Vieira, R.; Rebmann, G.; Su, D. S.; Keller, N.; Ledoux, M. J.; Schlägl, R. *Carbon* **2006**, *44*, 809.
- (176) Xia, W.; Bitter, J. H.; Su, D. S.; Qian, J.; Mühler, M. *Diamond Relat. Mater.* **2009**, *18*, 13.
- (177) Zhang, J.; Hu, Y. S.; Tessonniere, J. P.; Weinberg, G.; Maier, J.; Schlägl, R.; Su, D. S. *Adv. Mater.* **2008**, *20*, 1450.
- (178) Su, D. S.; Chen, X. W.; Weinberg, G.; Klein-Hofmann, A.; Timpe, O.; Hamid, S. B. A.; Schlogl, R. *Angew. Chem., Int. Ed.* **2005**, *44*, 5488.
- (179) Chen, X. W.; Su, D. S.; Schlägl, R. *Phys. Status Solidi B* **2006**, *243*, 3533.
- (180) Chen, X. W.; Su, D. S.; Hamid, S. B. A.; Schlägl, R. *Carbon* **2007**, *45*, 895.
- (181) Delgado, J. J.; Chen, X. W.; Su, D. S.; Hamid, S. B. A.; Schlägl, R. *J. Nanosci. Nanotechnol.* **2007**, *7*, 3495.
- (182) Chizari, K.; Deneuve, A.; Ersen, O.; Florea, I.; Liu, Y.; Edouard, D.; Janowska, I.; Begin, D.; Pham-Huu, C. *ChemSusChem* **2012**, *5*, 102.
- (183) Yan, H.; Su, D. S. *ChemCatChem* **2013**, DOI: 10.1002/cctc.201200758.
- (184) Alam, K.; Anghelescu, M. S.; Bradu, A. Computational model of porous media using true 3-D images. In *Heat Transfer in Multi-Phase Materials*; Öchsner, A., Murch, G. E., Eds.; Springer: Heidelberg, Germany, 2010; p 347.
- (185) Norimatsu, W.; Kusunoki, M. *Trans. JWRI* **2010**, *39*, 287.
- (186) Sun, K.; Yu, J.; Zhang, C.; Zhou, X. *Mater. Lett.* **2012**, *66*, 92.
- (187) Datye, A.; Wu, K.-H.; Gomes, G.; Kumari, L.; Li, W.; Lin, H.-T. *Ceram. Trans.* **2010**, *217*, 117.
- (188) Zhao, Y.; Watanabe, K.; Hashimoto, K. *Phys. Chem. Chem. Phys.* **2011**, *13*, 15016.
- (189) Xu, Z.; Buehler, M. J. *ACS Nano* **2009**, *3*, 2767.
- (190) Duong, H. M.; Nguyen, S. T. *Recent Pat. Eng.* **2011**, *5*, 209.
- (191) Liu, Y.; Nguyen, L. D.; Truong-Huu, T.; Liu, Y.; Romero, T.; Janowska, I.; Begin, D.; Pham-Huu, C. *Mater. Lett.* **2012**, *79*, 128.
- (192) Karousis, N.; Tagmatarchis, N.; Tasis, D. *Chem. Rev.* **2010**, *110*, 5366.
- (193) Boukhvalov, D. W.; Katsnelson, M. I. *J. Phys.-Condensed Matter* **2009**, *21*, 344205/1.
- (194) Yan, L.; Zheng, Y. B.; Zhao, F.; Li, S.; Gao, X.; Xu, B.; Weiss, P. S.; Zhao, Y. *Chem. Soc. Rev.* **2012**, *41*, 97.
- (195) Toebe, M. L.; van der Lee, M. K.; Tang, L. M.; Huis in 't Veld, M. H.; Bitter, J. H.; van Dillen, A. J.; de Jong, K. P. *J. Phys. Chem. B* **2004**, *108*, 11611.
- (196) Plomp, A. J.; Su, D. S.; de Jong, K. P.; Bitter, J. H. *J. Phys. Chem. C* **2009**, *113*, 9865.
- (197) van Dommelle, S.; de Jong, K. P.; Bitter, J. H. *Chem. Commun.* **2006**, 4859.
- (198) Cailu, X.; Junfeng, C.; Yan, C.; Qingyou, H.; Hahn, C.; Liaw, P. K.; Dehai, W. *Adv. Eng. Mater.* **2006**, *8*, 73.
- (199) Xing, Y. C.; Li, L.; Chusuei, C. C.; Hull, R. V. *Langmuir* **2005**, *21*, 4185.
- (200) Aviles, F.; Cauich-Rodriguez, J. V.; Moo-Tah, L.; May-Pat, A.; Vargas-Coronado, R. *Carbon* **2009**, *47*, 2970.
- (201) Bergeret, C.; Cousseau, J.; Fernandez, V.; Mevellec, J.-Y.; Lefrant, S. *J. Phys. Chem. C* **2008**, *112*, 16411.
- (202) Pumera, M.; Smid, B.; Veltruska, K. *J. Nanosci. Nanotechnol.* **2009**, *9*, 2671.
- (203) Byl, O.; Liu, J.; Yates, J. T. *Langmuir* **2005**, *21*, 4200.
- (204) Tsang, S. C.; Harris, P. J. F.; Green, M. L. H. *Nature* **1993**, *362*, 520.
- (205) Bubert, H.; Brandl, W.; Kittel, S.; Marginean, G.; Toma, D. *Anal. Bioanal. Chem.* **2002**, *374*, 1237.
- (206) Xia, W.; Jin, C.; Kundu, S.; Mühler, M. *Carbon* **2009**, *47*, 919.
- (207) Okpalugo, T. I. T.; Papakonstantinou, P.; Murphy, H.; McLaughlin, J.; Brown, N. M. D. *Carbon* **2005**, *43*, 153.
- (208) Kundu, S.; Wang, Y.; Xia, W.; Muhler, M. *J. Phys. Chem. C* **2008**, *112*, 16869.
- (209) Gosselink, R. W.; van den Berg, R.; Xia, W.; Mühler, M.; de Jong, K. P.; Bitter, J. H. *Carbon* **2012**, *50*, 4424.
- (210) Tessonniere, J.-P.; Rosenthal, D.; Hansen, W. T.; Hess, C.; Schuster, M. E.; Blume, R.; Girgsdies, F.; Pfänder, N.; Timpe, O.; Su, D. S.; Schlägl, R. *Carbon* **2009**, *47*, 1779.
- (211) Su, D. S. Nanocarbons: Characterization tools. In *Nanomaterials for the Life Sciences Vol. 9: Carbon Nanomaterials*; Kumar, C. S. S. R., Ed.; Wiley-VCH: Weinheim, Germany, 2011; p 358.
- (212) Datye, A. K.; Smith, D. J. *Catal. Rev.-Sci. Eng.* **1992**, *34*, 129.
- (213) Shao, L. D.; Zhang, W.; Armbruster, M.; Teschner, D.; Girgsdies, F.; Zhang, B. S.; Timpe, O.; Friedrich, M.; Schlägl, R.; Su, D. S. *Angew. Chem., Int. Ed.* **2011**, *50*, 10231.
- (214) Postole, G.; Auroux, A. Surface acid-base characterization of containing group IIIA catalysts by using adsorption microcalorimetry. In *Advances in Fluid Catalytic Cracking*; Occelli, M. L., Ed.; CRC Press: Boca Raton, FL, 2010; p 199.
- (215) Arrigo, R.; Schuster, M. E.; Wrabetz, S.; Girgsdies, F.; Tessonniere, J. P.; Centi, G.; Perathoner, S.; Su, D. S.; Schlägl, R. *ChemSusChem* **2012**, *5*, 577.
- (216) Ampelli, C.; Centi, G.; Passalacqua, R.; Perathoner, S. *Energy Environ. Sci.* **2010**, *3*, 292.
- (217) Gangeri, M.; Perathoner, S.; Caudo, S.; Centi, G.; Amadou, J.; Begin, D.; Pham-Huu, C.; Ledoux, M. J.; Tessonniere, J.-P.; Su, D. S.; Schlägl, R. *Catal. Today* **2009**, *143*, 57.
- (218) Centi, G.; Perathoner, S.; Wine, G.; Gangeri, M. *Green Chem.* **2007**, *9*, 671.
- (219) Centi, G.; Perathoner, S. *ChemSusChem* **2010**, *3*, 195.
- (220) Castillejos, E.; Bachiller-Baeza, B.; Rodríguez-Ramos, I.; Guerrero-Ruiz, A. *Carbon* **2012**, *50*, 2731.
- (221) Frank, B.; Wrabetz, S.; Khavryuchenko, O. V.; Blume, R.; Trunschke, A.; Schlägl, R. *ChemPhysChem* **2011**, *12*, 2709.
- (222) Arrigo, R.; Havecker, M.; Schlogl, R.; Su, D. S. *Chem. Commun.* **2008**, 4891.
- (223) Arrigo, R.; Havecker, M.; Wrabetz, S.; Blume, R.; Lerch, M.; McGregor, J.; Parrott, E. P. J.; Zeitler, J. A.; Gladden, L. F.; Knop-Gericke, A.; Schlogl, R.; Su, D. S. *J. Am. Chem. Soc.* **2010**, *132*, 9616.
- (224) Salmeron, M.; Schlägl, R. *Surf. Sci. Rep.* **2008**, *63*, 169.
- (225) Bluhm, H.; Hävecker, M.; Knop-Gericke, A.; Kiskinova, M.; Schlägl, R.; Salmeron, M. *MRS Bull.* **2007**, *32*, 1022.
- (226) Newberg, J. T.; Starr, D. E.; Yamamoto, S.; Kaya, S.; Kendelewicz, T.; Mysak, E. R.; Porsgaard, S.; Salmeron, M. B.; Brown, G. E., Jr.; Nilsson, A.; Bluhm, H. *J. Phys. Chem. C* **2011**, *115*, 12864.
- (227) Newberg, J. T.; Starr, D. E.; Yamamoto, S.; Kaya, S.; Kendelewicz, T.; Mysak, E. R.; Porsgaard, S.; Salmeron, M. B.; Brown, G. E., Jr.; Nilsson, A.; Bluhm, H. *Surf. Sci.* **2011**, *605*, 89.
- (228) Zhu, Z.; Tao, F. F.; Zheng, F.; Chang, R.; Li, Y.; Heinke, L.; Liu, Z.; Salmeron, M.; Somorjai, G. A. *Nano Lett.* **2012**, *12*, 1491.
- (229) Zhang, J.; Liu, X.; Blume, R.; Zhang, A. H.; Schlägl, R.; Su, D. S. *Science* **2008**, *322*, 73.
- (230) Rinaldi, A.; Tessonniere, J. P.; Schuster, M. E.; Blume, R.; Girgsdies, F.; Zhang, Q. A.; Jacob, T.; Hamid, S. B. A.; Su, D. S.; Schlägl, R. *Angew. Chem., Int. Ed.* **2011**, *50*, 3313.

- (231) Rosenthal, D.; Widmer, R.; Wagner, R.; Gille, P.; Armbruster, M.; Grin, Y.; Schlögl, R.; Groning, O. *Langmuir* **2012**, *28*, 6848.
- (232) Friedrich, H.; de Jongh, P. E.; Verkleij, A. J.; de Jong, K. P. *Chem. Rev.* **2009**, *109*, 1613.
- (233) Thomas, J. M.; Midgley, P. A. *ChemCatChem* **2010**, *2*, 783.
- (234) Midgley, P. A.; Ward, E. P. W.; Hungria, A. B.; Thomas, J. M. *Chem. Soc. Rev.* **2007**, *36*, 1477.
- (235) De Rosier, D. J.; Klug, A. *Nature* **1968**, *217*, 130.
- (236) Klug, A.; Crowther, R. A. *Nature* **1972**, *238*, 435.
- (237) Zewail, A. H. *Science* **2010**, *328*, 187.
- (238) Tessonner, J. P.; Ersen, O.; Weinberg, G.; Pham-Huu, C.; Su, D. S.; Schlögl, R. *ACS Nano* **2009**, *3*, 2081.
- (239) Friedrich, H.; Guo, S.; de Jongh, P. E.; Pan, X.; Bao, X.; de Jong, K. P. *ChemSusChem* **2011**, *4*, 957.
- (240) Zheng, W. Q.; Zhang, J.; Zhu, B.; Blume, R.; Zhang, Y. L.; Schlichte, K.; Schlögl, R.; Schüth, F.; Su, D. S. *ChemSusChem* **2010**, *3*, 226.
- (241) Midgley, P. A.; Weyland, M.; Thomas, J. M.; Gai, Pr.L.; Boyes, E. D. *Angew. Chem., Int. Ed.* **2002**, *41*, 3804.
- (242) Zhang, B.; Zhang, W.; Su, D. S. *ChemCatChem* **2011**, *3*, 965.
- (243) Zhang, B. S.; Zhang, W.; Su, D. S. *Microsc. Anal.* **2012**, *26*, 15.
- (244) Gontard, L. C.; Chang, L.-Y.; Hetherington, C.J. D.; Kirkland, A. I.; Ozkaya, D.; Dunin-Borkowski, R. E. *Angew. Chem., Int. Ed.* **2007**, *46*, 3683.
- (245) Su, D. S.; Jacob, T.; Hansen, T. W.; Wang, D.; Schlögl, R.; Freitag, B.; Kujawa, S. *Angew. Chem., Int. Ed.* **2008**, *47*, 5005.
- (246) Kotakoski, J.; Krasheninnikov, A. V.; Kaiser, U.; Meyer, J. C. *Phys. Rev. Lett.* **2011**, *106*, 105505/1.
- (247) Suenaga, K.; Koshino, M. *Nature* **2010**, *468*, 1088.
- (248) Hansen, P. L.; Wagner, J. B.; Helveg, S.; Rostrup-Nielsen, J. R.; Clausen, B. S.; Topsøe, H. *Science* **2002**, *295*, 2053.
- (249) Helveg, S.; López-Cartes, C.; Sehested, J.; Hansen, P. L.; Clausen, B. S.; Rostrup-Nielsen, J. R.; Abild-Pedersen, F.; Nørskov, J. K. *Nature* **2004**, *427*, 426.
- (250) Gai, P. L.; Calvino, J. J. *Annu. Rev. Mater. Res.* **2005**, *35*, 465.
- (251) Florea, I.; Ersen, O.; Arenal, R.; Ihiawakrim, D.; Messaoudi, C.; Chizari, K.; Janowska, I.; Pham-Huu, C. *J. Am. Chem. Soc.* **2012**, *134*, 9672.
- (252) Ichikawa, S.; Akita, T.; Okumura, M.; Haruta, M.; Tanaka, K.; Kohyama, M. *J. Electron Microsc.* **2003**, *52*, 21.
- (253) Su, D. S. *ChemCatChem* **2011**, *3*, 919.
- (254) Carlsson, J. M.; Hanke, F.; Linic, S.; Scheffler, M. *Phys. Rev. Lett.* **2009**, *102*, 166104/1.
- (255) Ao, Z.; Li, S. Hydrogenation of graphene and hydrogen diffusion behavior on graphene/graphane interface. In *Graphene Simulation*; Gong, J. R., Ed.; InTech: Rijeka, 2011; p 53.
- (256) Radovic, L. R. *J. Am. Chem. Soc.* **2009**, *131*, 17166.
- (257) Khavryuchenko, V. D.; Khavryuchenko, O. V.; Lisnyak, V. V. *Catal. Commun.* **2010**, *11*, 340.
- (258) Xu, S. C.; Irle, S.; Musaev, D. G.; Lin, M. C. *J. Phys. Chem. C* **2009**, *113*, 18772.
- (259) Hu, X. B.; Zhou, Z.; Lin, Q. X.; Wu, Y. T.; Zhang, Z. B. *Chem. Phys. Lett.* **2011**, *503*, 287.
- (260) Giannozzi, P.; Car, R.; Scsoles, G. *J. Chem. Phys.* **2003**, *118*, 1003.
- (261) Shan, B.; Cho, K. *Chem. Phys. Lett.* **2010**, *492*, 131.
- (262) Hu, X. B.; Wu, Y. T.; Li, H. R.; Zhang, Z. B. *J. Phys. Chem. C* **2010**, *114*, 9603.
- (263) Pramanik, A.; Kang, H. S. *J. Phys. Chem. C* **2011**, *115*, 10971.
- (264) Li, Z.; Chen, Z. X.; Kang, G. J.; He, X. *Catal. Today* **2011**, *165*, 25.
- (265) Banhart, F. *Nanoscale* **2009**, *1*, 201–213.
- (266) Wang, L.-L.; Khare, S. V.; Chirita, V.; Johnson, D. D.; Rockett, A. A.; Frenkel, A. I.; Mack, N. H.; Nuzzo, R. G. *J. Am. Chem. Soc.* **2006**, *128*, 131.
- (267) Qin, W.; Li, X. *Chem. Phys. Lett.* **2011**, *502*, 96.
- (268) Zoberbier, T.; Chamberlain, T. W.; Biskupek, J.; Kuganathan, N.; Eyhusen, S.; Bichoutskaia, E.; Kaiser, U.; Khlobystov, A. N. *J. Am. Chem. Soc.* **2012**, *134*, 3073.
- (269) Lv, Y.-A.; Cui, Y.-H.; Li, X.-N.; Song, X.-Z.; Wang, J.-G.; Dong, M. *Phys. E (Amsterdam, Neth.)* **2010**, *42*, 1746.
- (270) Kwon, K.; Jin, S.-a.; Pak, C.; Chang, H.; Joo, S. H.; Lee, H. I.; Kim, J. H.; Kim, J. M. *Catal. Today* **2011**, *164*, 186.
- (271) Seo, H. O.; Kim, K.-D.; Jeong, M.-G.; Kim, Y. D.; Choi, K. H.; Hong, E. M.; Lee, K. H.; Lim, D. C. *Macromol. Res.* **2012**, *20*, 216.
- (272) Lee, H.-Y.; Vogel, W.; Po-Jen Chu, P. *Langmuir* **2011**, *27*, 14654.
- (273) Gajendran, P.; Saraswathi, R. *Pure Appl. Chem.* **2008**, *80*, 2377.
- (274) Centi, G.; Lanzafame, P.; Perathoner, S. *Catal. Today* **2011**, *167*, 14.
- (275) Zinoviev, S.; Mueller-Langer, F.; Das, P.; Bertero, N.; Fornasiero, P.; Kaltschmitt, M.; Centi, G.; Miertus, S. *ChemSusChem* **2010**, *3*, 1106.
- (276) Braden, D. J.; Henao, C. A.; Heltzel, J.; Maravelias, C. C.; Dumesic, J. A. *Green Chem.* **2011**, *13*, 1755.
- (277) Wettstein, S. G.; Bond, J. Q.; Alonso, D. M.; Pham, H. N.; Datye, A. K.; Dumesic, J. *Appl. Catal., B* **2012**, *117–118*, 321.
- (278) Bezemer, G. L.; Bitter, J. H.; Kuipers, H. P. C. E.; Oosterbeek, H.; Holewijn, J. E.; Xu, X.; Kapteijn, F.; van Dillen, A. J.; de Jong, K. P. *J. Am. Chem. Soc.* **2006**, *128*, 3956.
- (279) den Breejen, J. P.; Radstake, P. B.; Bezemer, G. L.; Bitter, J. H.; Frøseth, V.; Holmen, A.; de Jong, K. P. *J. Am. Chem. Soc.* **2009**, *131*, 7197.
- (280) Perez-Alonso, F. J.; McCarthy, D. N.; Nierhoff, A.; Hernandez-Fernandez, P.; Strelbel, C.; Stephens, I. E. L.; Nielsen, J. H.; Chorkendorff, I. *Angew. Chem., Int. Ed.* **2012**, *51*, 4641.
- (281) Gu, J.; Zhang, Y.-W.; Tao, F. *Chem. Soc. Rev.* **2012**, *41*, 8050.
- (282) Barkhuizen, D.; Mabaso, I.; Viljoen, E.; Welker, C.; Claeyns, M.; van Steen, E.; Fletcher, J. C. Q. *Pure Appl. Chem.* **2006**, *78*, 1759.
- (283) Lei, Y.; Mahmood, F.; Lee, S.; Greeley, J.; Lee, B.; Seifert, S.; Winans, R. E.; Elam, J. W.; Meyer, R. J.; Redfern, P. C.; Teschner, D.; Schlögl, R.; Pellin, M. J.; Curtiss, L. A.; Vajda, S. *Science* **2010**, *328*, 224.
- (284) Teschner, D.; Borsodi, J.; Kis, Z.; Szentmiklosi, L.; Revay, Z.; Knop-Gericke, A.; Schlögl, R.; Torres, D.; Sautet, P. *J. Phys. Chem. C* **2010**, *114*, 2293.
- (285) Teschner, D.; Borsodi, J.; Wootsch, A.; Revay, Z.; Havecker, M.; Knop-Gericke, A.; Jackson, S. D.; Schlögl, R. *Science* **2008**, *320*, 86.
- (286) Abate, S.; Centi, G.; Perathoner, S.; Su, D. S.; Weinberg, G. *Appl. Catal., A* **2011**, *391*, 158.
- (287) Vogel, W.; He, W.; Huang, Q.-H.; Zou, Z.; Zhang, X.-G.; Yang, H. *Int. J. Hydrogen Energy* **2010**, *35*, 8609.
- (288) Abate, S.; Freni, M.; Arrigo, R.; Schuster, M. E.; Perathoner, S.; Centi, G. *ChemCatChem* **2013**, DOI: 10.1002/cctc.201200914.
- (289) Yoo, E. J.; Okada, T.; Akita, T.; Kohyama, M.; Honma, I.; Nakamura, J. *J. Power Sources* **2011**, *196*, 110.
- (290) Shim, J. Ho; Jung, H. J.; Lee, Y.; Lee, C. *Bull. Chem. Soc. Jpn.* **2011**, *84*, 1276.
- (291) Ji, X.; Banks, C. E.; Holloway, A. F.; Jurkschat, K.; Thorogood, C. A.; Wildgoose, G. G.; Compton, R. G. *Electroanalysis* **2006**, *18*, 2481.
- (292) Prati, L.; Villa, A. *Catalysts* **2012**, *2*, 24.
- (293) Abate, S.; Arrigo, R.; Schuster, M. E.; Perathoner, S.; Centi, G.; Villa, A.; Su, D.; Schlögl, R. *Catal. Today* **2010**, *157*, 280.
- (294) Cavani, F.; Centi, G.; Perathoner, S.; Trifiro, F. *Sustainable Industrial Processes*; Wiley-VCH: Weinheim, Germany, 2010.
- (295) Centi, G.; Perathoner, S.; Abate, S. Direct synthesis of hydrogen peroxide: Recent advances. In *Modern Heterogeneous Oxidation Catalysis*; Mizuno, N., Ed.; Wiley-VCH: Weinheim, Germany, 2009; p 253.
- (296) Centi, G.; Perathoner, S. *Catal. Today* **2009**, *143*, 145.
- (297) Abate, S.; Perathoner, S.; Centi, G. *Top. Catal.* **2011**, *54*, 718.
- (298) Abate, S.; Lanzafame, P.; Perathoner, S.; Centi, G. *Catal. Today* **2011**, *169*, 167.
- (299) Cotarca, L.; Eckert, H. *Phosgenations—A Handbook*; Wiley-VCH: Weinheim, Germany, 2003.

- (300) Mitchell, C. J.; van der Borden, W.; van der Velde, K.; Smit, M.; Scheringa, R.; Ahrika, K.; Jones, D. H. *Catal. Sci. Technol.* **2012**, *2*, 2109.
- (301) Volodina, V. A.; Kozlovskii, A. A.; Kuzina, S. I.; Mikhailov, A. I. *High Energy Chem.* **2008**, *42*, 311.
- (302) Li, Y.-P.; Cao, H.-B.; Liu, C.-M.; Zhang, Y. *J. Hazard. Mater.* **2007**, *148*, 158.
- (303) Qi, B.; Lin, F.; Bai, J.; Liu, L.; Guo, L. *Mater. Lett.* **2008**, *62*, 3670.
- (304) Hee, H. B.; Hyun, S. D.; Sung, Y. C. *Tetrahedron Lett.* **1985**, *26*, 6233.
- (305) Larsen, J. W.; Freund, M.; Kim, K. Y.; Sidovar, M.; Stuart, J. L. *Carbon* **2000**, *38*, 655.
- (306) Gao, Y.; Ma, D.; Wang, C.; Guan, J.; Bao, X. *Chem. Commun.* **2011**, *47*, 2432.
- (307) Li, B.; Xu, Z. *J. Am. Chem. Soc.* **2009**, *131*, 16380.
- (308) Pacosova, L.; Kartusch, C.; Kukula, P.; van Bokhoven, J. A. *ChemCatChem* **2011**, *3*, 154.
- (309) Zhang, J.; Su, D. S.; Blume, R.; Schlögl, R.; Wang, R.; Yang, X.; Gajovic, A. *Angew. Chem., Int. Ed.* **2010**, *49*, 8640.
- (310) Su, D. S.; Maksimova, N. I.; Mestl, G.; Kuznetsov, V. L.; Keller, V.; Schlögl, R. *Carbon* **2007**, *45*, 2145.
- (311) Liu, X.; Frank, B.; Zhang, W.; Cotter, T. P.; Schlögl, R.; Su, D. S. *Angew. Chem., Int. Ed.* **2011**, *50*, 3318.
- (312) Mochalin, V. N.; Shenderova, O.; Ho, D.; Gogotsi, Y. *Nat. Nanotechnol.* **2012**, *7*, 11.
- (313) McGregor, J.; Huang, Z.; Parrott, E. P. J.; Zeitler, J. A.; Nguyen, K. L.; Rawson, J. M.; Carley, A.; Hansen, T. W.; Tessonniere, J.-P.; Su, D. S.; Teschner, D.; Vass, E. M.; Knop-Gericke, A.; Schlögl, R.; Gladden, L. F. *J. Catal.* **2010**, *269*, 329.
- (314) Frank, B.; Zhang, J.; Blume, R.; Schlögl, R.; Su, D. S. *Angew. Chem., Int. Ed.* **2009**, *48*, 6913.
- (315) Frank, B.; Blume, R.; Rinaldi, A.; Trunschke, A.; Schlögl, R. *Angew. Chem., Int. Ed.* **2011**, *50*, 1.
- (316) Frank, B.; Blume, R.; Rinaldi, A.; Trunschke, A.; Schlögl, R. Nanocarbons as catalyst for selective oxidation of acrolein to acrylic acid. *DGMK Tagungsbericht* **2011**, *2011–2*, 211 (Preprints of the DGMK-Conference “Catalysis: Innovative Applications in Petrochemistry and Refining”, 2011).
- (317) Liang, C.; Xie, H.; Schwartz, V.; Howe, J.; Dai, S.; Overbury, S. H. *J. Am. Chem. Soc.* **2009**, *131*, 7735.
- (318) Ni, S.; Li, Z.; Yang, J. *Nanoscale* **2012**, *4*, 1184.
- (319) Song, S.; Yang, H.; Rao, R.; Liu, H.; Zhang, A. *Catal. Comm.* **2010**, *11*, 783.
- (320) Yu, H.; Peng, F.; Tan, J.; Hu, X.; Wang, H.; Yang, J.; Zheng, W. *Angew. Chem., Int. Ed.* **2011**, *50*, 3978.
- (321) Yang, X.; Yu, H.; Peng, F.; Wang, H. *ChemSusChem* **2012**, *5*, 1213.
- (322) Luo, J.; Peng, F.; Yu, H.; Wang, H. *Chem. Eng. J.* **2012**, *204–206*, 98.
- (323) Pohorecki, R.; Baldyga, J.; Moniuk, W.; Podgorska, W.; Zdrojowski, A.; Wierzchowski, P. T. *Chem. Eng. Sci.* **2001**, *56*, 1285.
- (324) Morozan, A.; Jegou, P.; Pinault, M.; Campidelli, S.; Jousselme, B.; Palacin, S. *ChemSusChem* **2012**, *5*, 647.
- (325) Yang, L.-J.; Jiang, S.-J.; Zhao, Y.; Zhu, L.; Chen, S.; Wang, X.-Z.; Wu, Q.; Ma, J.; Ma, Y.-W.; Hu, Z. *Angew. Chem., Int. Ed.* **2011**, *50*, 7132.
- (326) Kim, Y. S.; Shin, J. Y.; Jeon, H. J.; Cha, A.; Lee, C.; Lee, S.-g. *Chem.-Asian J.* **2013**, *8*, 232.
- (327) Ma, Y.; Sun, L.; Huang, W.; Zhang, L.; Zhao, J.; Fan, Q.; Huang, W. *J. Phys. Chem. C* **2011**, *115*, 24592.
- (328) Jo, K.; Lee, J.-S.; Cho, J.; Kim, B.-S. *Preprints-Am. Chem. Soc., Div. Energy Fuels* **2012**, *57*, 87.
- (329) Kwon, K.; Jin, S.; Cheon, J. Y.; Joo, S. H. *Langmuir* **2012**, *28*, 991.
- (330) Biddinger, E. J.; Ozkan, U. S. *J. Phys. Chem. C* **2010**, *114*, 15306.
- (331) Lyth, S. M.; Nabae, Y.; Islam, N. M.; Kuroki, S.; Kakimoto, M.; Miyata, S. *J. Nanosci. Nanotechnol.* **2012**, *12*, 4887.
- (332) Choi, C. H.; Park, S. H.; Woo, S. I. *J. Mater. Chem.* **2012**, *22*, 12107.
- (333) Ziwu, L.; Feng, P.; Hongjuan, W.; Hao, Y.; Wenxu, Z.; Jian, Y. *Angew. Chem., Int. Ed.* **2011**, *50*, 3257.
- (334) Ziwu, L.; Feng, P.; Hongjuan, W.; Hao, Y.; Jun, T.; Lili, Z. *Catal. Commun.* **2011**, *16*, 35.
- (335) Ziwu, L.; Feng, P.; Hongjuan, W.; Hao, Y.; Wenxu, Z.; Xianyong, W. *J. Nat. Gas Chem.* **2012**, *21*, 257.
- (336) Wong, W. Y.; Daud, W. R. W.; Mohamad, A. B.; Kadhum, A. A. H.; Majlan, E. H.; Loh, K. S. *Diamond Relat. Mater.* **2012**, *22*, 12.
- (337) Vazquez-Arenas, J.; Higgins, D.; Chen, Z.; Fowler, M.; Chen, Z. *J. Power Sources* **2012**, *205*, 215.
- (338) Kim, H.; Lee, K.; Woo, S. I.; Jung, Y. *Phys. Chem. Chem. Phys.* **2011**, *13*, 17505.
- (339) Wiggins-Camacho, J. D.; Stevenson, K. J. *J. Phys. Chem. C* **2011**, *115*, 20002.
- (340) Centi, G.; Perathoner, S.; Vazzana, F. Catalysis using guest single and mixed oxides in host zeolite matrices. In *Catalysis by Unique Metal Ion Structures in Solid Matrices*; Centi, G., Bell, A. T., Wichterlová, B., Eds.; Springer-Verlag: Dordrecht, The Netherlands, 2001; p 165.
- (341) Cejka, J.; Centi, G.; Perez-Pariente, J.; Roth, W. *J. Catal. Today* **2012**, *179*, 2.
- (342) de Jongh, P. E.; Adelhelm, P. *ChemSusChem* **2010**, *3*, 1332.
- (343) Tessonniere, J. P.; Pesant, L.; Ehret, G.; Ledoux, M. J.; Pham-Huu, C. *Appl. Catal. A* **2005**, *288*, 203.
- (344) Pan, X.; Fan, Z.; Chen, W.; Ding, Y.; Luo, H.; Bao, X. *Nat. Mater.* **2007**, *6*, 507–511.
- (345) Chen, W.; Pan, X.; Willinger, M. G.; Su, D. S.; Bao, X. *J. Am. Chem. Soc.* **2006**, *128*, 3136.
- (346) Chen, W.; Fan, Z.; Pan, X.; Bao, X. *J. Am. Chem. Soc.* **2008**, *130*, 9414.
- (347) Yang, Z.; Guo, S.; Pan, X.; Wang, J.; Bao, X. *Energy Environ. Sci.* **2011**, *4*, 4500.
- (348) Serp, P.; Castillejos, E. *ChemCatChem* **2010**, *2*, 41.
- (349) Khlobystov, A. N. *ACS Nano* **2011**, *5*, 9306.
- (350) Ertl, G.; Knözinger, H.; Schüth, F.; Weitkamp, J. *Handbook of Heterogeneous Catalysis*; Wiley-VCH: Weinheim, Germany, 2008; Vol. 8, p 2501.
- (351) Baaziz, W.; Begin-Colin, S.; Pichon, B. P.; Florea, I.; Ersen, O.; Zafeiratos, S.; Barbosa, R.; Begin, D.; Pham-Huu, C. *Chem. Mater.* **2012**, *24*, 1549.
- (352) Mao, Z. G.; Sinnott, S. B. *J. Phys. Chem. B* **2000**, *104*, 4618.
- (353) Striolo, A. *Nano Lett.* **2006**, *6*, 633.
- (354) Chen, X.; Cao, G. X.; Han, A. J.; Punyamurtula, V. K.; Liu, L.; Culligan, P. J.; Kim, T.; Qiao, Y. *Nano Lett.* **2008**, *8*, 2988.
- (355) Zhang, H. W.; Ye, H. F.; Zheng, Y. G.; Zhang, Z. Q. *Microfluid. Nanofluid.* **2011**, *10*, 403.
- (356) Ye, H. F.; Zhang, H. W.; Zheng, Y. G.; Zhang, Z. Q. *Microfluid. Nanofluid.* **2011**, *10*, 1359.
- (357) Liu, Y. C.; Moore, J. D.; Roussel, T. J.; Gubbins, K. E. *Phys. Chem. Chem. Phys.* **2010**, *12*, 6632.
- (358) Nakamura, Y.; Ohno, T. *Chem. Phys. Lett.* **2012**, *539–540*, 123.
- (359) Majumder, M.; Chopra, N.; Andrews, R.; Hinds, B. *J. Nature* **2005**, *438*, 44.
- (360) Holt, J. K.; Park, H. G.; Wang, Y. M.; Stadermann, M.; Artyukhin, A. B.; Grigoropoulos, C. P.; Noy, A.; Bakajin, O. *Science* **2006**, *312*, 1034.
- (361) Majumder, M.; Chopra, N.; Hinds, B. *J. ACS Nano* **2011**, *5*, 3867.
- (362) Sears, K.; Dumée, L.; Schütz, J.; She, M.; Huynh, C.; Hawkins, S.; Duke, M.; Gray, S. *Materials* **2010**, *3*, 127.
- (363) Schmidt, L. D.; Goralski, C. T., Jr. *Stud. Surf. Sci. Catal.* **1997**, *110*, 491.
- (364) Sun, H.; Blass, S.; Michor, E.; Schmidt, L. *Appl. Catal. A* **2012**, *445–446*, 35.
- (365) Skinner, M. J.; Michor, E. L.; Fan, W.; Tsapatsis, M.; Bhan, A.; Schmidt, L. D. *ChemSusChem* **2011**, *4*, 1151.

- (366) Dibán, N.; Aguayo, A. T.; Bilbao, J.; Urtiaga, A.; Ortiz, I. Membrane reactors for in situ water removal: A review of applications. *Ind. Eng. Chem. Res.* **2013**, DOI: 10.1021/ie3029625.
- (367) Jhang, S. H.; Margariska, M.; Skourski, Y.; Preusche, D.; Grifoni, M.; Wosnitza, J.; Strunk, C. *Phys. Rev. Lett.* **2011**, *106*, 096802/1.
- (368) Appelhans, D. J.; Lin, Z.; Lusk, M. T. *Phys. Rev. B: Condens. Matter Mater. Phys.* **2010**, *82*, 073410/1.
- (369) Vogg, R.; Pal, S.; Pati, S. K.; Rao, C. N. R. *J. Phys.: Condens. Matter* **2008**, *20*, 215211/1.
- (370) Zhang, H.; Pan, X.; Liu, J.; Qian, W.; Wei, F.; Huang, Y.; Bao, X. *ChemSusChem* **2011**, *4*, 975.
- (371) Leary, R.; Westwood, A. *Carbon* **2011**, *49*, 741.
- (372) Chen, J.; Li, B.; Zheng, J.; Zhao, J.; Zhu, Z. *J. Phys. Chem. C* **2012**, *116*, 14848.
- (373) Guai, G. H.; Li, Y.; Ng, C. M.; Li, C. M.; Chan-Park, M. B. *ChemPhysChem* **2012**, *13*, 2566.
- (374) Centi, G.; Perathoner, S. Advanced photocatalytic materials by nanocarbon hybrid materials. In *Nanocarbon Hybrids*; Eder, D., Schlägl, R., Eds.; De Gruyter: Berlin, Germany, 2013, in press.
- (375) Su, D. S.; Centi, G. *J. Energy Chem.* **2013**, *22*, 151.
- (376) Li, X.; Qin, Y.; Picraux, S. T.; Guo, Z.-X. *J. Mater. Chem.* **2011**, *21*, 7527.
- (377) Yuan, Q.; Xu, Z.; Yakobson, B. I.; Ding, F. *Phys. Rev. Lett.* **2012**, *108*, 245505/1.
- (378) Kim, J.; Page, A. J.; Irle, S.; Morokuma, K. *J. Am. Chem. Soc.* **2012**, *134*, 9311.
- (379) Picher, M.; Navas, H.; Arenal, R.; Quesnel, E.; Anglaret, E.; Jourdain, V. *Carbon* **2012**, *50*, 2407.
- (380) Hembram, K. P. S. S.; Rao, G. M. *Mater. Lett.* **2012**, *72*, 68.
- (381) Singh, D. K.; Iyer, P. K.; Giri, P. K. *Int. J. Nanosci.* **2011**, *10*, 49.
- (382) Carlsson, J. M.; Scheffler, M. *Phys. Rev. Lett.* **2006**, *96*, 046806/1.
- (383) Tessonner, J.-P.; Villa, A.; Majoulet, O.; Su, D. S.; Schlägl, R. *Angew. Chemie Int. Ed.* **2009**, *48*, 6543.
- (384) Chen, C.-Y.; Jafvert, C. T. *Environ. Sci. Technol.* **2010**, *44*, 6674.
- (385) Luo, Y.; Heng, Y.; Dai, X.; Chen, W.; Li, J. *J. Solid State Chem.* **2009**, *182*, 2521.
- (386) Liang, Y. T.; Vijayan, B. K.; Gray, K. A.; Hersam, M. C. *Nano Lett.* **2011**, *11*, 2865.
- (387) Huang, H.; Sun, D.; Wang, X. *J. Phys. Chem. C* **2011**, *115*, 19405.
- (388) Centi, G.; Gangeri, M.; Fiorello, M.; Perathoner, S.; Amadou, J.; Bégin, D.; Ledoux, M. J.; Pham-Huu, C.; Schuster, M. E.; Su, D. S.; Tessonner, J.-P.; Schlägl, R. *Catal. Today* **2009**, *147*, 287.
- (389) Kim, G.; Jhi, S.-H. *ACS Nano* **2011**, *5*, 805.
- (390) Moldovan, M. S.; Bulou, H.; Dappe, Y. J.; Janowska, I.; Bégin, D.; Pham-Huu, C.; Ersen, O. *J. Phys. Chem. C* **2012**, *116*, 9274.
- (391) Li, Y.; Sun, C.; Yu, C.; Wang, C.; Liu, Y.; Song, Y. Graphene oxide and its applications in catalysis. *Adv. Mater. Res.* **2012**, *476–478* (Pt. 2, New Materials and Processes), 1488.
- (392) Chen, D.; Feng, H.; Li, J. *Chem. Rev.* **2012**, *112*, 6027.
- (393) Agnoli, S.; Granozzi, G. *Surf. Sci.* **2013**, *609*, 1.
- (394) Huang, C.; Li, C.; Shi, G. *Energy Environ. Sci.* **2012**, *5*, 8848.
- (395) Tan, L.-L.; Chai, S.-P.; Mohamed, A. R. *ChemSusChem* **2012**, *5*, 1868.
- (396) Han, L.; Wang, P.; Dong, S. *Nanoscale* **2012**, *4*, 5814.
- (397) Antolini, E. *Appl. Catal., B* **2012**, *123–124*, 52.
- (398) Krishnan, D.; Kim, F.; Luo, J.; Cruz-Silva, R.; Cote, L. J.; Jang, H. D.; Huang, J. *Nano Today* **2012**, *7*, 137.
- (399) Wang, H.; Maiyalagan, T.; Wang, X. *ACS Catal.* **2012**, *2*, 781.
- (400) Xiang, Q.; Yu, J.; Jaroniec, M. *Chem. Soc. Rev.* **2012**, *41*, 782.
- (401) Scheuermann, G. M.; Rumi, L.; Steurer, R.; Bannwarth, W.; Mülhaupt, R. *J. Am. Chem. Soc.* **2009**, *131*, 8262.
- (402) Dreyer, D. R.; Jarvis, K. A.; Ferreira, P. J.; Bielawski, C. W. *Polymer Chem.* **2012**, *3*, 757.
- (403) Dreyer, D. R.; Bielawski, C. W. *Adv. Funct. Mater.* **2012**, *22*, 3247.
- (404) Dreyer, D. R.; Jarvis, K. A.; Ferreira, P. J.; Bielawski, C. W. *Macromolecules* **2011**, *44*, 7659.
- (405) Dreyer, D. R.; Jia, H.-P.; Todd, A. D.; Geng, J.; Bielawski, C. W. *Org. Biomol. Chem.* **2011**, *9*, 7292.
- (406) Jia, H.-P.; Dreyer, D. R.; Bielawski, C. W. *Tetrahedron* **2011**, *67*, 4431.
- (407) Jia, H.-P.; Dreyer, D. R.; Bielawski, C. W. *Adv. Synth. Catal.* **2011**, *353*, 528.
- (408) Kumar, A. V.; Rao, K. R. *Tetrahedron Lett.* **2011**, *52*, 5188.
- (409) Verma, S.; Mungse, H. P.; Kumar, N.; Choudhary, S.; Jain, S. L.; Sain, B.; Khatri, O. P. *Chem. Commun.* **2011**, *47*, 12673.
- (410) Ji, J. Y.; Zhang, G. H.; Chen, H. Y.; Wang, S. L.; Zhang, G. L.; Zhang, F. B.; Fan, X. B. *Chem. Sci.* **2011**, *2*, 484.
- (411) Boukhvalov, D. W.; Dreyer, D. R.; Bielawski, C. W.; Son, Y.-W. *ChemCatChem* **2012**, *4*, 1844.
- (412) Wang, S.; Nai, C. T.; Jiang, X.; Pan, Y.; Tan, C. H.; Nesladek, M.; Xu, Q. H.; Loh, K. P. *J. Phys. Chem. Lett.* **2012**, *3*, 2332.
- (413) Jahan, M.; Bao, Q. L.; Loh, K. P. *J. Am. Chem. Soc.* **2012**, *134*, 6707.
- (414) Pan, Y. H.; Wang, S.; Kee, C. W.; Dubuisson, E.; Yang, Y. Y.; Loh, K. P.; Tan, C. H. *Green Chem.* **2011**, *13*, 3341.